NASA Technical Paper 3537

1995

Flight Test of the X-29A at High Angle of Attack: Flight Dynamics and Controls

Jeffrey E. Bauer
Robert Clarke
John J. Burken
Dryden Flight Research Center
Edwards, California

National Aeronautics and Space Administration

Office of Management

Scientific and Technical Information Program

CONTENTS

TABLES

FIGURES

ABSTRACT

The NASA Dryden Flight Research Center has flight tested two X-29A aircraft at low and high angles of attack. The high-angle-of-attack tests evaluate the feasibility of integrated X-29A technologies. More specific objectives focus on evaluating the high-angle-of-attack flying qualities, defining multiaxis controllability limits, and determining the maximum pitch-pointing capability. A pilot-selectable gain system allows examination of tradeoffs in airplane stability and maneuverability. Basic fighter maneuvers provide qualitative evaluation. Bank-angle captures permit qualitative data analysis.

This paper discusses the design goals and approach for high-angle-of-attack control laws and provides results from the envelope expansion and handling qualities testing at intermediate angles of attack. Comparisons of the flight test results to the predictions are made where appropriate. The pitch rate command structure of the longitudinal control system is shown to be a valid design for high-angle-of-attack control laws. Flight test results show that wing rock amplitude was overpredicted and aileron and rudder effectivenesses were underpredicted. Flight tests show the X-29A airplane to be controllable in all axes, with no nose wandering, up to 40° angle of attack.

INTRODUCTION

The NASA Dryden Flight Research Center (NASA Dryden) X-29A program was structured to test the X-29A no. 1 airplane at low angles of attack and the no. 2 airplane at high angles of attack. The low-angle-of-attack testing included evaluating and improving handling qualities.[1, 2] The high-angle-of-attack tests assessed the predictive techniques for high angle of attack and the feasibility of the integrated X-29A technologies. These technologies include a 4.9 percent–thick supercritical wing with no leading-edge devices but with variable-camber control trailing-edge devices. In addition, the aircraft has a close-coupled canard and large negative static margin. More specific objectives focused on evaluating the high-angle-of-attack flying qualities, defining multiaxis controllability limits, and determining the maximum pitch-pointing capability.[3, 4]

Recent emphasis has been placed on the ability of an aircraft to operate beyond maximum lift. It has been theorized for some time that the forward-swept wing has several advantages in this flight regime.[5, 6] The configuration was designed to be departure resistant and to maintain significant roll control at high angles of attack. To further investigate the potential of a forward-swept wing at high angles of attack, the X-29A military utility and agility test program was initiated in 1986 as a follow-on to the low-angle-of-attack program.[1, 2 7–10]

This paper provides results from the envelope expansion and handling qualities testing at intermediate angles of attack. Topics include envelope expansion, flight test techniques, and flight test results. Comparisons of the flight test results to the predictions are made where appropriate.

AIRCRAFT DESCRIPTION

The X-29A aircraft is a single-seat, single-engine fighter class aircraft (fig. 1). An F-5 forebody is used forward of the pilot station, and F-16 integrated servo-actuators are used for all except the strake actuators. The cockpit has conventional dial display gauges (fig 2). No cathode-ray-tube screens or head-up displays are used.

The wing has a thin, 4.9 percent–thick streamwise supercritical airfoil section with a 29.27° forward sweep along the leading edge and a –33.73° quarter-chord sweep. The wing structure includes aeroelastically tailored graphite-epoxy covers to help provide the stiffness needed to overcome the torsional divergence problems associated with forward-swept wings. The wing is relatively simple, employs full-span trailing-edge flaps, and does not use leading-edge devices. These double-hinged flaps also provide discrete variable camber.

The three surfaces used for pitch control are the all-moving, close-coupled canards; symmetric wing flaps; and aft-fuselage strake flaps. The lateral–directional axes are controlled using differential wing flaps and a conventional rudder. Table 1 shows critical airplane geometry and mass characteristics. A more complete description of the aircraft has previously been provided.[10]

The second X-29A airplane, built concurrently with the first, was modified for high-angle-of-attack flight research by adding support structure to the tail and a spin chute (fig. 3).[11] The chute is designed to recover the aircraft from an upright or inverted spin or deep stall and is contained in a canister installed at the base of the vertical tail. The chute measures 19 ft in diameter with riser lengths of 75 ft. The chute mechanism

was tested on the ground and in the air. Deployment speed is limited to a maximum of 180 kn equivalent airspeed and is accomplished by a redundant set of pyrotechnics. After deployment, the chute can be jettisoned by unlocking the mechanical jaws that hold the chute to the aircraft. If that mechanism fails, explosive bolts that would release the jaws can be fired.

The cockpit was also modified for high-angle-of-attack testing. Large angle-of-attack and yaw rate gauges, spin chute status displays, and spin recovery indicators were added to the cockpit. Figure 2 shows the spin recovery indicators, which consist of four arrows showing stick positioning and two dots indicating rudder pedal positioning. A single-needle pressure altimeter replaced the clock. For high angles of attack, a yaw string was placed on the windshield to aid the pilot.

Commands generated on the ground and uplinked to the horizontal and vertical flightpath command needle in the attitude direction indicator instrument were used for flightpath targeting.[12] This instrument allowed the pilot to easily capture and hold angles of attack for high-angle-of-attack test points. The needle deflection was proportional to the error between the target angle of attack and the measured angle of attack. Similarly, the vertical needle showed the error between the measured and the targeted sideslip angle. The horizontal and vertical needles were important in high-angle-of-attack maneuvers, assisting the pilots in flying more precise test points. The pilots were able to concentrate on a single instrument to receive attitude, target-angle-of-attack error, and target-sideslip error information.

The upper surface of the right wingtip and the left side of the vertical stabilizer tip had stripes painted on them. The stripes were added in case a spin necessitated aircraft orientation identification from long-range optics.

Flight Control System

This subsection describes flight control system (FCS) modifications that were made to allow exploration of the high-angle-of-attack envelope. The architecture of the FCS was largely unchanged from that developed and tested in the low-angle-of-attack program.

The FCS was designed to allow maneuvering of the airplane at high angles of attack without using rudder pedal inputs. The lateral stick commanded stability axis roll rate, and the longitudinal stick commanded a combination of pitch rate, normal acceleration, and angle of attack.[13, 14] Rudder pedals commanded washed-out stability axis yaw rate.

Mode Logic

The X-29A FCS uses two basic modes. The primary mode is a normal digital (ND) mode; the backup mode is an analog reversion (AR) mode. Several degraded modes are also possible when sensor failures prompt a reconfiguration. A new digital mode, NORMHI, was created for high-angle-of-attack testing. This mode is identical to the ND mode, but it prevents the automatic downmoding to the AR mode that occurs when surface commands exceed predetermined rates.

The new NORMHI mode prevents the reasonability test from causing the downmode to the AR mode during critical high-angle-of-attack maneuvers or out-of-control situations. The reasonability test is a logic that was developed in an attempt to prevent generic software errors from leading to loss of the airplane. For high angles of attack, the commands in the digital computers are still limited to reasonable rates; only the automatic downmoding to the AR mode is precluded. Pilot action is required to select the backup mode in the event of a generic software failure.

The AR mode was unchanged for the second X-29A airplane. Six-degree-of-freedom nonlinear simulation found that the AR mode would provide marginal recovery capability at high angles of attack. Simulation studies showed that this FCS would have poor damping of the predicted wing rock. The simulation showed that if the pilot were to allow the wing rock motion to fully develop, the inertial coupling would be strong enough that the angle of attack could not be reduced below 40°. Previous low-angle-of-attack envelope expansion philosophy was to test the primary ND and backup AR modes under all flight conditions. This philosophy was not followed for the X-29A high-angle-of-attack envelope expansion, and only the NORMHI mode was tested.

Design Requirements

The FCS was required to retain the low-angle-of-attack flight characteristics and control law structure that had been used previously on X-29A no. 1. The FCS was also required to ensure that spins would not be easily entered. An active spin prevention system was incorporated into the FCS to meet that requirement.

Additional design guidelines were developed using the Langley differential maneuvering simulation. Table 2 shows these guidelines. The aircraft dynamics from the six-degree-of-freedom simulation were compared to the guidelines. The guidelines were not used for linear models. Generally, the X-29A FCS met these design guidelines. Yaw rates for neutral lateral controls were predicted to be small based upon the small asymmetries present in the simulation database. Predicted angle-of-attack recovery was favorable, exhibiting a smooth onset from high-angle-of-attack conditions. Adverse sideslip during rolling maneuvers and wing rock were predicted to be within the Langley guidelines. Proverse sideslip was expected to sometimes exceed the guideline. The angle-of-attack variation was also predicted to be within the guidelines even though the control laws did not compensate for inertial pitching moments caused by commanded roll rates.

Design Technique

The high-angle-of-attack control laws were designed using conventional techniques combined with the X-29A nonlinear batch and real-time simulations. Linear analysis was used to examine stability margins and generate time histories that were compared with the nonlinear simulation results to validate the margins. The linear analysis included conventional Bode stability margins, time history responses, and limited, structured singular-value analysis in the lateral–directional axes.

In the pitch axis, stability margins at high-angle-of-attack conditions were predicted to be higher than the stability margins at equivalent low-angle-of-attack conditions. In the lateral–directional axes, however, the unstable wing rock above 35° angle of attack dominated the response in linear and nonlinear analysis. Feedback gains that stabilized the linear airplane models showed an unstable response in the nonlinear simulation. This unstable response was caused by rate saturation of the ailerons. The FCS configuration kept the feedback gains at a reasonable level to control the high frequency instability but did not completely control the low-frequency (bounded) lateral–directional instability (wing rock).

Longitudinal Control Law Design

At high angles of attack, the X-29A pitch stick commanded a blend of pitch rate and angle of attack. The choice of the controlled variable followed a different philosophy than that of other high-angle-of-attack aircraft that primarily use angle-of-attack command systems.[15, 16] The combination of feedbacks used in the X-29A FCS provided more of a pitch rate command system with weak angle-of-attack feedback. The pitch axis trim schedule provided small positive stick forces at 1-*g*, high-angle-of-attack conditions. Approximately 1-in. deflection, or 8 lbf, was required to hold 40° angle of attack.

For the most part, the basic low-angle-of-attack ND longitudinal axis control laws remained unchanged for the NORMHI mode at high angles of attack. No gains in the longitudinal axis were scheduled with angle of attack, but several feedback paths were switched in and out as a function of angle of attack. The following changes were made in the design of the high-angle-of-attack control laws for the X-29A longitudinal axis (fig. 4):

- The automatic camber control (ACC) schedules were modified to reduce transonic canard loads and to provide optimum lift-to-drag ratio canard and strake flap positioning by increasing slightly the reference canard position in a 20° to 38° angle-of-attack range.
- Airspeed feedback was faded out and angle-of-attack feedback was faded in to control a slow, divergent angle of attack. Airspeed feedback was not appropriate to control the instability that developed at high angles of attack; angle-of-attack measurement provided the best feedback because the divergence was almost purely angle of attack.
- Active negative angles of attack and *g*-force limiters were added to prevent potential nosedown pitch tumble entries or inverted hung stall problems.
- The single, redundant, attitude-heading reference system feedbacks were faded out because the attitude information only provides gravity compensation for pilot inputs and normal acceleration feedback. The lack of redundancy and the relatively small benefit did not warrant the risk of system failure at high-angle-of-attack conditions.
- Symmetric flaperon limit was reduced from 25° to 21°. Because high-gain roll rate feedback is required to prevent wing rock and the wing flaperons are shared symmetrically and asymmetrically, 4° of flaperon deflection were reserved for aileron

commands. The flaperons were commanded with differential commands that had priority. Otherwise, the ACC schedule would have commanded the wing flaperons on the symmetric limit at high angles of attack and resulted in a coupling of the wing rock and longitudinal control loop through the symmetric flaperon.

Roll and Yaw Control Law Design

In the lateral axes, the airplane was controlled with conventional ailerons and rudder. The ailerons had priority over symmetric flaperon deflections in the control laws. The control laws were designed in this manner because all roll control is provided by the ailerons while pitch control is provided by canards, strake flaps, and symmetric flaperons.

In the lateral–directional axes, the control laws were changed significantly for high angles of attack from the original low-angle-of-attack FCS. Figure 5 shows a full-state type feedback structure. The high-angle-of-attack changes, for the most part, simplified the control law structure flown on X-29A no. 1. The new control laws required many gains to be scheduled with angles of attack. Several were just faded to constants, while four command and feedback gains used three angle-of-attack breakpoints for table lookup. These three angle-of-attack breakpoints were the maximum allowed because of computer space limitations. Computer speed limitations required that a multirate gain lookup structure be incorporated.

Because the angle of attack was expected to change rapidly, the angle-of-attack portion of the gains was updated to 20 Hz. Mach number and altitude were updated to 2.5 Hz. The control law changes and reasons for them are as follows:

- The forward-loop integrator in the lateral axis was removed at high angles of attack. This removal eliminated a problem with the integrator saturating and causing a pro-spin flaperon command.
- The majority of lateral–directional feedbacks were eliminated. This feedback elimination left only high-gain, roll-rate-to-aileron feedback and washed-out stability axis yaw rate feedback to rudder paths. The high-gain roll damper was used to suppress the wing rock that developed near maximum lift. The washed-out stability axis yaw rate feedback helped control sideslip during maneuvers under high-angle-of-attack conditions.
- Pilot forward-loop gains were simplified, leaving only lateral-stick-to-aileron, lateral-stick-to-rudder, and rudder-pedal-to-rudder gains. The lateral stick gearing was changed from second-order nonlinear gearing to linear gearing at high angles of attack. A washout filter was used in parallel with the aileron-to-rudder interconnect (ARI) gain to provide additional initial rudder deflection in response to rudder command.
- Spin prevention logic was added. The logic commanded up to full rudder and aileron deflection if the yaw rate exceeded 30 deg/sec at an angle of attack $\geq 40°$ for upright spins or an angle of attack $\leq -25°$ for inverted spins. The pilot command gain was increased to allow the pilot sufficient authority to override any of these automatic inputs.

Pilot-Selectable Gain

To aid in research and allow for unexpected problems in flight testing, several changes were incorporated in the FCS. These changes included a pilot-selectable gain capability to allow two gains to be independently varied. These two gains could each have five values. This feature was used to evaluate, in flight, gain modifications to the control laws. Initially, the roll-rate-to-aileron gain, *K2*, and ARI gain, *K27*, were varied. Later, the lateral roll command gain, *K13*, and the *K27* were varied.

Concerns about severe wing rock led to a slow build-up in angle of attack using the pilot-selectable gain variations. The airplane roll response was heavily damped, and the pilot-selectable gain system was used to examine reductions in feedback gain. The response of the airplane was approximately 20 percent faster with the reduced roll-rate-to-aileron feedback gain than with the baseline gain. No objectionable wing rock developed because of the lower gain.

Pilot-selectable gain was also used to increase the roll performance of the X-29A airplane at high-angle-of-attack conditions.[17] The stability axis roll rates almost doubled in the 20° to 30° angle-of-attack region at 200 kn. This increased roll performance was accomplished using a 75 percent increase in the *K13* and an 80 percent increase in the *K27*. Increases in rates were possible throughout much of the high-angle-of-attack envelope but usually were not as dramatic as this example. Only small degradation occurred in the roll

coordination. Above this angle-of-attack region, uncommanded reversals occurred. These uncommanded reversals were caused by control surface saturation and a corresponding lack of coordination that manifested as increased sideslip.

The pilot-selectable gain concept proved to be a valuable research tool for testing simple control law changes before the full FCS changes were made. The ability to fly different FCS gains, back-to-back, on the same flight resulted in more accurate comparisons. This ability was especially important when the changes resulted in subtle flying qualities differences.

Flow Angle and Pitot-Static Measurement Systems

Accurate angle-of-attack measurement was very important because this measurement was a primary gain-scheduling parameter as well as a feedback to longitudinal and lateral–directional axes. Accurate airspeed information was also important to control conditional stability of the lateral and longitudinal axes at high angles of attack. Stability margins would be compromised if errors were large.

Two of the three angle-of-attack sensors were located on each side of the airplane and had a range limited to 35°. The location and range of these sensors were considered inadequate for testing, and two options were considered to solve the inadequacy. The first option was to mount two additional angle-of-attack vanes on the noseboom. This option was mechanized and flown on X-29A no. 1 for evaluation and was found to have excellent characteristics. The second option was to install NACA booms and angle-of-attack vanes on the wingtips. This option was not implemented because roll rate corrections for the large lateral offsets would have been required, and the flight control computers did not allow such corrections.

The modification to include two additional angle-of-attack vanes on the noseboom proved to be a good one. Only once during the high-angle-of-attack program did the three vanes not compare. This anomaly occurred during a recovery from a high-angle-of-attack test point. Figure 6 shows the time history of the recovery maneuver. The figure reflects that as sideslip exceeded 20°, the left rear angle-of-attack vane exceeded the sensor tolerance of 5° and was declared failed. This incident occurred during a recovery from 50° angle of attack. The airplane continued to operate on the two remaining sensors and was in no danger. The noseboom angle-of-attack measurements became less reliable above 35° angle of attack.

To obtain accurate measurement of airspeed at high-angle-of-attack conditions caused by local flow effects, three pitot probe locations were investigated. Belly probes were tested on a wind-tunnel model and were found to change the aerodynamics. Swivel probes could not be used on the noseboom because they were unable to be flight qualified for installation forward of engine inlets on a single-engine airplane. Side probes were expected to have poor characteristics at high angles of attack. Because an alternate location could not be found, the decision was made to use a single-string noseboom pitot-static probe at high angles of attack.

The high-angle-of-attack FCS had to be highly reliable. Three or more sensors were generally used to provide redundancy, but for impact pressure at high angles of attack, the FCS relied on a single noseboom probe with two independent sensors. For most of the high-angle-of-attack region, the side pitot-static probes performed as they had on the X-29A no. 1. Discrepancies were observed in the 7° to 12° angle-of-attack region. As angle of attack increased above 30°, measurement of impact pressure became less reliable. Above 45° true angle of attack (52° indicated), the side probes stalled, resulting in impact pressures of zero inches of mercury.

Simulation

Simulations were used extensively for evaluating the high-angle-of-attack control laws. A high-angle-of-attack aerodynamic database was obtained from many X-29A wind-tunnel tests. Wind-tunnel rotary balance data and forced oscillation data[18] were combined with spin-tunnel data to provide dynamic derivative estimates for inclusion in the simulation model. The aerodynamic model was valid for an angle-of-attack range from –50° to 90°, a sideslip range from –30° to 30°, and transonic speeds.[19, 20]

The simulations included a full, nonlinear, real-time piloted simulation consisting of hardware-in-the-loop, airplane-in-the-loop, and all FORTRAN implementations; batch-processed simulations; and linearized equations of motion simulations. Each of these simulations was essential to verification and validation of the control laws.

The piloted simulations were used for designing and testing the FCS as well as for training pilots during the high-angle-of-attack envelope expansion. The batch simulations were used to generate time history and frequency response comparisons to the hardware-in-the-loop results and to conduct an engineering analysis between high-angle-of-attack flights. The linear analysis results were compared with the nonlinear simulations and provided stability margin estimates for the rigid and aeroservoelastic models.

The aircraft-in-the-loop simulation was used during initial verification and validation of the high-angle-of-attack control system to accomplish the following:

- Verify the open-loop frequency response characteristics of sensor-to-control surface paths
- Verify the FCS-rigid body stability open-loop characteristics
- Verify that no closed-loop resonance exists on rigid jack supports
- Verify that maximum hydraulic demands of the high-gain FCS would be met by the normal and emergency airplane hydraulic systems
- Perform a complete end-to-end confidence check of the airplane systems

TEST AND PROCEDURES

Figure 7 shows the aircraft flight envelope. The original high-angle-of-attack control laws were designed for speeds up to Mach 0.6 and were later cleared to Mach 0.75. The envelope was intended to be expanded to Mach 0.9, but time constraints did not permit the necessary design, verification, and validation efforts.

Envelope Expansion

Maneuvers were developed to carefully expand the high-angle-of-attack envelope. These maneuvers were referred to as integrated test blocks (ITBs). Each ITB consisted of a series of test maneuvers at a given angle of attack. The ITBs were designed to obtain concurrent test data for several research engineering disciplines, including flight controls, aeroservoelastics, and aerodynamics.

Three ITBs were initially defined for the high-angle-of-attack envelope expansion with progressively more aggressive maneuvers in each. After five expansion flights, the ITBs were modified to obtain the necessary data more efficiently. The modified ITBs were as follows:

ITB 1	Pitch authority check Stabilized point Large input, 3-axis raps and pulses Half-throw aileron and rudder rolls Steady heading to 5° sideslip
ITB 2	Steady heading to 10° sideslip or full input Full input aileron and rudder rolls Full stick, 360° aileron roll

The high-angle-of-attack envelope expansion above 10° angle of attack began with ITB 1 flown from 1-*g* entries in 5° angle-of-attack increments. When necessary, intermediate trim points were flown at 2.5° increments. The ITB 2 for a given angle of attack was flown when the ITB 1 expansion had been completed for an angle of attack of 10° higher than the given angle of attack. Above 40° angle of attack, the entire ITB 1 was not performed but was replaced by a directional control check maneuver. The pilot stabilized the airplane at the target angle of attack for as long as possible before the forebody yawing exceeded limits. The 1-*g* expansion was completed to a target angle of attack of 55°, and the ITB 2 was performed to 45° angle of attack.

Windup turn or split-S entries were performed at 160, 200, 250, and 270 kn calibrated airspeed. For all airspeeds, the envelope was expanded above 10° angle of attack by the same process used for the 1-*g* expansion. The ITBs were essentially the same. During the initial accelerated expansion, the aft stick limit was reached at approximately 25° angle of attack. Further expansion was not possible without sacrificing airspeed, so the pitch stick authority was increased to allow the accelerated expansion to continue.

Piloted Simulation and Updates

Extensive use was made of piloted simulation during the high-angle-of-attack expansion. Before each flight, the pilot used the simulator to become familiar with the test points and the predicted behavior of the aircraft. Changes were made to the test maneuvers as required. Engineers monitored strip charts at the simulator to watch for any unusual aircraft behavior and set flight limits accordingly. This monitoring also allowed the engineers to become familiar with the anticipated aircraft behavior. The strip charts were often used in the

control room to verify the simulation and the test team's understanding of the dynamics of the aircraft.

The piloted simulation was updated based on the flight data. This update process consisted of several steps. The first step involved analyzing the data to separate force and moment contributions caused by aerodynamics, inertias, kinematics, and gyroscopics. From these data, initial surface derivative estimates were made. The second step involved using these estimates to run the parameter estimation program, pEst,[21] to refine estimates of the aircraft aerodynamic derivatives for small rates and sideslips. The third step involved using a batch simulation to verify estimates for large amplitude maneuvers. In this step, derivatives were adjusted in the simulation until the desired degree of accuracy in matching the aircraft and simulation responses was achieved. No rotary derivatives were updated. Once the estimates were judged to be satisfactory, a parameter variation study was conducted to help define real-time operating limits. The data were also extrapolated to the next flight condition.

A more detailed explanation of the updating method has previously been described.[4, 22] The updates were easily added or deleted without altering the baseline aerodynamic data. This technique of updating the simulation was a powerful tool during the envelope clearance and postflight analysis. The simulator was always able to keep the response of the aircraft bounded even though it was unreliable for accurately predicting the flying qualities of the vehicle. When the aircraft did not behave as predicted, the cause could quickly be determined by using the parameter variation study that had been conducted before each flight.

The challenge for the test team was to perform the sensitivity study so that any undesirable aircraft responses were bounded by the simulation. The flight data would then indicate how to modify the simulation. Using the simulation in this way was invaluable for reducing the risk during the high-angle-of-attack envelope expansion.

RESULTS AND DISCUSSION

This section discusses the flight test results and is divided into three subsections. The first subsection documents the observed characteristics and compares them, where appropriate, with the preflight predictions. The second subsection addresses the flying qualities research accomplished. The third subsection discusses a structural interaction with the FCS.

Flight Characteristics and Correlation With Preflight Predictions

This subsection documents the observed characteristics of the X-29A airplane at high angles of attack. Where appropriate, the flight test results are compared with preflight predictions. The preflight predictions were generated from both wind-tunnel and dynamically scaled drop-model tests. The drop model for the X-29A airplane[23] was an unpowered, 22 percent–scaled geometric replica that was dropped from a helicopter. The model was dynamically scaled to the weight, center of gravity, and inertia of the full-scale vehicle.

Wing Rock and Lateral Control Power

Much attention was given to the predicted wing rock characteristics during design and verification of the flight control laws. These predictions were based upon wind-tunnel estimates[24, 25] and were supported by drop-model flight tests. The unaugmented drop-model roll departed at 32° angle of attack. A roll damper was added to the FCS to prevent the departure. A gain of 0.88 deg/(deg/sec) reduced the wing rock magnitudes over the unaugmented model (fig. 8).[23] However, roll rates as high as 30 deg/sec existed for angles of attack below 40°. Rates reported for subscale tests are equivalent full-scale values.

Above 40° angle of attack, roll rates approached 150 deg/sec. Large noseup pitching moments were generated as a result of the large oscillations by a combination of inertial and aerodynamic coupling. A gain of 2.0 deg/(deg/sec) was finally used in the drop model to suppress the high roll rates in the 40° angle-of-attack region. Additional details about the tests and their results have previously been given.[23, 24]

These results, along with the results from ground-based testing, were used to develop the aerodynamic models for the control law design simulation used at NASA Dryden. The simulation at NASA Dryden predicted that wing rock would occur between 30° and 45° angle of attack and at approximately 60°. Wing rock magnitude was predicted to be composed of ±30 deg/sec of roll rate, ±10° to 15° of bank angle, and ±10° of sideslip. Preflight predictions were that 35°

angle of attack would be the maximum attainable before wing rock would dominate the flight characteristics and prevent additional expansion.

For the full-scale airplane, buffet began at approximately 12° to 15° angle of attack. The buffet was light, becoming moderate at approximately 20° angle of attack. Above 20° angle of attack, the buffet was once again light.

Wing rock began at approximately 16° angle of attack and was characterized by bank-angle changes of less than 5° at 0.9 Hz. Because of the randomness of the frequency and magnitude, the pilots characterized this motion as wing drop rather than wing rock. Because of the small magnitude of the motion, the wing rock did not detract from the handling of the aircraft in the 16° to 20° angle-of-attack region. In fact, while maneuvering, the pilots commented that they were unaware of its presence.

Figure 9 is a time history of the wing drop characteristic. At 40° angle of attack, the wing rock had increased to a ±14 deg/sec roll rate at 0.4 Hz. This rate was considerably less than the ±30 deg/sec roll rate predicted for that angle-of-attack region. In fact, the wing rock was absent in the presence of 1° to 2° sideslip. Figure 10 shows a time history of the wing rock experienced near 40° angle of attack. Figure 11 shows the magnitude of the bank angle oscillation as a function of angle of attack during wing rock.

The reduced wing rock is attributed to the higher-than-predicted (less unstable) roll damping and increased aileron control power. Preflight predictions for roll rate in the 30° angle-of-attack region were 10 to 15 deg/sec. Actual roll rates were 40 deg/sec, supporting the belief that aileron effectiveness had been underpredicted. As a result, however, some of the FCS gains were inappropriate. The pilot-selectable gain feature of the FCS proved to be valuable in assessing what more appropriate gains might be. Analysis determined that roll-rate-to-aileron gain could be reduced to a maximum of 0.48 deg/(deg/sec) without significantly increasing wing rock. Lowering this gain resulted in approximately 20 percent faster-than-predicted roll rates.

Rudder power was predicted to begin decreasing at approximately 20° angle of attack.[4] Testing showed that rudder power between 20° and 40° angle of attack was larger than predicted.[22] Above 40° angle of attack, rudder effectiveness decreased to predicted values. In general, roll coordination was better than expected. Pilot comments were favorable relative to other aircraft. The airplane showed no differences between rolling left and rolling right. The better-than-predicted rudder effectiveness above 20° is believed responsible for the good lateral–directional characteristics above 20° angle of attack. As a result of the reduced magnitude of the wing rock and better-than-expected roll coordination, all axis maneuvering was performed through 45° angle of attack.

Aileron control power was greater than predicted for large aileron deflections, but the opposite was true for small deflections. During the aerodynamic update process, a breakpoint was added at 6° of deflection. This inclusion of a breakpoint had an interesting effect when linear analysis was conducted. If the linearization was performed over a small step size (for example, ±1°), the lesser effectiveness was used. In the case of the X-29A airplane at 30° angle of attack, using the small step size resulted in the open-loop poles being unstable. If the step size of the linearization for the aileron was increased so that the greater effectiveness was used (in this case, ±8°), the open-loop poles became stable. Figure 12 shows the pole locations. The linearization was performed using the updated aerodynamic data set.

Having an unstable system for small deflections and a stable system for large deflections leads to a bounded limit cycle. Small aileron deflections resulted in an unstable dutch roll mode, allowing wing rock to occur. During maneuvering, larger aileron deflections were applied, resulting in a stable dutch roll mode and eliminating the wing rock. This result is consistent with the pilots' comments that the wing rock and drop were unnoticeable while maneuvering.

This event illustrates the importance of obtaining accurate estimates of control effectiveness over reasonable control deflection ranges. For the X-29A airplane, the original aileron effectiveness was determined in the wind tunnel from ±10° deflections, resulting in predictions of larger effectiveness at lower deflections than existed. Caution must also be used when conducting linear analysis to ensure the step size of the linearization is appropriate.

Pitching Moment Characteristics

The pilots consistently found the pitch rate capability of the X-29A airplane inadequate. Figure 13 shows the predicted maximum noseup and nosedown pitch rates as a function of Mach number. Three low-speed points from these data were flown. Figure 14 shows the

comparison of the flight data with simulation predictions made using the baseline aerodynamic model. The close agreement between the data and the predictions leads to high confidence in the predicted maximum pitch rates for this angle-of-attack range. The pitch rates in figure 13 are highly dependent upon the stick inputs. For the simulation runs, two types of inputs were made: a full-aft stick step and a doublet. The doublet input consisted of full-aft stick followed by full-forward stick timed to try to force the control surfaces to maximum rates.

Figure 13 clearly shows that the X-29A aircraft would require rates approximately 50 percent higher to be comparable with the F-18 aircraft at low-speed conditions. Examination of peak actuator rates shown in figure 15 reveals that the X-29A airplane was using nearly all of its capability with the current gains. Increases in the canard actuator rates commensurate with the increases in pitch rate would be required to achieve higher pitch rates. Similar increases in the flaperon and strake flaps might also be required, but these surfaces are less significant in the X-29A pitch response. In fact, flight experience has shown no degradation with the rate limiting.

Other flight data showed that the simulation was conservative and that the actuators showed higher rate capability than that modeled in the simulation. The FCS did not use software rate limiters. All control surfaces were allowed to move at the hardware rate limits. The asymmetric behavior of the strake rate is believed to be caused by hinge moments that opposed the noseup behavior and helped during the nosedown command.

The simulation showed that most of the actuator rate was used controlling the unstable airplane response (fig. 14). Close examination shows that for the full-aft stick input, the initial response is trailing-edge-down for the canard and trailing-edge-up for the flaperon and strake flap. As is typical for an unstable pitch response, the surfaces then move quickly in the opposite direction to unload and control the unstable response. This subsequent movement is typically much larger than the initial motion and more demanding of the actuator rates, especially at low dynamic pressure where large control surface motion is required.

Figure 16 shows the lower-than-predicted pitch control capability as the difference between the solid lines and flight data points. As a result of the lower-than-predicted pitching moment coefficient, C_m, nosedown capability was carefully monitored during the expansion and was the first item checked at each new flight condition. Minimum nosedown aerodynamic pitching moment for the X-29A airplane was predicted to be nearly twice that recommended for a class IV fighter.[26] The actual nosedown capability was only slightly better than the guideline.

Despite this, the X-29A airplane experienced nosedown recovery hangup because of inertial coupling from yaw asymmetries. During several recoveries, pitch rate was momentarily reduced to 0 deg/sec. Based on the data available where all three pitch surfaces were saturated and the aircraft continued to pitch down, it is believed that the aircraft achieved neutral or slightly positive static stability at high angles of attack. Angle-of-attack expansion, however, was limited above 60° because of the limited nosedown moment capability. Also, above 50° angle of attack, more stringent center-of-gravity limits were imposed. Despite these restrictions, pitch pointing was demonstrated to 67° angle of attack.

One problem encountered during envelope expansion was limited pitch authority at 25° angle of attack during 160- and 200-kn entries. The original FCS design allowed the pilot to command 5.4-g increments at high speed and 1.0-g increments at low speed. To counter the limited pitch authority problem, the incremental g was increased to 7.0 g at high speed and 2.0 g at low speed. These increases greatly improved the situation, but the pilot still had insufficient control authority at high-speed, high-angle-of-attack points above 200 kn. Another gain change would have been difficult because such a change would affect the pitch sensitivity. The X-29A pilots noted that, during 1-g flight at angles of attack of 35° and 40°, an increased sensitivity of the longitudinal control was evident, but compensation for this sensitivity was easily accomplished. Table 3 provides stick displacement and force data.

Yaw Asymmetries

Preflight predictions anticipated a slow yaw divergence at approximately 60° angle of attack. In flight, the characteristics were quite good up to 40° angle of attack. Above 40°, however, several asymmetries were noticed. Starting at approximately 43° angle of attack, a nose-right asymmetry (C_{n_o} = 0.02) developed. This asymmetry could be countered by applying the stick and rudder in advance of the yaw. At 47° angle of attack, a left yaw developed of the same magnitude as

the yaw to the right. The left yaw could not be completely halted with stick and rudder application, but sufficient pitch and roll control was maintained.

Above 50° angle of attack, the direction of the asymmetry was difficult to determine. Rudder control power was essentially nonexistent above 45° angle of attack. Aileron control power above 40° angle of attack was positive but weak. The aircraft exhibited a graceful degradation of controllability. The pilots were easily able to recognize this degradation and compensate for it by simply pushing forward on the stick to decrease the angle of attack. This characteristic allowed guest pilots to fly the aircraft to the limits of the cleared envelope on their first flight after a limited amount of simulation time.

Flying Qualities Research

Every control system designer faces the challenge of providing sufficient control without compromising basic system stability. Using aerodynamic models developed through extensive wind-tunnel testing, an acceptable FCS was developed for the X-29A airplane. However, differences between the aerodynamic predictions and the airplane's flight characteristics allowed for significant improvement in maneuverability without compromising stability margins. The objective of the handling qualities research was to examine the tradeoff between maneuverability and controllability in the high-angle-of-attack control laws of the X-29A airplane.

Early results from the envelope expansion phase showed room for improvement in the 15° to 30° angle-of-attack region. The improvements were made using the pilot-selectable gain capability. This test mode allowed back-to-back comparisons among several FCS gain configurations that often showed subtle differences in flight characteristics. Appendix A shows the linearized aerodynamic and FCS characteristics for 15°, 25°, and 30° angles of attack at 200 kn. Appendix B is a summary of pilot comments.

Both qualitative and quantitative maneuvers were used. Qualitative maneuvers consisted of basic fighter maneuvers (BFMs) and were used to determine which set of gains were preferred by the pilots.[27] The BFMs were viewed as more representative of the way the aircraft might be flown in an air combat engagement. The quantitative maneuvers were used to identify response characteristic trends between the different gain combinations. The gains varied were the roll command and the ARI gains. Figure 17 highlights these gains. The gains were varied as follows:

Group	Roll command gain, percent	Aileron-to-rudder gain, percent
A	100	100
B	150	140
C	175	180

Three BFM conditions were tested. The BFMs included one-circle fight, rolling scissors, and lateral gross acquisition maneuvers.[28] These maneuvers have previously been explained in detail.[27] The quantitative maneuver was a 180° bank angle capture starting at a 90° bank angle and rolling over the top. This maneuver was selected because earlier work determined that maximum roll rates would be reached during a roll through 180° of bank angle.

The earlier work also provided information on agility, defined here as the time to roll through 45° and 90°, and on time to roll and capture 180°. A matrix of airspeeds (160, 200, and 250 kn) and angles of attack (1 *g*; 15°, 25°, and 30°) was used for the quantitative maneuvers (table 4). Because of limited flight time, only the 200-kn column and 25° angle-of-attack row of the matrix were successfully completed. Two maneuvers per gain setting at each condition were selected for analyses. Each maneuver had to satisfy angle-of-attack, airspeed, and altitude limits in order for it to be used. The requirements were relaxed for the 250-kn points because at high angles of attack, airspeed could not be maintained during the roll.

The pilots were expected to prefer the gain set with the highest roll command, group C. In figure 18, the quantitative data show group-C gains had slightly higher stability axis roll rates than group-B gains had, as expected. Figure 19 shows group-C gains also had correspondingly higher body axis yaw rates than were seen using group B-gains. To determine if the amount of body axis yaw rate generated to coordinate the rolls for group C was excessive, the amount of body axis yaw rate required to coordinate the stability axis roll rate in figure 18 is plotted in figure 19.

For groups B and C, the amount of yaw rate was adequate to provide the required coordination.

Coordination was examined in detail because it was believed that coordination would have a significant impact on the pilots' comments. Emphasis was placed on groups B and C because the roll rate capability of group A was recognized as inadequate for the task. The roll command gain was too low.

Figure 20 shows a typical 180° bank angle capture. This particular maneuver used group-B gains. At approximately 2 sec, the pilot commanded full-right stick to roll to the opposite 90°. As the aileron responded, roll rate and sideslip began to build to positive values. Roll rate built to approximately 30 deg/sec before the angle of sideslip reached a positive value. Once sideslip became positive at approximately 2.5 sec, roll rate began to decrease. In this case, sideslip built to approximately 2.0° as roll rate decreased to approximately 15 deg/sec.

This reduction in roll rate is caused by the adverse sideslip and the large positive dihedral.[22] Adverse sideslip is defined as sideslip where roll rate and sideslip have the same signs. Rolling with adverse sideslip tends to reduce angle of attack.[29] As roll rate decreases, sideslip decreases and eventually becomes negative, resulting in proverse sideslip accelerating the roll to almost 50 deg/sec. During this period, the pilot maintained full-lateral stick.

The trends discussed in regard to figure 20 are the same for group-B and group-C maneuvers. Using group-C gains, slightly larger sideslips developed than had with group-B gains (fig. 21). In 1-g maneuvering above 30° angle of attack, roll hesitation and some reversals were encountered when using roll command gains higher than baseline gains. As airspeed increased, the hesitation and reversals subsided. The hesitation and reversals were caused by rudder position-limiting permitting adverse sideslip to build.

Figure 21 shows sideslip as a function of angle of attack for rolls at various angles of attack. These data were tabulated as though the roll were to the left, when in actuality data from both left and right rolls were used. Even though rudder effectiveness was higher than expected, it was insufficient to generate the required yawing moment to coordinate the rolls at high angles of attack and roll rates (fig. 22). The rudder reaches its position limit at 25° angle of attack for group-C gains and at 30° angle of attack for group-B gains. The rudder does not reach its position limit for the baseline gains.

Because the rudder was consistently position-limiting for group-C gains, an attempt was made to determine what effect this position-limiting might have on the sideslip buildup. For this investigation, position-limiting of the ailerons was also considered. Figure 23 presents maximum absolute value for the aileron positions at the 200-kn test points. All of the instances of position-limiting occurred during the capture part of the maneuver.

Figure 24 shows a time history for group C at a 200-kn, 25° angle of attack where both rudder and aileron position-limiting occurred. The rudder position-limited for approximately 0.4 sec during the roll initiation when an attempt to generate coordinating yaw rate was made. Sideslip reached only 2° adverse during this portion of the maneuver. This magnitude is the same magnitude of sideslip that developed during the group-B maneuver at 30° angle of attack (fig. 20). In that case, the rudder position-limited for 0.2 sec during the roll initiation. Interestingly, the rate of change of sideslip is greater for the group-B gains than for group-C gains.

As figure 24 shows, the largest sideslip excursions occurred when the ailerons and rudder were position-limited. This condition only occurred when the pilot attempted to stop the roll rate and capture position. A significant increase in the rate of sideslip change does not occur because the surfaces reached their position limits. Therefore, it was concluded that position-limiting did not significantly detract from aircraft coordination.

The reason a significant change in sideslip did not result is that both the rudder and aileron position-limited. At the beginning of the maneuver (approximately 4.5 sec) only the rudder position-limited. The change of sideslip rate changed sign, although sideslip did not reach a large value. This change of sign indicates the need to limit roll capability when the rudder position-limits in order to maintain roll coordination.

Rate limiting was also investigated as a potential cause of coordination problems. In all cases examined, only a very small percentage exhibited rate limiting. When rate limiting did occur, it did not last longer than 0.2 sec. Therefore, it was concluded that rate limiting had no effect on aircraft coordination during these maneuvers.

To determine the preferred combination of gains, pilot comments were studied. Comments were recorded during flights, postflight debriefings, and discussions with the pilots after testing was concluded. Appendix B contains a compilation of pilot comments. Emphasis was placed on their comments regarding the BFMs (not the 180° bank angle captures) because it was believed that these tasks represented more realistic maneuvering of the aircraft.

Based on comments recorded during the flights and postflight debriefings, no clear preference existed between the two highest roll command gains, groups B and C. A desire for even higher roll rates, however, was expressed. Independent interviews with the project pilots after test phase completion revealed the pilots' preference for group-B gains (the next-to-highest roll command gain). The consensus seemed to be that groups B and C exhibited the same amount of roll rate but that group C had a noticeable amount of yaw rate making it less desirable. Note that the majority of the rolling during the BFMs occurred between 160 and 180 kn and at 25° angle of attack. Some rolls were initiated above 200 kn, but as angle of attack was maintained, the airspeed bled down to below 200 kn. One interesting trend was noticed in the BFMs. Of the rolls performed at airspeeds in excess of 200 kn, the majority were for group-C gains.

The problem for the control system designer is that the pilots preferred additional roll capability but objected to the amount of yaw rate present with the group-C gains. To provide roll rates higher than those group C provided, greater yaw rates would be required to coordinate the aircraft. The high yaw rates were precisely what was disliked about group-C gains. In response to pilot comments about the yaw rate associated with group-C gains, an investigation of lateral acceleration at the cockpit station was made.

The comments regarding yaw rate were believed to actually be complaints regarding the lateral acceleration at the cockpit station. Because lateral acceleration could not be measured at the cockpit station, the measured acceleration near the aircraft center of gravity was used and corrected to the pilot station. The noise level of the pitch, roll, and yaw accelerometers was too high in the angle-of-attack range of interest, so the rate sensor information was differentiated to compute accelerations. These signals were also noisy and thus were heavily filtered. The filtering allowed for peaks and trends to be more easily identified; however, it corrupted the data to the extent that quantitative assessment of the acceleration was not possible. All signals were filtered in the same way to avoid time skews. These data should only be used to identify trends.

Figure 25 shows an example of the filtering effects. The top trace represents cockpit acceleration with limited filtering. The bottom trace is the same data after additional filters were applied. Note the reduction in magnitude. The bottom trace was used to identify the trends in these data.

The lateral acceleration analysis was conducted by computing the lateral acceleration at the pilot station and the individual components of that acceleration. Peak accelerations were examined for the entire maneuver and for just the roll initiation. Figure 26 shows the data for the 200-kn points at roll initiation. From these data, no clear trend with gain set is evident.

Figure 27 shows the peak lateral acceleration at the cockpit for the 200-kn maneuvers. Below 25° angle of attack, no consistent trend was evident. At 30° angle of attack, however, a clear trend between the groups was apparent. In general, these peaks in lateral acceleration occurred during the capture task. Without more evidence of lateral accelerations consistently larger with group-C gains than with group-B or baseline gains, it was concluded that the pilots were not confusing lateral acceleration with yaw rate cues.

During the guest pilot portion of the program, a pilot with considerable high-angle-of-attack experience had the opportunity to fly group B-and group-C gains. The resulting comments were consistent with engineering expectations. Specifically, the pilot commented that group C provided greater roll rates and the levels of yaw rate were not discomforting. During the earlier high-angle-of-attack program, the pilot had the opportunity to regularly experience high levels of yaw rate. A certain amount of "conditioning" is believed to be required before a pilot becomes comfortable with these, and higher, yaw rates. Experience during this earlier high-angle-of-attack program supports this belief.[30, 31] Pilots with experience flying maneuvers at high angles of attack that generated large amounts of yaw rate had become conditioned to it. Guest pilots evaluating the system who were not accustomed to those levels of yaw rate were uncomfortable with the system.

The logical next step in this work will be to understand how to deal with the yaw rate during a tracking task. A metric for high-angle-of-attack flying qualities at 30° angle of attack has already been proposed[32] and examined using the available X-29A data. The metric design criterion is based on the roll mode time constant and wind axis roll rate. The criterion was developed using piloted simulations with a perfectly coordinated (0° sideslip) control system. The task was to aggressively acquire the target aircraft within the allowed 65-mil lateral error with no overshoot and within the desired time. Ratings for the X-29A airplane were obtained from a lateral gross acquisition task modeled after this task. Because the X-29A airplane did not have a gun

sight, acquisition to a specific accuracy was not possible. The task for the X-29A airplane consisted of positioning a target F-18 aircraft 1000 ft above and 1500 ft ahead of the X-29A airplane at an altitude of 25,000 ft, traveling at 180 kn calibrated airspeed. The target aircraft then rolled 90° and pulled to 30° angle of attack when signaled by the X-29A pilot. Next, the X-29A pilot selected maximum power, pulled to 30° angle of attack, and rolled about the velocity vector to grossly acquire the target aircraft.

The X-29A airplane could not perfectly coordinate stability axis rolls. Figure 21 shows that sideslips were generally kept within a 5° band of 0°. Also, the roll mode time constant was plotted against stability axis roll rate instead of wind axis roll rate. The difference between the two rates is the contribution of sideslip. Because sideslips were small, the difference between the stability axis and wind axis rates lies within the accuracy of the measurement.

The roll mode time constant was estimated by fitting a first-order delay of the pilot lateral stick to the flight data. A pure time delay and a vertical offset were also included. The wing rock that was present made fitting stability axis roll rate difficult. The wing rock superimposed on the roll gave the impression of much faster time constants in most cases. To avoid this problem, body axis yaw rate was fit instead. Because the wing rock experienced by the X-29A airplane was almost pure body axis, the yaw rate did not have the problem with the wing rock that the stability axis roll rate did.

The only difference between a fit of body axis yaw rate and stability axis roll rate for this simple model was the gain. Therefore, the time constant, time delay, and offset could be obtained using body axis yaw rate. A simple gain change was all that would be required to then match stability axis roll rate. Note that this approach works because no delay in the yaw rate response exists. This lack of delay resulted from the interconnect. If a delay in the yaw rate response had occurred, then this approach would not have been appropriate. Therefore, the application of this analysis approach is limited.

Figure 28 shows results from this approach. This figure shows the match for body axis yaw and stability axis roll rates. Only the gain is changed between the two fits. This approach results in significantly slower roll mode time constants than have been previously published.[27, 33] This approach better represents the X-29A capability because it avoids the corruption of the roll rate by the wing rock.

Roll mode time constant data for the X-29A airplane were collected at 160 and 200 kn at 30° angle of attack from the 180° bank-angle captures. Figure 29 shows these data. These airspeeds represent the region of airspeeds flown during the BFM and lateral gross acquisition maneuvers and for which the ratings were obtained. The quantitative maneuvers were used to obtain time constants and roll rates because the BFM data did not support that kind of analysis. Conditions were matched as closely as possible between the maneuvers.

Figure 30 shows the group-B and -C regions and the proposed criterion boundaries.[32] Both regions were given Cooper-Harper ratings[34] of 4 or 5 and overall assessments between level 1 and level 2 by the pilots.[27, 33] Pilot comments such as "like lots of roll power," "roll rate is fine," "put stick in, comes across very carefree," and "very impressed with roll rate," imply that the proposed criterion is overly restrictive.

Structural Dynamics Interaction With the Flight Control System

At high angles of attack, vertical fin buffeting caused by forebody vortex interaction was encountered. The FCS was strongly affected through the excitation of several structural modes that were seen on the roll rate gyroscope signal.[35] The buffet intensity was as high as 110 *g* peak-to-peak at the tip of the vertical fin. The buffet caused fatigue concerns for the vertical stabilizer.

The vertical fin vibration excited the roll rate gyroscope signal and, through high-gain feedback, caused the flaperon actuators to attempt to track this high-frequency signal. Flight tests showed an unexpected hydraulic system problem resulted from this flaperon command. During a 360° full-stick aileron roll, the left outboard flaperon hydraulic logic indicator showed a failure of the control logic for this actuator.

The most probable explanation for this failure is that a flow restriction existed in the hydraulic lines that drive the left outboard flap, and this restriction showed up when large, high-frequency demands were placed on the actuator. Postflight analysis also showed that the measured left outboard flap rates were approximately 7 to 8 deg/sec lower than rates for the right outboard flaperon. Because the roll rate gyroscope signal did not originally use any structural notch filters, the vertical fin first-bending (15.8 Hz), wing bending

antisymmetric (13.2 Hz), and fuselage lateral bending (11.1 Hz) structural modes showed up in the commands to the ailerons.

Figure 31 shows the response of the roll rate gyroscope signal. The figure shows that most of the vertical tail buffet is transferred to the roll rate gyroscope signal through the vertical fin first-bending mode. Analyses of the flight data showed that the g level increased proportionately with dynamic pressure. Notch filters and a software gain reduction on roll rate feedback were used as the long-term FCS solution to the problem. Before these changes, 50 percent of the maneuvers in the region where failures occurred indicated left outboard flap hydraulic logic failures. After the changes were made, these failure conditions rarely occurred, and entry conditions with buffet levels even more severe than previous ones were encountered without incident.

SUMMARY OF RESULTS

The X-29A forward-swept-wing aircraft was flight tested at high angles of attack at the NASA Dryden Flight Research Center. A classic control law design utilizing a combination of pitch rate and angle of attack for longitudinal control was developed. The lateral and directional axes were changed significantly from the low-angle-of-attack flight control system. A pilot-selectable gain was included in the design which was utilized in flying qualities assessment and control law gain changes at high angles of attack.

Preflight predictions were that wing rock would limit the useful angle-of-attack range to 35°. The actual wing rock magnitude was less than one-half of what was predicted, and that amount was attenuated whenever sideslip was present. This actuality allowed the roll-rate-to-aileron gain to be reduced to one-fourth of the value suggested from the preflight data and subscale model tests. The cleared envelope was extended to 67° angle of attack at 1 g and Mach 0.75 at low angle of attack. All axis maneuvering was cleared to 45° angle of attack at 1 g. The reduced wing rock was believed to have resulted from higher roll damping and increased aileron control power for large aileron deflections.

Roll coordination was better than expected, and rudder effectiveness was higher than predicted, between 20° and 40° angle of attack. Aileron power was larger than predicted for deflections greater than 6° but smaller than predicted for deflections less than 6°. Because of the difference in effectiveness, a bounded limit cycle existed. Yaw asymmetries developed above 40° angle of attack. Diminished aileron and rudder power was not sufficient to overpower these asymmetries.

Predictions of noseup and nosedown pitch capabilities matched flight results up through 40° angle of attack. Differences in noseup pitching moment above 40° angle of attack required more canard deflection than predicted. Large yaw asymmetries led to several pitch hangups during maneuvers above 50° angle of attack at aft center-of-gravity conditions even though the X-29A airplane met recommended nosedown control power guidelines. Canard position limits prevented simple modifications to provide additional nosedown authority. The X-29A noseup and nosedown maximum pitch rates were limited by the high level of static instability and control surface rate limits. At low airspeeds, new actuators with a minimum of a 50-percent higher rate would have been required to achieve rates comparable to those of the F-18 airplane.

Wind-tunnel and drop-model predictions of a poor high-angle-of-attack aircraft were not validated by the flight test program. Flight test showed the X-29A airplane to be a good aircraft up to 40° angle of attack. The X-29A airplane has provided the background for fine-tuning our ground-based predictive techniques for high-angle-of-attack aircraft.

The instability did not prevent the aircraft from operating at high angles of attack, but it did limit performance. Because the aircraft did not become as statically stable as predicted at higher angles of attack, the pitch authority was required to control the instability rather than improve pitch performance. The full-span flaperons provided good roll control. Roll control was not compromised by the fact that the wing did not use leading-edge devices.

The pilot-selectable gain system was used extensively to examine tradeoffs in airplane stability and maneuverability. Basic fighter maneuvers were flown to provide qualitative evaluation. Bank angle captures of 180° were flown between 160 and 200 kn and 1 g through 30° angle of attack for quantitative data analysis. Roll and yaw gains were increased to improve roll performance. A gain increase that used the maximum rudder authority produced the best pilot comments. Further increasing the gain produced rudder saturation that degraded the turn coordination. This configuration was not preferred by the pilots, even though it had more roll performance.

Limited pilot ratings from the basic fighter maneuvers were used to evaluate the proposed 30° angle-of-attack criterion. Roll mode time constant was estimated by fitting a first-order system to time histories of the stability axis roll rate. The proposed criterion does not predict the X-29A ratings adequately.

Dryden Flight Research Center
National Aeronautics and Space Administration
Edwards, California, December 7, 1994

APPENDIX A

LINEAR MODELS

Figure A-1 shows the linear matrices. The linear matrices were obtained from the updated aerodynamic data set for control surface step sizes of 8°.

The following are constant data for the linear models:

S	= 185.0000	I_{xx}	= 4547.0608
b	= 27.2000	I_{yy}	= 51887.9466
$\bar{c}$	= 7.2160	I_{zz}	= 57063.4365
Empty wt	= 14524.0000	I_{xz}	= 2558.9667
Fuel wt	= 1052.0000	XCG	= 450.70
Total wt	= 15576.000	YCG	= 0.00
		ZCG	= 64.62

Figures A-2 and A-3 show the block diagrams for the longitudinal and lateral–directional control systems.

Table A-1 provides the transfer functions for the block diagrams given in figures A-2 and A-3.

The following are lateral–directional gains as a function of angle of attack. Refer to figure 5 for definitions.

Gain	α		
	15°	25°	30°
K2	–1.79924	–3.67639	–4.62445
K17	0.758387	0.845741	0.889859
K27	–0.0357338	–0.0510411	–0.0587721

APPENDIX B

PILOT COMMENTS

These pilot comments were recorded during the flight or in the postflight debriefing. Speeds are given in knots calibrated airspeed. Where a word or words were undecipherable, [???] has been used.

Flight 82, Pilot B

One-circle fight with an F-18 airplane at 25,000 ft, 250 kn, group B—Stick aft stop. The F-18 started on an advantage; started 1000 ft behind. Started there, kept the advantage, and did not increase it. Does roll better.

One-circle fight with an F-18 airplane at 25,000 ft, 250 kn, group C—Group B has much better rolling. Rolling compensated for the lack of nose authority. Roll felt better at group B.

General comments during return to base—Like group B; lot of roll power. Still stick-limited. The angle of attack got high. Group C, not too easy to see much difference. Group B, quality better. Get up against aft stick stop with other two [with baseline and group C].

Flight 90, Pilot B

90/90 roll capture at 20,000 ft, 200 kn, 30° angle of attack, group B; 0/60/0 rolls at 20,000 ft, 200 kn, 15° angle of attack, group C; One-circle fight at 25,000 ft, 250 kn, 15° angle of attack, group B—Group C is not as good as group B at 30° angle of attack [BFM]. The X-29A roll rate gave it lateral agility advantage over the F-18; took advantage of this by keeping aircraft loaded up during BFM. Roll capture tasks are difficult with the higher roll rates [especially 0 to 90]. Overshoots were common; anticipation is required. Stick was sensitive. Looking in cockpit [Attitude Direction Indicator] rather than outside to capture bank was unnatural. Bank angle is difficult to define at high angles of attack. This is a poor closed-loop task. Little correlation between roll capture task [roll rate too high] and BFM [roll capability good].

Flight 91, Pilot A

90/90 roll capture at 20,000 ft, 200 kn, 30° angle of attack, group B; 90/0 roll capture at 20,000 ft, 200 kn, 25° angle of attack, group C; 360 roll transient at 20,000 ft, 200 kn, 30° angle of attack, group B

Group B—Slight roll hesitation during roll. Not a ratchet. Lateral acceleration felt good. Roll rate may be too high for this task. Aircraft is less powered than simulation [???] more airspeed in flight.

Group C—Quite a ride. Stick is very sensitive around neutral and requires lots of anticipation. Holding angle of attack and capturing roll angle is very difficult.

One-circle fight with an F-18 airplane at 25,000 ft, 250 kn, group B—At one time, would have liked more pitch authority at a 30° angle of attack to pull it around [30° angle of attack limit]. Noticed an improved roll rate when rolling over top. Rolled over top to get into trail gun position.

Flights 94 and 95, Pilot C

90/90 roll captures at 20,000 ft, 200 kn, 1 *g*, 15° angle of attack, groups A, B, and C—Tried to do them as quickly as possible; needed to lead arrestment. Impressive roll rates. Noticeable unload at 15° angle-of-attack rolls. No noticeable lateral accelerations. Did not notice difference between groups B and C but was having trouble with the task.

Lateral gross acquisition at 25,000 ft, 180 kn, 30° angle of attacks, groups A, B, and C— Poor pitch acceleration; sluggish. Versus an F-18 is good. Pitch acceleration is what pilot goes for. Pitch stick force and displacement are too large. Roll differences between groups A and B. Group B roll acceleration is surprising—one try, target right there after I rolled. Group B at a 30° angle of attack—noticed roll ratcheting. Sometimes the target didn't keep the X-29A at 8 or 4 o'clock. Timing has to be worked out with target.

Flight 96, Pilot A

90/90 roll capture at 20,000 ft, 200 kn, 1 *g*, 15°, 25°, and 30° angle of attack, group B

1 *g*—Roll rate onset and maximum roll rate are very nice. Gross acquisition—may be interesting to look at coupling.

15° angle of attack—For maneuvering, not good for capture task.

25°, 30° angle of attack—Roll rate slower, still adequate for maneuvering. Good for capture task.

25° angle of attack—Roll rate and acceleration crisp. As lateral stick command gain decreased, capture task was easier.

Cooper-Harper Ratings—1 *g:* 4–5; 15° angle of attack: 5; 25° angle of attack: 3; 30° angle of attack: couldn't get first try, second try overshot 30, couldn't get 90° roll angle at start.

General Comments—Faster roll rate onset the better. I question the applicability of this task as a measure of roll agility. For repeatability, the test requires full lateral stick; however, I would ease off stick when acquiring target.

Flight 98, Pilot C

Lateral gross acquisition at 25,000 ft, 180 kn, 30° angle of attack, group A—Can do the final job of acquiring the target but can not get around the corner. Cooper-Harper rating: 7. Inadequate roll rate. Time delay is too large. Group A roll rate onset is nowhere near fast enough.

Flight 101, Pilot B

90/90 roll captures at 20,000 ft, 200 kn: 1 *g*, groups B and C; 15° angle of attack, groups B and C; 25° angle of attack, group B; 30° angle of attack, group A

Group B—Smoother; good for captures. Not enough roll acceleration.

Group C—Faster; more acceleration. Pretty controllable. Pilots will back off on stick for their own capture criteria or for their own use. Pilots like faster roll acceleration. For capture start with full stick, back off and then reverse to stop roll is optimum. Like group C for the air-to-air, outer-loop task. First attempt, saw ratcheting in roll. Second attempt, didn't see it.

Flight 103, Pilot B

90/90 roll captures at 20,000 ft: 160 kn, 25° angle of attack, group A; 250 kn, 25° angle of attack, groups A, B and C; 200 kn, 30° angle of attack, group C

Roll rates with groups C and B are higher and preferred over group A, with group C maybe slightly higher. Group B is preferred for roll capture task over group C because group C has too much lateral–directional problems [less roll coupling]. At 250 kn, 25° angle of attack, group C rolls faster.

Flight 104, Pilot C

90/90 roll captures at 20,000 ft, 160 kn, 1 *g* and 25° angle of attack, groups A, B, C—Didn't notice a lot of difference in coordination between groups B and C at high angle of attack. At 1 *g*, group B is much better than group C. Group C, especially at lower, slower speeds, feel a hitch in lateral acceleration that is unexpected [forces pilot to instinctively back off on lateral stick]. Group B is smooth everywhere. Preferred groups B and C roll rate over group A. Lateral acceleration is not large enough to cause problem (group B over group C for BFM), but is large enough to tell aircraft is not responding to commands.

Lateral gross acquisition at 25,000 ft, 180 kn, 30° angle of attack, groups B and C.

Group C—No remarkable difference, but task is so inconsistent I would rather not draw any valid conclusions. Done when chase was under the nose. Got 3/4 of it done and he [the F-18 pilot] went under the nose. Good roll rate; little overshoot. A roll hesitation or lurch when rolling through wings level causes hesitation in lateral stick.

Group B—Roll rate okay. Blind [chase under the nose]. Got buried under nose. Liked roll rate.

General Comments—Would have liked higher roll acceleration [lower time constant] even with groups B and C. Slow roll acceleration was not noticed in roll captures. [Seemed like pilot wanted more roll capability in group C.] Difficulty in setting up—initial conditions difficult. Timing has to be right [think pilot was rolling too soon]. Target is below nose at 90° roll angle. Would like more pitch rate and pitch acceleration during pull to a 30° angle of attack. Giving a rating is not easy because of the difficulty in setup and pitch

portion. Would give groups B and C a Cooper-Harper rating of 4–5 for the lateral task. Task is not consistent.

Flight 108, Pilot C

Rolling scissors with an F-18 opponent at 25,000 ft, Mach 0.6, group B—Liked roll rate—no need to go faster. No cues on stick for angle of attack—little disturbing. Pulled aft and got angle-of-attack overshoot. Looked down at needles to see what angle of attack was and felt yaw accelerate at same time. Got the advantage initially. Forced to respect angle-of-attack buildup and be tentative with maneuvering. I suggest starting at 200 rather than 250 kn to allow more maneuvering evaluation at high angle of attack. Like the roll rate. Little advantage initially, then F-18 had advantage so I pulled higher. No angle-of-attack cues on stick; this is distracting. Roll rate is fine.

Flight 110, Guest Pilot A

1-*g* orientation at 20,000 ft; 25°, 35°, and 45° angle of attack; group A—25° angle of attack rolls well with coordinating rudder. Angle of attack is easier to control than simulation. 35° angle of attack—roll rate no good—small.

360° roll at 25,000 ft, 1 *g*, 25° angle of attack, group A—Not impressed.

360° roll at 25,000 ft, 1 *g*, 35° angle of attack, group B and group C—No comments.

90/90 captures at 20,000 ft, 200 kn, 25° angle of attack, group C—Rolled better than group B—had to compensate when rolling out.

90/90 capture at 20,000 ft, 200 kn, 30° angle of attack, group B—Rolled better and is easier to stop.

Flat scissors at 25,000 ft, Mach 0.6—No comments.

Flight 111, Pilot C

Rolling scissors with an F-18 opponent at 25,000 ft, Mach 0.6: 29° maximum angle of attack, group B; 40° maximum angle of attack, group B; 44° maximum angle of attack, group B; 38° maximum angle of attack, group C; 31° maximum angle of attack, group C; 33° maximum angle of attack, group A

Groups C and B—No difference in roll rates; adequate rates. No coordination problems. Sink like a brick during rolls. [Aft stick to 30°–35° angle of attack where pilot wants to maneuver, but angle of attack increases to 50°.] No cues for angle-of-attack buildup such as buffet, increase, lateral acceleration, or stick force or position. [Forces pilot to be reluctant, hesitant in maneuvering.] Not a carefree airplane. F-18 can maneuver with head out cockpit; X-29A can't.

Group A—Much more sluggish. Overall Cooper-Harper rating for rolling scissors task: 3 roll; 5 overall. Rolling scissors experiment should force both aircraft to high angles of attack. Sufficient roll rate and that initial advantage could be gained over F-18. However, as the engagement continued, the superior specific excess power of the F-18 allowed it to return to a neutral situation.

Flight 112, Guest Pilot B

Above 250 kn—Nice flying, responsive flying qualities.

Orientation at 20,000 ft, 1 *g*; 15°, 25°, and 50° angle of attack—Buffet at 20° angle of attack; wing rock above 25°–30° angle of attack. Got used to wing rock and high angle of attack. Felt very comfortable at 50° angle of attack first time there. At 30°– 35° angle of attack, mild wing rock and cockpit noise.

360° roll at 20,000 ft, 1 *g*, 25° angle of attack group A and group B. Orientation at 20,000 ft, 35° angle of attack, group B—Used some rudder with group B, did not notice difference in roll rate. Roll rate and precision were fine. Velocity vector roll disorienting—difficult to know when to stop. Group A—slow roll rates even more noticeable at high angle of attack. Angle of attack control very easy, easier than simulation.

Rolling scissors with an F-18 opponent at 20,000 ft, Mach 0.6: 52° maximum angle of attack, group B; 44° maximum angle of attack, group B; 43° maximum angle of attack, group C; 49° maximum angle of attack, group A

Group B—Nice handling. Enjoyed it; easy and comfortable to fly. The BFM was really fun, able to use X-29A's high-angle-of-attack capability to get in F-18's rear hemisphere. Able to gain 3/9 [3 and 9 o'clock positions] every time by aggressively losing speed and spitting F-18 out in front. Aircraft did what I wanted. When reaching 52° angle of attack, felt no yaw rate or acceleration cues. Lack of continued pitch rate

with aft stick and ground angle-of-attack call alerted me to angle of attack; would not have recovered otherwise. Did not hear angle-of-attack warning tone. Did not notice difference between groups B and C. Did not notice difference between groups B and C and group A unless at full-lateral stick. Did not notice wing rock or buffet during rolling scissors. Never let off on aft stick—wanted to bleed off more speed.

90/90 roll captures at 20,000 ft, 200 kn, 25° angle of attack, group B—Rolled quickly—good roll rate. Was aggressive in getting there quickly [???] to overshooting of opposite 90. Did not notice side force.

Flight 115, Pilot A

Raps and pulses at 20,000 ft, 1 *g*, 50° angle of attack, group B—Above 50° angle of attack, aircraft yawed off; full-right rudder did not stop it. Came back off angle of attack and yaw came under control. Yaw off at 50° angle of attack seemed slower than at 45° angle of attack.

Rolling scissors with an F-18 opponent at 25,000 ft, 215–250 kn: 47° maximum angle of attack, group B; 45° maximum angle of attack, group C; 44° maximum angle of attack, group B; 45° maximum angle of attack, group C; 42° maximum angle of attack, group C—Didn't feel yaw rate. Aircraft felt real stable. Pitch needs more. Roll is adequate; used full stick. Would like more stick. Ability to keep aircraft loaded and roll is a significant advantage in close-in, tight fight. End game was that X-29A was in a more favorable position than the F-18 airplane. Initial move gave X-29A the advantage. Would like more pitch authority for angle of attack. Change to point and shoot (angle of attack > 40°–45°). Authority is there but not utilized because of angle of attack limits. [Pilot received angle-of-attack calls at 30° and 40°.]

Group B—Used full-lateral stick on a routine basis. Gives good roll rates, but more would be better since full stick was used routinely. Roll rates are good, acceptable, but would like more. More would be nice. Airplane felt real stable. Initial move puts [???] nicely behind. Like to have more pitch authority. Good roll authority but using full stick. Would like the high rates without using full stick [lateral].

Group C—No difference with group B. Felt yaw rate more. Felt rates more at lower angles of attack. With group C, more aware during initial move of the yawing motion of the airplane. Let him [F-18 pilot] get away, then the F-18 got the advantage (pitch-pointing authority). More aware of yaw during the initial inputs. Need more pitch authority at low speeds. Didn't feel yaw rate. It [the X-29A airplane] loaded in roll, put in front of the F-18. The F-18 could compensate. Need a little more pitch authority. Only momentary advantages. Really like the feedback forces, unlike the F-18, but not aware of the angle of attack. Very impressed with the roll rate. Put stick in; comes across very carefree. Flew the maneuver with head out of the cockpit. Ginger with angle of attack. Liked the roll rates.

Groups B and C—Initial roll rate onset is acceptable. Don't notice wing rock during the BFM. Tactically, wouldn't mind pitching X-29A up to a 70° angle of attack for a snapshot.

Flight 116, Guest Pilot C

Pilot orientation at 20,000 ft, 1 *g*; 15°, 35°, and 50° angle of attack—Angle-of-attack control was precise. Aircraft was easier to fly than simulation. Stick forces were lighter and stick displacements were smaller than F-18. [Would have overcontrolled the aircraft in pitch if pilot did not simulate beforehand.] Saw no tendency for the aircraft to yaw off at 50° angle of attack. Controllability and precision are good—close to the F-18 HARV.

Lateral–directional raps and doublets at 20,000 ft, 1 *g*, 50° angle of attack—Little aircraft response. Trouble getting sideslip—only difficult maneuver. Clearly better for precision maneuvers than the F-18—no excursion in the parameters.

360° roll at 20,000 ft, 1 *g*, 35° angle of attack, group B—Rolls significantly better than an unaugmented F-18 (higher roll rate and precision). Was impressed. Looks like the F-18 HARV.

360° roll at 20,000 ft, 1 *g*, 35° AOA, group C—Slightly higher roll rate, although difficult to tell the difference with group B. Controllable. Used heading change to tell when 360° rolls were complete.

90/90 roll capture at 20,000 ft, 200 kn, 25° angle of attack, group B—Very happy with the aircraft. Precise control; very smooth flying.

Rolling scissors with an F-18 opponent at 25,000 ft, 215–250 kn: 35° maximum angle of attack, group B; 33° maximum angle of attack, group C; 55° maximum angle of attack, group C—Very impressed. Very pleased with the loaded roll rates. Liked the light stick forces; allows carefree maneuvering. Would have

liked angle-of-attack feedback. [There were none which caused pilot to be tentative with maneuvering. The pilot didn't feel like all the angle-of-attack capability that was there was used.] Would have liked more angle-of-attack capability and more pitch-pointing capability [pitch rate and acceleration] at all angles of attack. The X-29A beats the F-18 in roll; the F-18 beats the X-29A in pitch. Higher angle of attack would have allowed me to take advantage of a snapshot opportunity [greater than 45–50° angle of attack]. [The BFM experiment was good because the pilot stayed at a moderate angle of attack to roll. This allowed the BFM to stay a true rolling scissors and allowed the pilot to see the benefits of higher roll performance at a higher angle of attack.] Didn't notice wing rock during the BFM. Would like to see the X-29A with the F-18 HARV as the opponent—a good experiment because the X-29A would enjoy a specific energy advantage, but maneuvering disadvantage at a high angle of attack. Significantly better at these angles of attack than the F-18. There was no way the F-18 was going to get an advantage in these engagements.

Flight 117, Pilot B

360° roll at 25,000 ft, 1 *g*, 45° angle of attack, group B—Aircraft attitude and motion are very unique. It was strange being able to rotate the aircraft at a 45° angle of attack through 360°—mostly heading change.

Flight 118, Pilot A

0/60/0 maneuver at 25,000 ft, 1 *g*, 40° angle of attack, group C—Simulator predicted aircraft characteristics well. Good that we didn't fly 360s here.

Flight 119, Pilot B

Formation flying (fingertip and close trail) with an F-18 airplane at 10,000 to 20,000 ft, Mach 0.6 to 0.8.

Group B—A little jerky, but may be pilot gain. Group B increase over group A was not noticed here. Not very sensitive. Satisfactory; no deficiencies. Cooper-Harper rating: 3.

Group C—Does not appear to be any deficiencies. Group B a little smoother than group C; less stick input and take out with group B. More "hunting" with group C; more stick activity. Group B really seems to be the superior control law.

Group A—Can't compare—done at low altitude with turbulence present.

General comments—Not a big difference between groups A, B, and C. No pilot-induced oscillation tendencies. Negative proof—maximum roll rate afforded by gain change. Does not hurt during this task.

Flight 120, Pilot C

360° roll at 25,000 ft, 1 *g*, 40° angle of attack, group B—Felt the roll rate accelerating, came off full lateral stick. Roll winds up, especially the last 180°. Neutral stick on recovery—roll did not want to stop at first.

0/60/0 maneuver at 25,000 ft, 1 *g*, 45° angle of attack, group B—Came off with stick to recover; momentarily rolled more to right, even with left stick. [First time that the pilot felt the aircraft did not respond to commands.]

360° roll at 25,000 ft, 1 *g*, 30° angle of attack, group B—Nominal.

360° roll at 25,000 ft, 1 *g*, 35° angle of attack, group B—Felt a little like higher angles of attack at end; landed.

NOMENCLATURE

Abbreviations and Acronyms

ACC	automatic camber control
ARI	aileron-to-rudder interconnect
BFM	basic fighter maneuver
FCS	flight control system
FS	fuselage station
ITB	integrated test block
NACA	National Advisory Committee for Aeronautics
NASA	National Aeronautics and Space Administra-tion
pEst	parameter estimation program

Symbols

b	wing span, ft
BMAX	rudder pedal command gain, deg/percent
$\bar{c}$	chord, ft
C_m	pitching moment coefficient
C_{n_o}	yawing moment coefficient at zero sideslip
GF1	symmetric flap gain, deg/deg
GMAX	pitch stick command gain, *g*/percent
GS1	strake flap gain, deg/deg
GYCWSH	rudder pedal-to-aileron washout filter time constant, sec
G_{lim}	pitch stick limit gain, rad/sec
G_{n_z}	normal acceleration gain, (rad/sec)/*g*
G_q	pitch rate gain, (deg/sec)/(deg/sec)
$G_{\dot{q}}$	pitch acceleration gain, (deg/sec)/(deg/sec sec)
I_{xx}	moment of inertia about the *x*-axis, slug-ft^2
I_{xz}	cross product of inertia, slug-ft^2
I_{yy}	moment of inertia about the *y*-axis, slug-ft^2
I_{zz}	moment of inertia about the *z*-axis, slug-ft^2
K2	roll-rate-to-aileron gain, (deg/sec)/(deg/sec)
K3	$\dot{\beta}$-to-aileron gain, (deg/sec)/(deg/sec)
K4	n_y-to-aileron gain, (deg/sec)/*g*
K13	lateral roll command gain, (deg/sec)/(deg/sec)
K14	rudder pedal-to-aileron gain, (deg/sec)/percent
K17	$\dot{\beta}$-to-rudder gain, deg/(deg/sec)
K18	lateral acceleration-to-rudder gain, deg/*g*
K27	aileron-to-rudder gain, deg/(deg/sec)
K_{α_2}	pitch axis angle-of-attack feedback gain, (rad/sec)/(ft/sec)
n_y	lateral acceleration, *g*
n_z	normal acceleration, *g*
PMAX	lateral stick command gain, (deg/sec)/percent
p	roll rate, deg/sec
q	pitch rate, deg/sec
r	yaw rate, deg/sec
S	reference area, ft^2
s	Laplace operator
V	velocity, ft/sec
V_T	true velocity, kn
XCG	longitudinal center of gravity location, in.
XKI1	pitch axis forward loop integrator gain, deg/deg
XKI3	lateral axis forward loop integrator gain, deg/deg
XKP1	pitch axis forward loop proportional gain, deg/(deg/sec)
XKP3	lateral axis forward loop proportional gain, deg/(deg/sec)
XKP4	yaw axis forward-loop proportional gain, deg/(deg/sec)
YCG	lateral center of gravity location, in.
ZCG	vertical center of gravity location, in.
α	angle of attack, deg
$\dot{\beta}$	rate of change of sideslip, deg/sec
θ	pitch angle, deg
τ_s	roll command filter time constant
ϕ	roll angle, deg

REFERENCES

[1]Bosworth, John T. and Cox, Timothy H., *A Design Procedure for the Handling Qualities Optimization of the X-29A Aircraft*, NASA TM-4142, 1989.

[2]Cox, Timothy H. and Powers, Bruce G., *Flying Qualities Experience With the X-29A Aircraft*, NASA TP-3340, 1993.

[3]Walchli, Lawrence A. and Smith, Rogers E., "Flying Qualities of the X-29A Forward Swept Wing Aircraft," *Flying Qualities*, AGARD-CP-508, Feb. 1991, pp. 25-1–25-13.

[4]Pellicano, Paul, Krumenacker, Joseph, and Vanhoy, David, "X-29 High Angle-of-Attack Flight Test Procedures, Results, and Lessons Learned," SFTE 21st Annual Symposium, Garden Grove, California, Aug. 1990.

[5]Spacht, G., "The Forward Swept Wing: A Unique Design Challenge," AIAA-80-1885, Aug. 1980.

[6]Grafton, Sue B., Gilbert, William P., Croom, Mark A., and Murri, Daniel G., "High Angle-of-Attack Characteristics Of A Forward-Swept Wing Fighter Configuration," AIAA-82-1322, Aug. 1982.

[7]Gera, Joseph, "Dynamics and Controls Flight Testing of the X-29A Airplane," AIAA-86-0167, Jan. 1986.

[8]Gera, Joseph, and Bosworth, John T., *Dynamic Stability and Handling Qualities Tests on a Highly Augmented, Statically Unstable Airplane*, NASA TM-88297, 1987.

[9]Chacon, Vince and McBride, David, *Operational Viewpoint of the X-29A Digital Flight Control System*, NASA TM-100434, 1988.

[10]Gera, J., Bosworth, J. T., and Cox, T. H., *X-29A Flight Test Techniques and Results: Flight Controls*, NASA TP-3121, 1991.

[11]Walchli, Lawrence A., Ryan, Robert J., and Smith, Wade R., "X-29 High Angle-Of-Attack Flight Test," WL-TR-93-3003, Jan. 1992.

[12]Meyer, R. R., and Schneider, E. T., "Real-Time Pilot Guidance System for Improved Flight Test Maneuvers," AIAA-83-2747, Nov. 1983.

[13]Clarke, Robert and Webster, Fred, "Design of the X-29A High-Alpha Flight Control System," *High-Angle-of-Attack Projects and Technology Conference*, NASA CP-3207, Apr. 1992, pp. 15–27.

[14]Clarke, Robert, Burken, John, Bauer, Jeffrey, Earls, Michael, Knighton, Donna, and McBride, David, "Development and Flight Test of the X-29A High Angle-of-Attack Flight Control System," *High-Angle-of-Attack Technology*, Vol. 1, NASA CP-3149, Part 3, 1992, pp. 1275–1313.

[15]Pahle, Joseph W., Powers, Bruce, Regenie, Victoria, Chacon, Vince, Degroote, Steve, and Murnyak, Steven, *Research Flight-Control System Development for the F-18 High Alpha Research Vehicle*, NASA TM-104232, 1991.

[16]Huber, Peter and Galleithner, Hans, "Control Laws/Flying Qualities and Flight Test Results," *High-Angle-of-Attack Projects and Technology Conference*, NASA CP-3207, Apr. 1992, pp. 171–188.

[17]Bauer, Jeffrey and Clarke, Robert, "X-29 High Alpha Control System Improvements," *High-Angle-of-Attack Projects and Technology Conference*, NASA CP-3207, Apr. 1992, pp. 29–47.

[18]O'Connor, Cornelius, Ralston, John, and Bernhart, Billy, *An Incremental Rotational Aerodynamic Math Model Of The X-29 Airplane From 0° Through 90° Angle-Of-Attack*, AFWAL-TR-88-3067, Sept. 1988.

[19]Whipple, Raymond D. and Ricket, Jonathan L., *Low-Speed Aerodynamic Characteristics of a 1/8-Scale X-29A Airplane Model at High Angles of Attack and Sideslip*, NASA TM-87722, 1986.

[20]Ralston, John N., *Rotary Balance Data and Analysis for the X-29A Airplane for an Angle-of-Attack Range of 0° to 90°*, NASA CR-3747, 1984.

[21]Murray, James E. and Maine, Richard E., *pEst Version 2.1 Users Manual*, NASA TM-88280, 1987.

[22]Webster, Fredrick R. and Purifoy, Dana, *X-29 High Angle-Of-Attack Flying Qualities*, AFFTC-TR-91-15, July 1991.

[23]Fratello, David J., Croom, Mark A., Nguyen, Luat T., and Domack, Christopher S., "Use of the Updated NASA Langley Radio-Controlled Drop-Model Technique for High-Alpha Studies of the X-29A Configuration," AIAA-87-2559, Aug. 1987.

[24]Croom, Mark A., Whipple, Raymond D., Murri, Daniel G., Grafton, Sue B., and Fratello, David J., "High-Alpha Flight Dynamics Research On The X-29 Configuration Using Dynamic Model Test Techniques," SAE-881420, Oct. 988.

[25]Murri, Daniel G., Nguyen, Luat T., and Grafton, Sue B., *Wind-Tunnel Free-Flight Investigation of a Model of a Forward-Swept-Wing Fighter Configuration*, NASA TP-2230, 1984.

[26]Nguyen, Luat T. and Foster, John V., *Development of a Preliminary High-Angle-of-Attack Nose-Down Pitch Control Requirement for High-Performance Aircraft*, NASA TM-101684, 1990.

[27]Smith, W. and Pellicano, P., "X-29 High Angle-of-Attack Military Utility Flight Test Results," AIAA-92-4080, Aug. 1992.

[28]Shaw, Robert L., *Fighter Combat: Tactics and Maneuvering*, Naval Institute Press, Annapolis, Maryland, 1985.

[29]Nguyen, Luat T., Ogburn, Marilyn E., Gilbert, William P., Kibler, Kemper S., Brown, Phillip W., and Deal, Perry L., *Simulator Study of Stall/Post-Stall Characteristics of a Fighter Airplane With Relaxed Longitudinal Static Stability*, NASA TP-1538, 1979.

[30]Gera, Joseph, "Simulation as an Analysis Tool in Flight Testing a Modified Control System on the F-14 Airplane," SES/SFTE Aircraft Test and Evaluation Symposium, Patuxent River, Maryland, Mar. 1982.

[31]Nguyen, Luat T., Gilbert, William P., Gera, Joseph, Iliff, Kenneth W., and Enevoldson, Einar K., "Application Of High-α Control System Concepts To A Variable-Sweep Fighter Airplane," AIAA Atmospheric Flight Mechanics Conference, Danvers, Massachusetts, Aug. 1980.

[32]Riley, David R. and Drajeske, Mark H., "Relationships Between Agility Metrics and Flying Qualities," SAE-901003, Apr. 1990.

[33]Huband, G. W. and Gillard, W. J., "X-29 High-Angle-of-Attack Flight Testing," *Aerospace Engineering*, vol. 13, no. 7, July 1993, pp. 11–17.

[34]Cooper, George E. and Harper, Robert P., Jr., *The Use of Pilot Rating in the Evaluation of Aircraft Handling Qualities*, NASA TN-D-5153, 1969.

[35]Voracek, David F. and Clarke, Robert, *Buffet Induced Structural/Flight-Control System Interaction of the X-29A Aircraft*, NASA TM-101735, 1991.

TABLES

Table 1: The X-29A no. 2 geometry and mass characteristics.

Weight, lb	14,583–18,518
Height, ft	14.3
Length, ft	48.1
Longitudinal center of gravity, in.	443.5–454.0
Moment of inertia, nominal, slug-ft^2:	
I_{xx}	4,600
I_{yy}	53,000
I_{zz}	56,000
I_{xy}	2,500
Wing:	
Span, ft	27.2
Mean aerodynamic chord, ft	7.22
Area, ft^2	185.0
Aspect ratio	4.0
Leading-edge sweep, deg	–29.27
Taper ratio	0.4
Dihedral angle, deg	0
Total flap area, ft^2	14.32
Hinge line, percent of wing chord	75
Flap deflection limits, deg	–10/+25 (trailing edge down)
Canard:	
Span, ft	13.63
Area, ft^2	37.0
Aspect ratio	1.47
Taper ratio	0.32
Deflection limits, deg	–60/+30 (trailing edge down)
Vertical tail:	
Span, ft	5.5
Area, ft^2	33.75
Aspect ratio	2.64
Taper ratio	0.32
Rudder area, ft^2	7.31
Hinge line, percent of tail chord	70
Rudder deflection limits, deg	±30
Strake flap:	
Half span, ft	2.1
Area, ft^2	5.21
Root chord, ft	2.5
Deflection limits, deg	±30

Table 2. High-angle-of-attack design guidelines.

1-g trim flight $\alpha \geq 20°$			
Neutral lateral controls	$\lvert r \rvert$ < 10 deg/sec after 10 sec positive angle-of-attack recovery with forward stick; no tuck tendency		
1-g trim flight and accelerated flight $20° \leq \alpha \leq 40°$			
Wing rock	$\alpha < 35°$	No sustained wing rock	
	$\alpha > 35°$	$\lvert \Delta\phi \rvert < 15°$	
Lateral maneuver	$\Delta\beta$ adverse	$\Delta\beta$ proverse	$\lvert \Delta\alpha \rvert$
1/2 stick Δ 30° roll No roll rate reversal	3°	none	3°
Full stick Δ 60° roll No roll rate reversal	7°	2°	7°
Full stick Δ 360° roll No roll rate reversal	9°	5°	12°

Table 3. Longitudinal and lateral stick characteristics.

	Longitudinal		Lateral
Displacement, in.	Original	Modified	±3.2
fore	3	1.5	
aft	–2.5	–1.25	
Stick gradient, lb/in.	8	8	2

Table 4. Matrix of test points for flying qualities research.

	Group	160 kn calibrated airspeed	200 kn calibrated airspeed	250 kn calibrated airspeed
1 g	A	complete	complete	
	B	complete	complete	
	C	complete	complete	
15° α	A		complete	
	B		complete	
	C		complete	
25° α	A	complete	complete	complete
	B	complete	complete	complete
	C	complete	complete	complete
30° α	A	complete	complete	
	B	complete	complete	
	C	complete	complete	

Table A-1. An s-plane description of continuous dynamic elements.

Dynamic element	s-plane description
Canard actuator	$\frac{(0.885)\ (20.2)\ (71.4)^2\ (144.9)}{(s+20.2)\left[s^2+2\,(0.736)\ (71.4)\,s+(71.4)^2\right](s+144.9)}$
Symmetric flap actuator	$\frac{(20.2)\ (71.4)^2\ (144.9)}{(s+20.2)\left[s^2+2\,(0.736)\ (71.4)\,s+(71.4)^2\right](s+144.9)}$
Strake actuator	$\frac{(50)\ (100)\ (325)^2}{(s+50)\ (s+100)\left[s^2+2\,(0.7)\ (325)\,s+(325)^2\right]}$
Differential flap actuator	$\frac{(54.1)^2\,(71.4)^2}{\left[s^2+2\,(1.53)\ (54.1)\,s+(54.1)^2\right]\left[s^2+2\,(0.735)\ (71.4)\,s+(71.4)^2\right]}$
Rudder actuator	$\frac{(54.1)^2\,(71.4)^2}{\left[s^2+2\,(1.53)\ (54.1)\,s+(54.1)^2\right]\left[s^2+2\,(0.735)\ (71.4)\,s+(71.4)^2\right]}$
Time delay	$\frac{100}{s+100}$
Pitch rate fuselage vertical bending notch filter	$\frac{s^2+2\,(0.2)\ (68)\,s+(68)^2}{s^2+2\,(0.5)\ (68)\,s+(68)^2}$
Pitch rate fuselage second vertical bending notch filter	$\left[\frac{120}{133}\right]^2\ \frac{s^2+2\,(0.05)\ (133)\,s+(133)^2}{s^2+2\,(0.50)\ (120)\,s+(120)^2}$
Pitch rate fuselage second vertical bending–wing second bending notch filter	$\left[\frac{160}{150}\right]^2\ \frac{s^2+2\,(0.071)\ (150)\,s+(150)^2}{s^2+2\,(0.70)\ (160)\,s+(160)^2}$
Yaw rate fuselage lateral bending notch filter	$\frac{s^2+2\,(0.1)\ (70)\,s+(70)^2}{s^2+2\,(0.7)\ (70)\,s+(70)^2}$
Normal acceleration fuselage vertical bending notch filter	$\frac{s^2+2\,(0.1)\ (70)\,s+(70)^2}{s^2+2\,(0.7)\ (70)\,s+(70)^2}$
Normal acceleration noseboom vertical bending–canard pitch–fuselage second vertical bending notch filter	$\left[\frac{150}{128}\right]^2\ \frac{s^2+2\,(0.10)\ (128)\,s+(128)^2}{s^2+2\,(0.70)\ (150)\,s+(150)^2}$
Lateral acceleration fuselage lateral bending notch filter	$\frac{s^2+2\,(0.1)\ (68)\,s+(68)^2}{s^2+2\,(0.5)\ (68)\,s+(68)^2}$

Table A-1. Concluded.

Dynamic element	s-plane description
Canard position fuselage vertical bending notch filter	$\frac{s^2 + 2(0.14)(68)s + (68)^2}{s^2 + 2(0.70)(68)s + (68)^2}$
Pitch rate gyroscope signal	$\frac{(137)^2}{s^2 + 2(0.704)(137)s + (137)^2}$
Roll rate gyroscope signal	$\frac{(157)^2}{s^2 + 2(0.701)(157)s + (157)^2}$
Yaw rate gyroscope signal	$\frac{(137)^2}{s^2 + 2(0.704)(137)s + (137)^2}$
Prefilter	$\frac{200}{s + 200}$
Roll rate notch filter	$\frac{s^2 + 14.2755s + 10,106.5}{s^2 + 142.1482s + 10,106.5}$

FIGURES

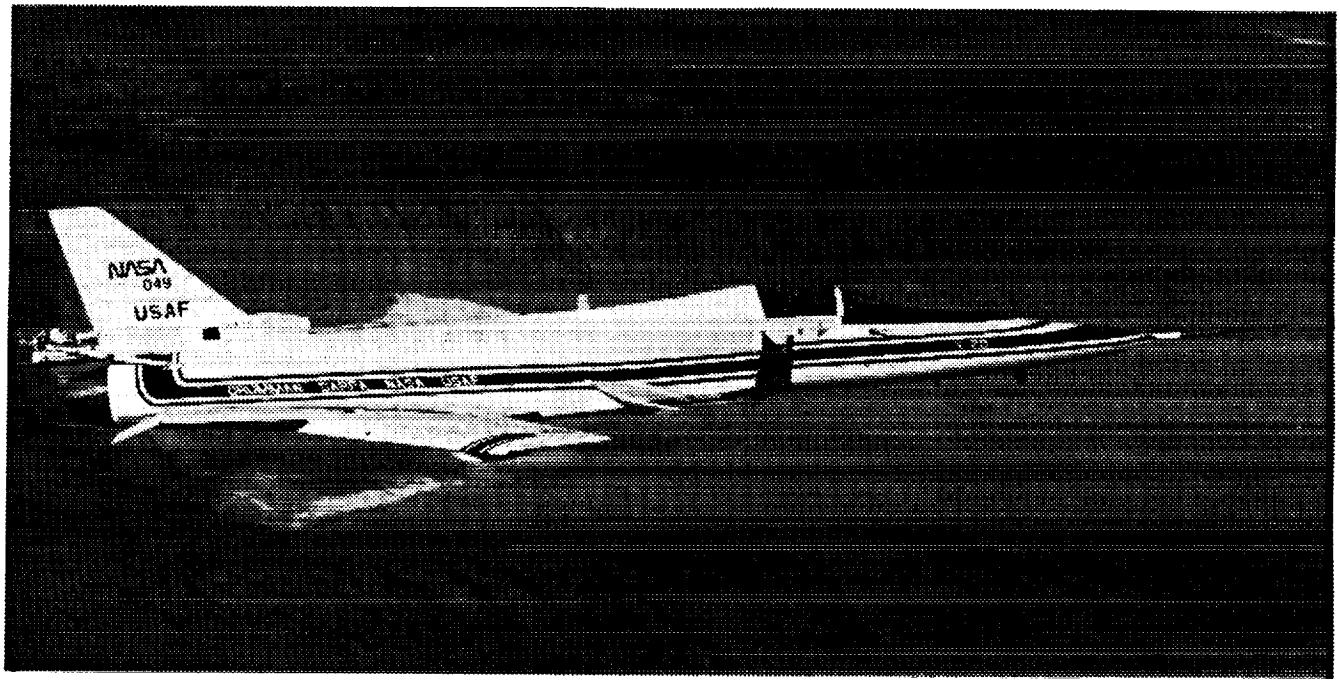

EC90-0048-17

Figure 1. The X-29A no. 2 test airplane.

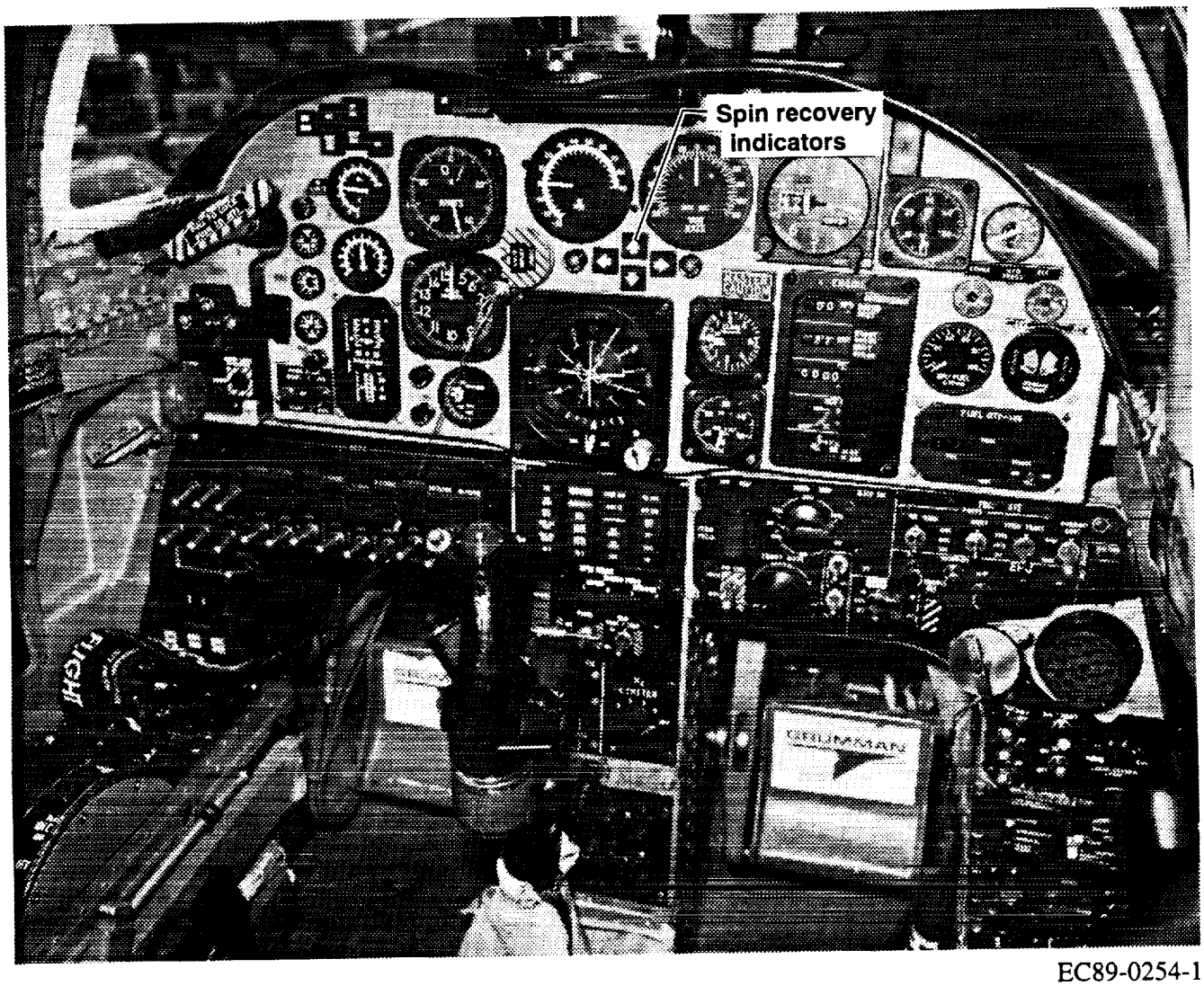

EC89-0254-1

Figure 2. The X-29A no. 2 cockpit displays.

EC89-0216-2

Figure 3. The X-29A no. 2 spin chute assembly.

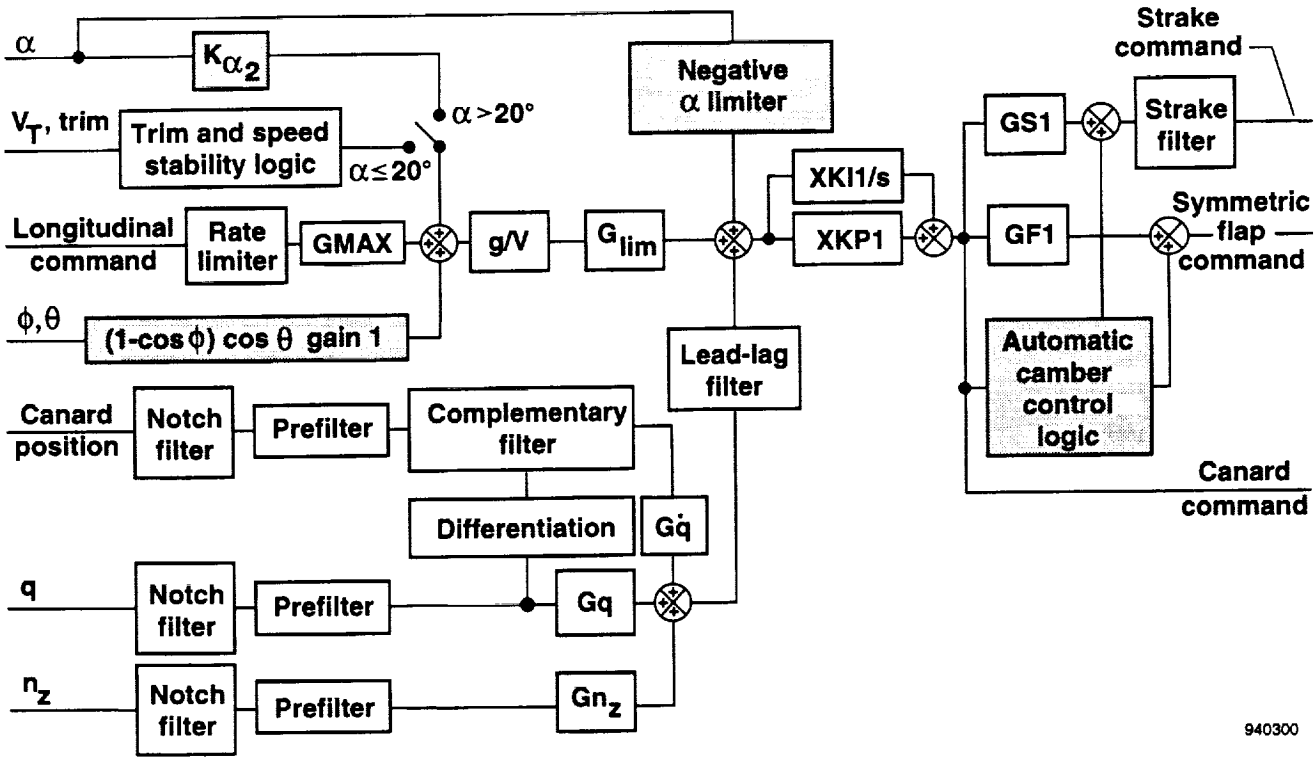

Figure 4. The X-29A longitudinal control system. The highlighted blocks represent changes made for high angle of attack.

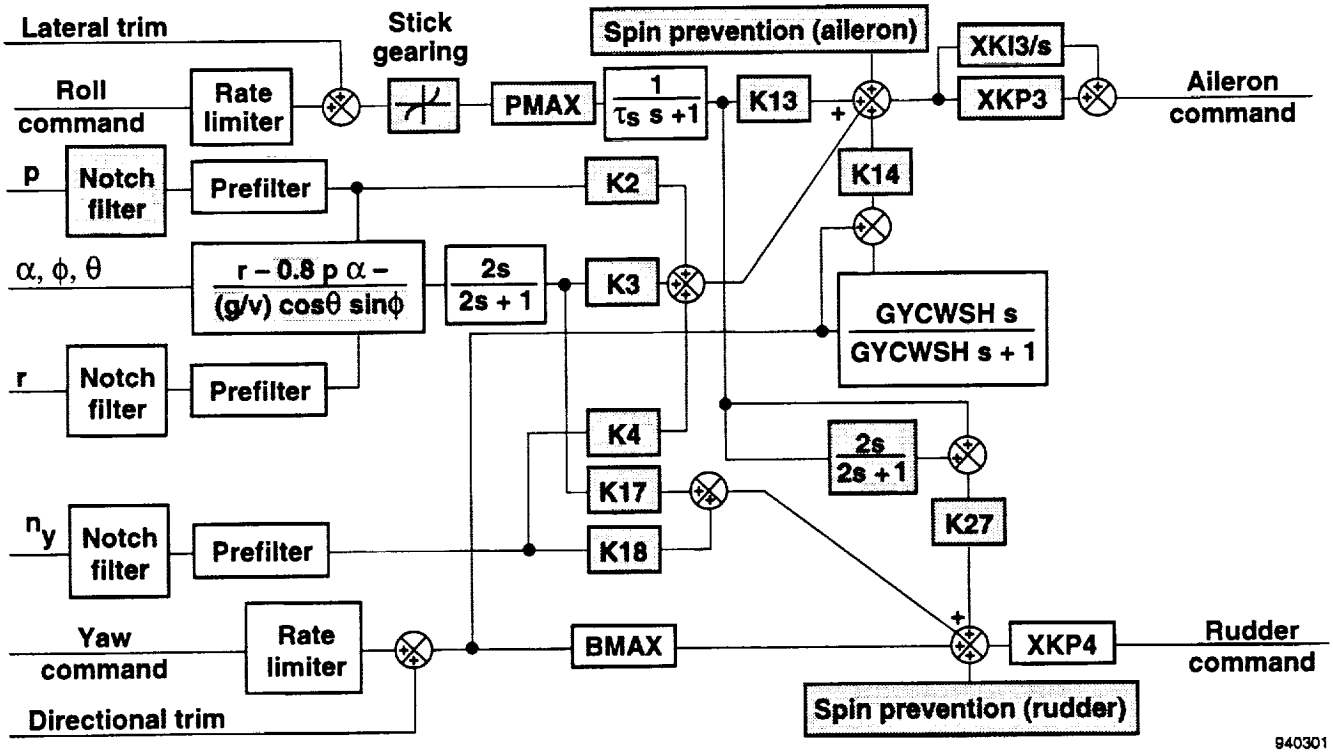

Figure 5. The X-29A lateral–directional control system. The highlighted blocks represent changes made for high angle of attack.

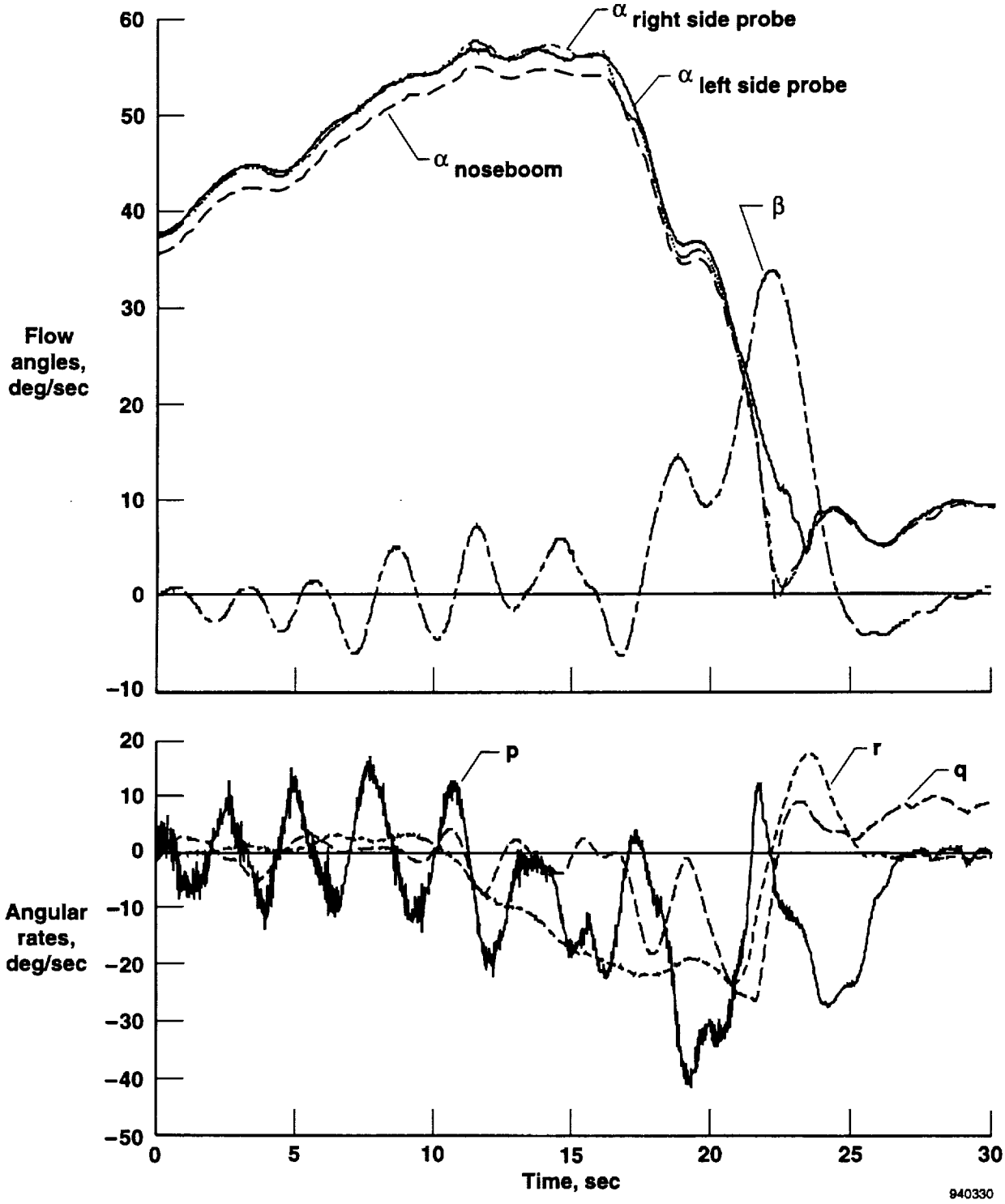

Figure 6. Time histories of the angle-of-attack redundancy management failure from flight 27. The failure was detected at 22.65 sec.

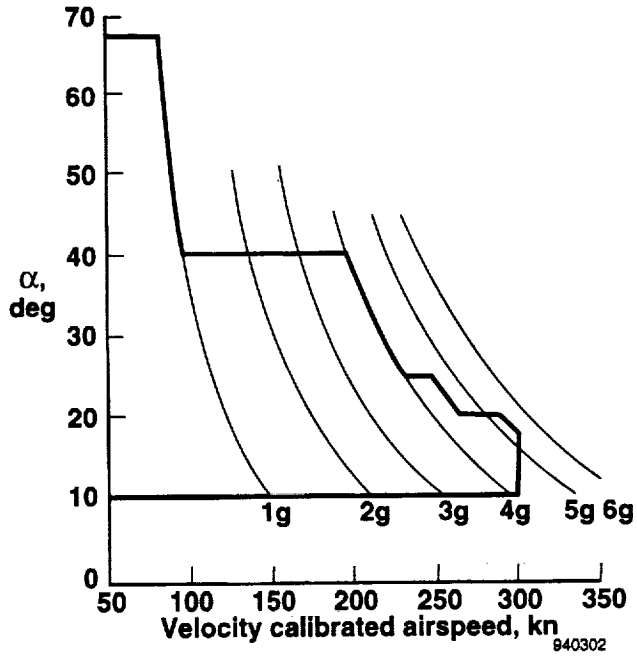

Figure 7. The X-29A high-angle-of-attack envelope.

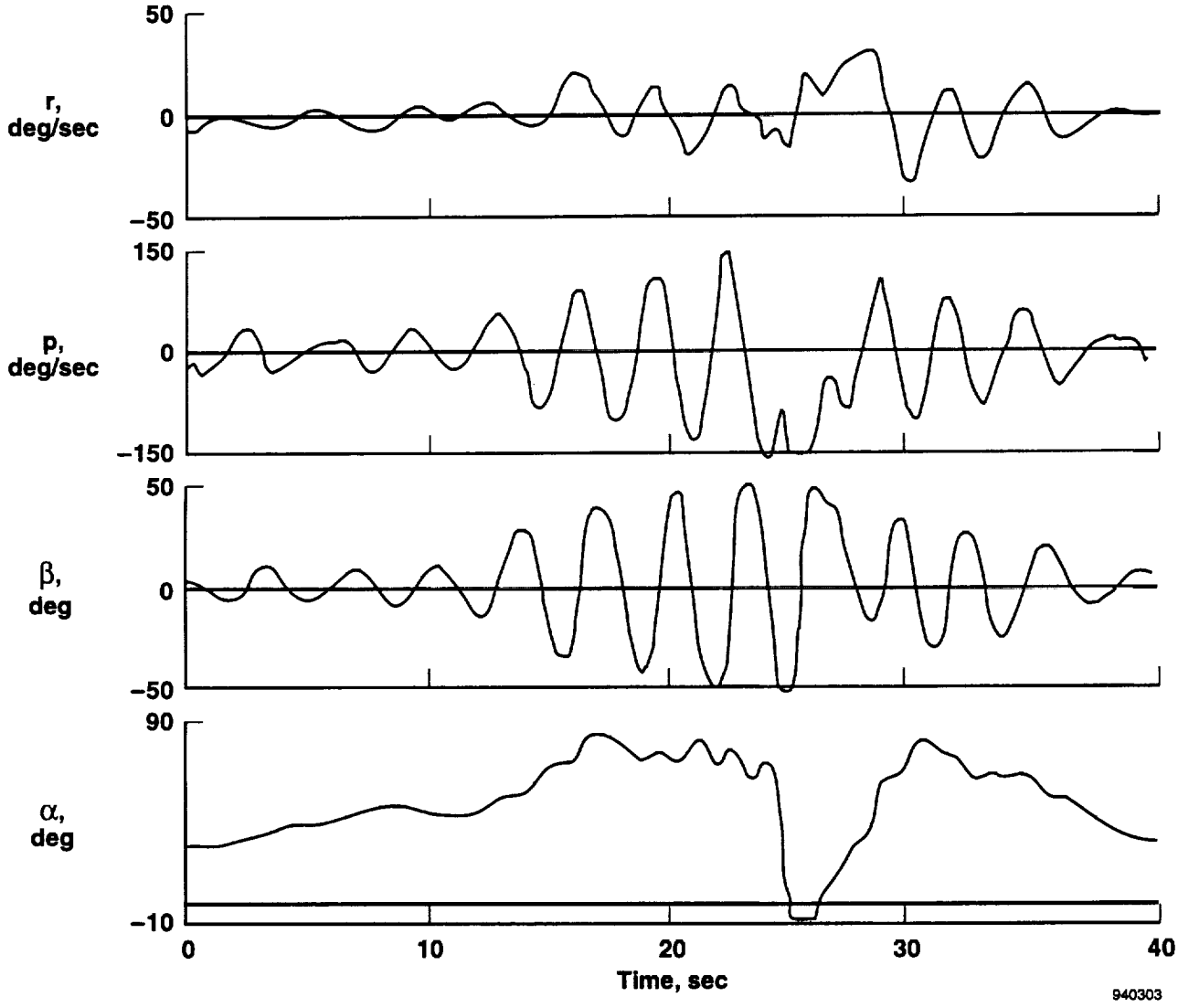

Figure 8. Drop-model wing rock with a 0.88 deg/(deg/sec) roll damping gain (reproduced from reference 23).

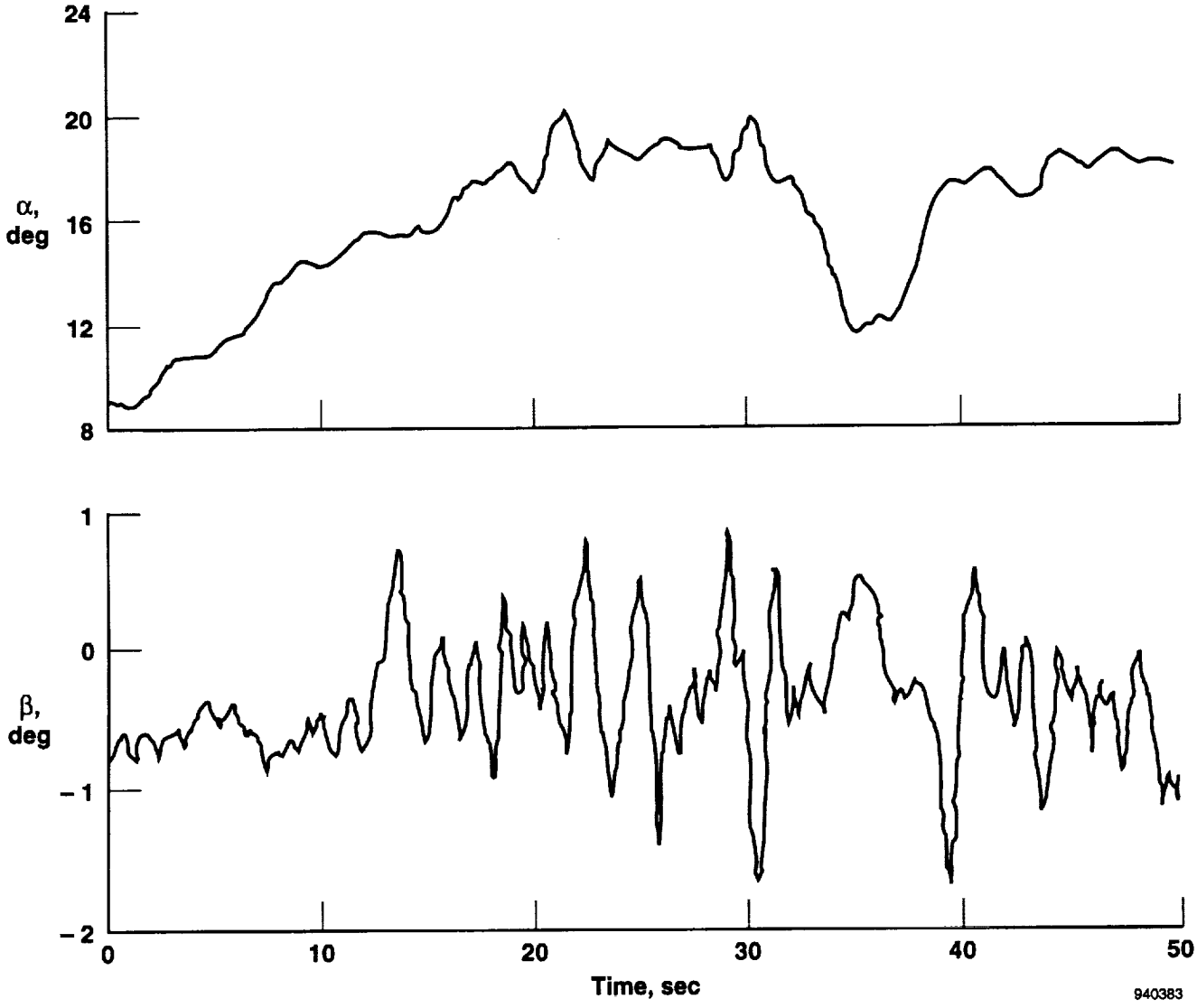

Figure 9. Wing drop time history.

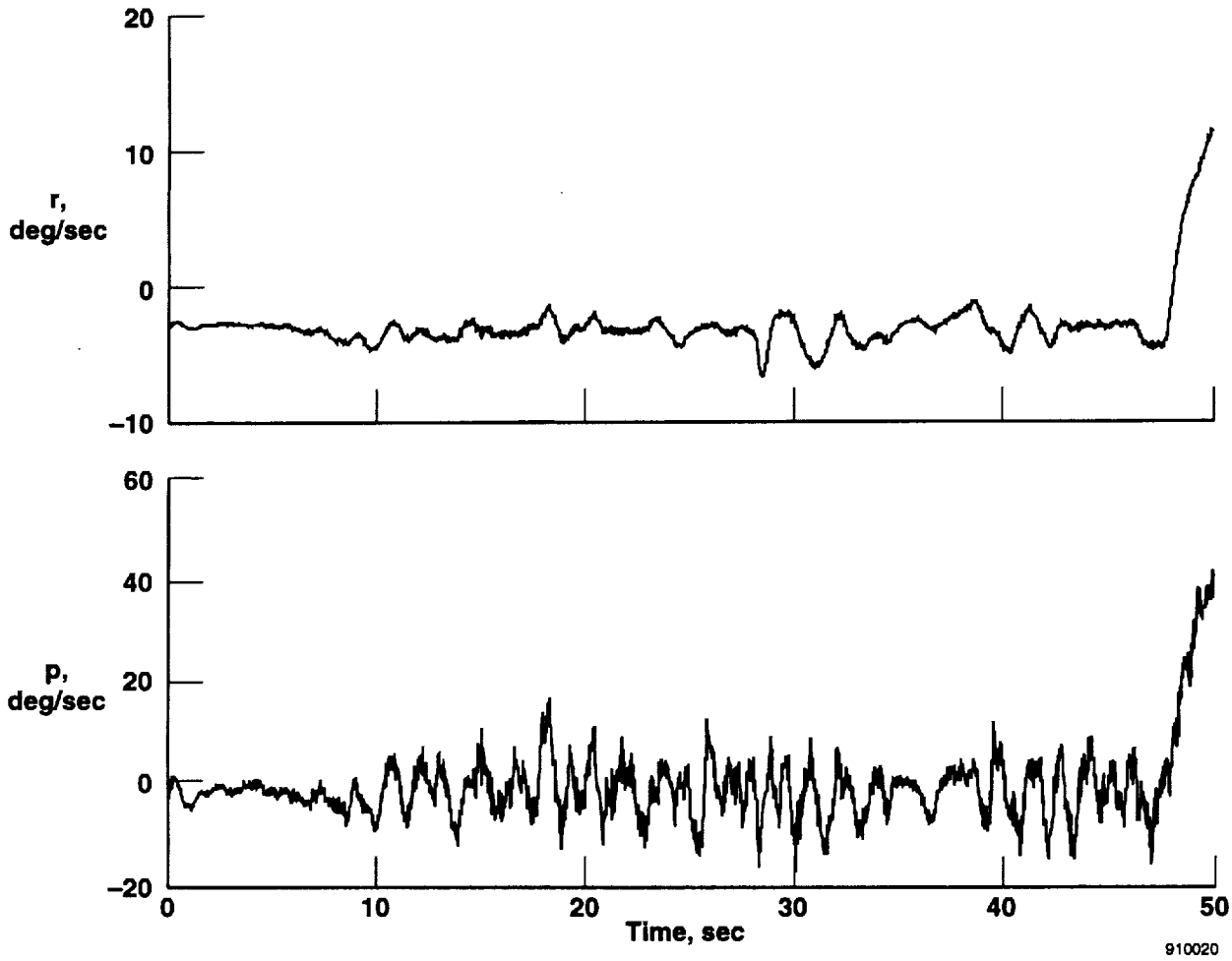

Figure 9. Continued.

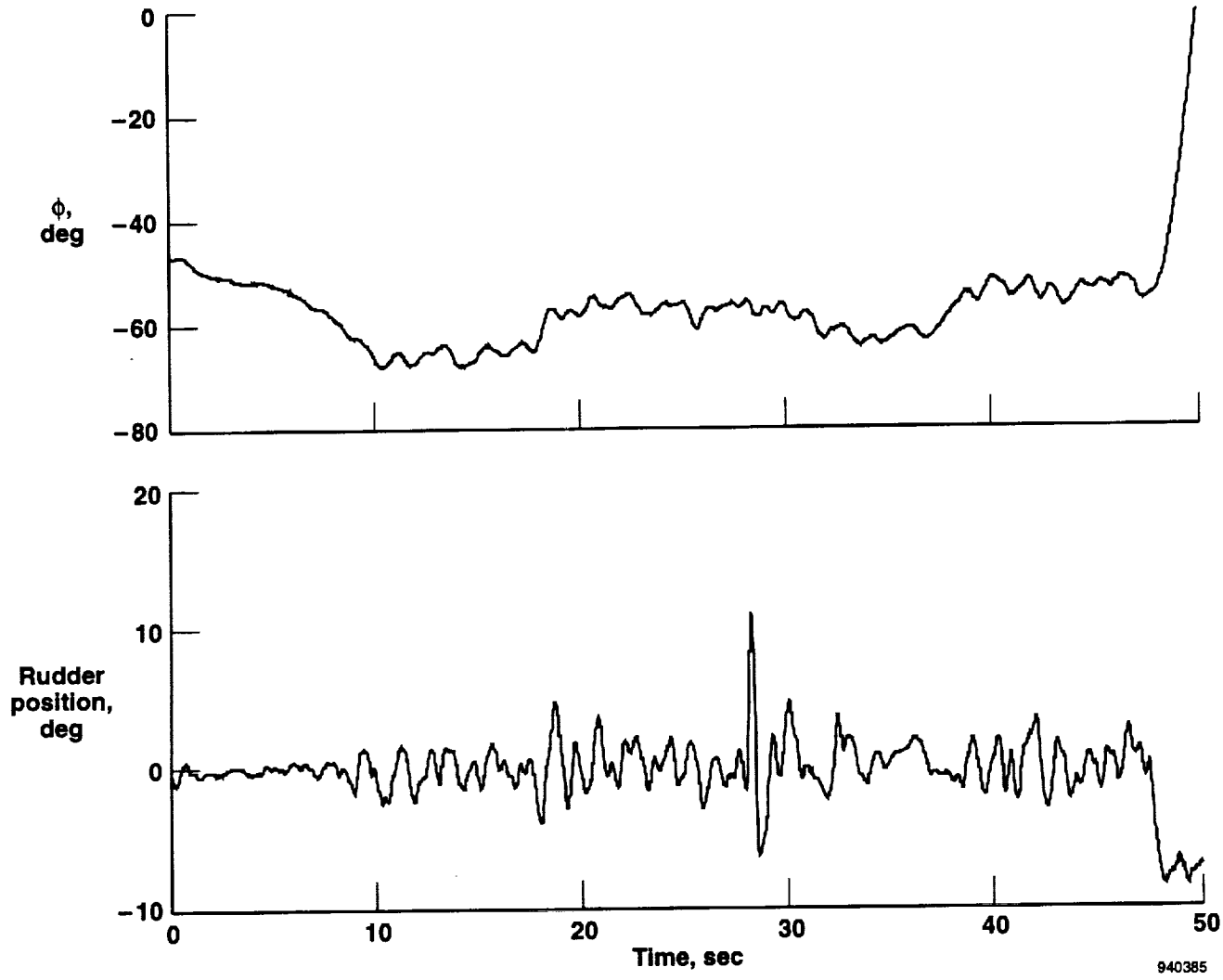

Figure 9. Continued.

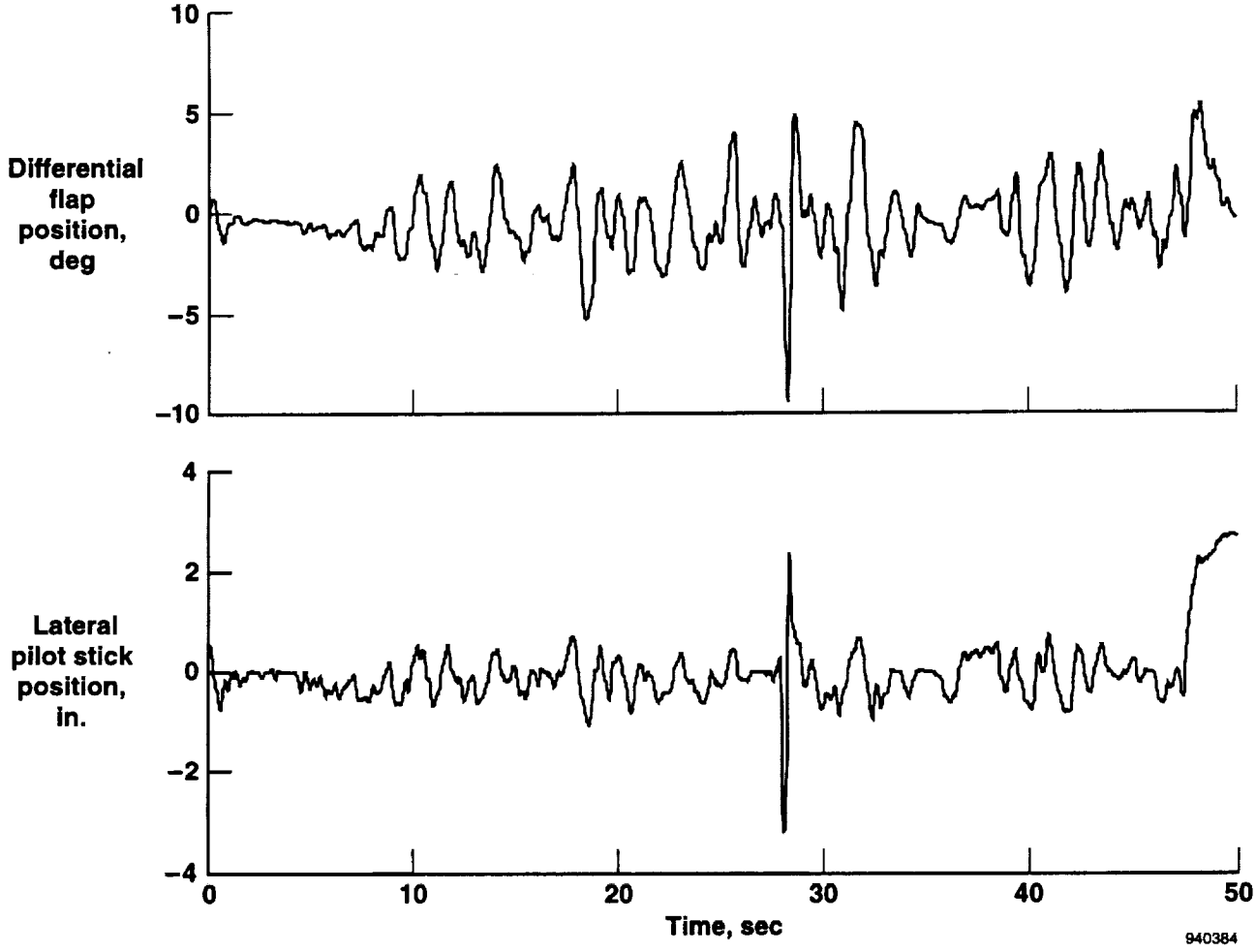

Figure 9. Concluded.

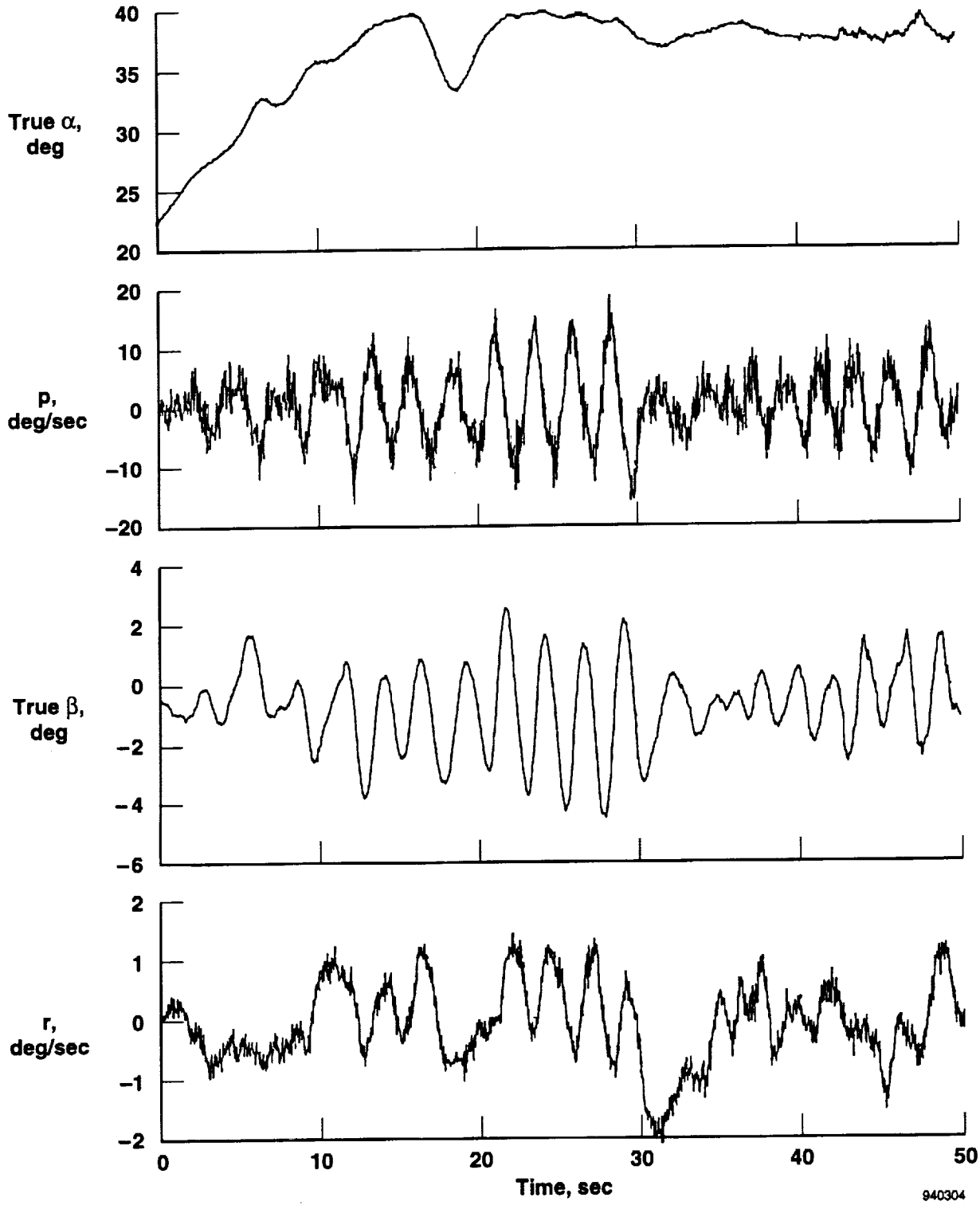

Figure 10. Wing rock time history.

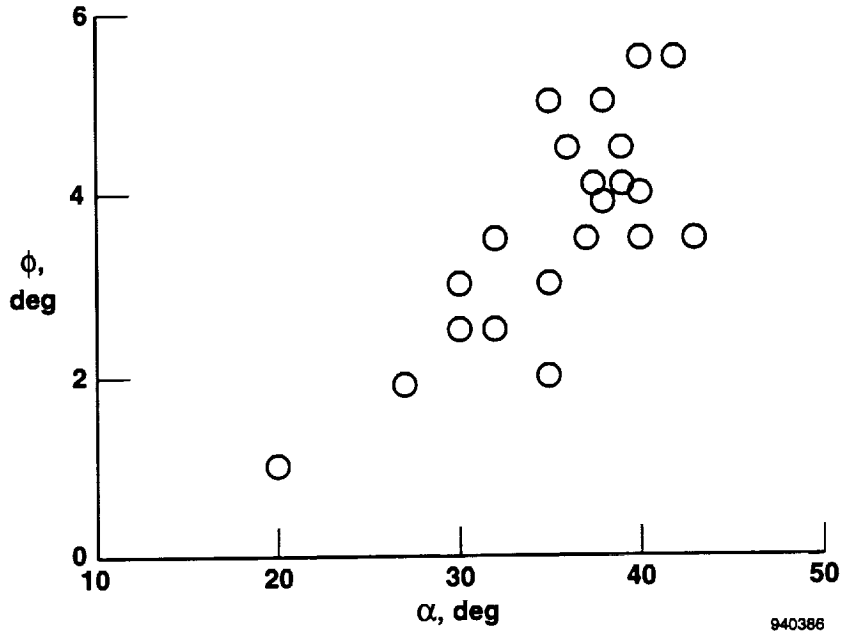

Figure 11. Magnitude of bank angle oscillation as a function of angle of attack during wing rock.

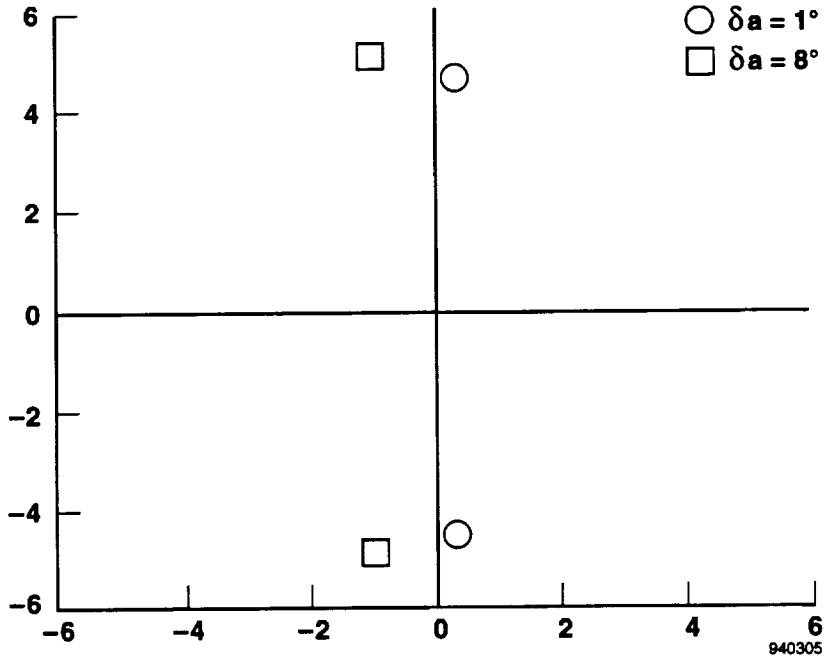

Figure 12. Open-loop dutch roll pole locations.

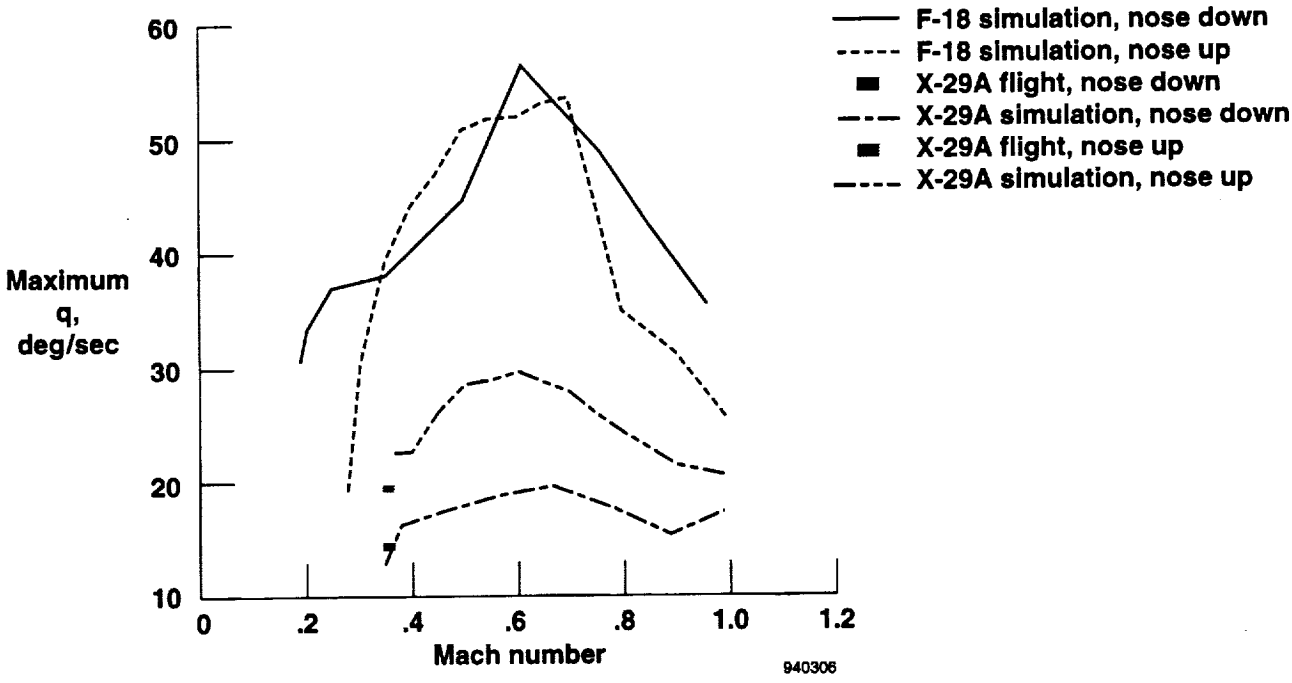

Figure 13. Pitch rate comparison.

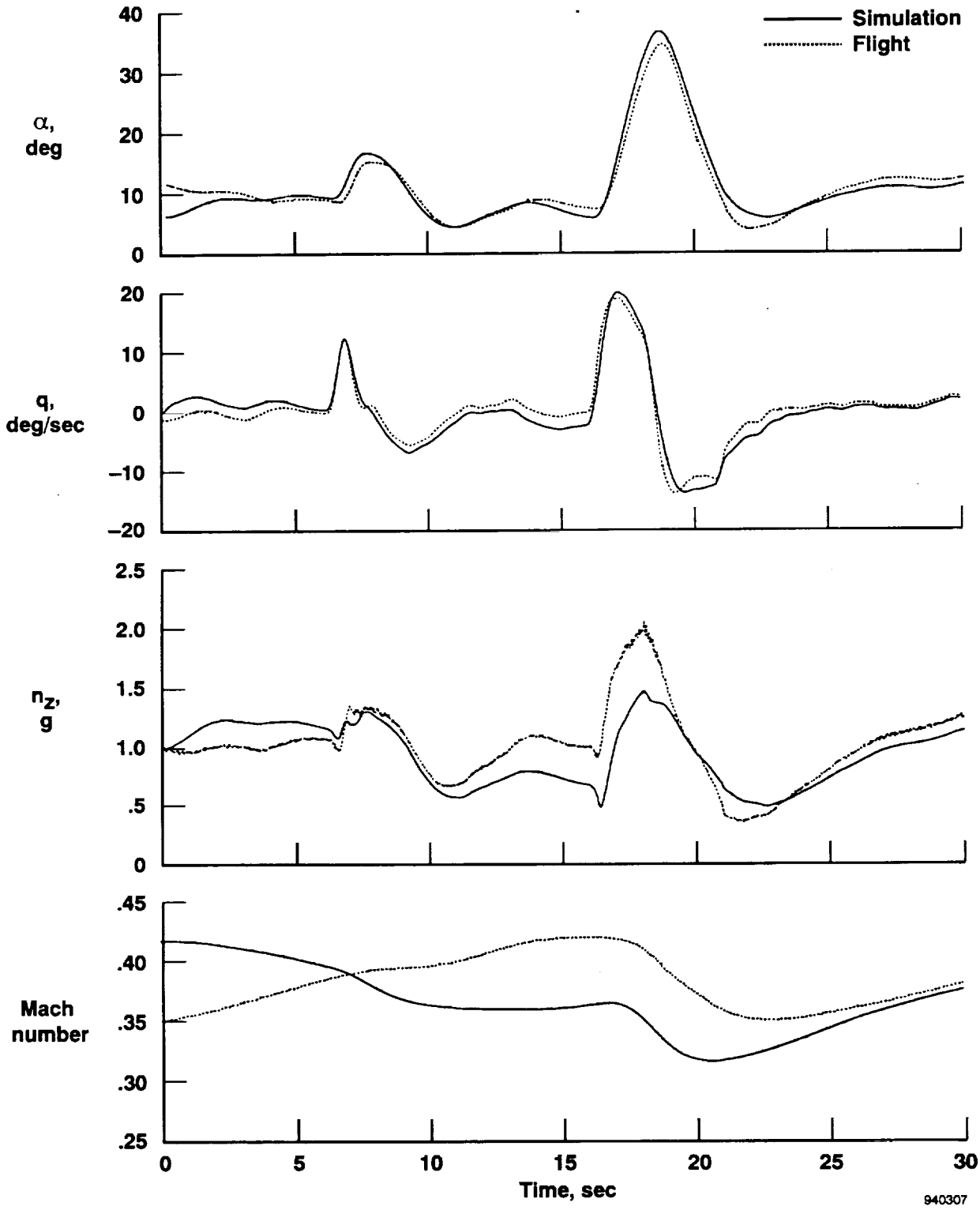

Figure 14. Simulation match to flight data for pitching maneuver.

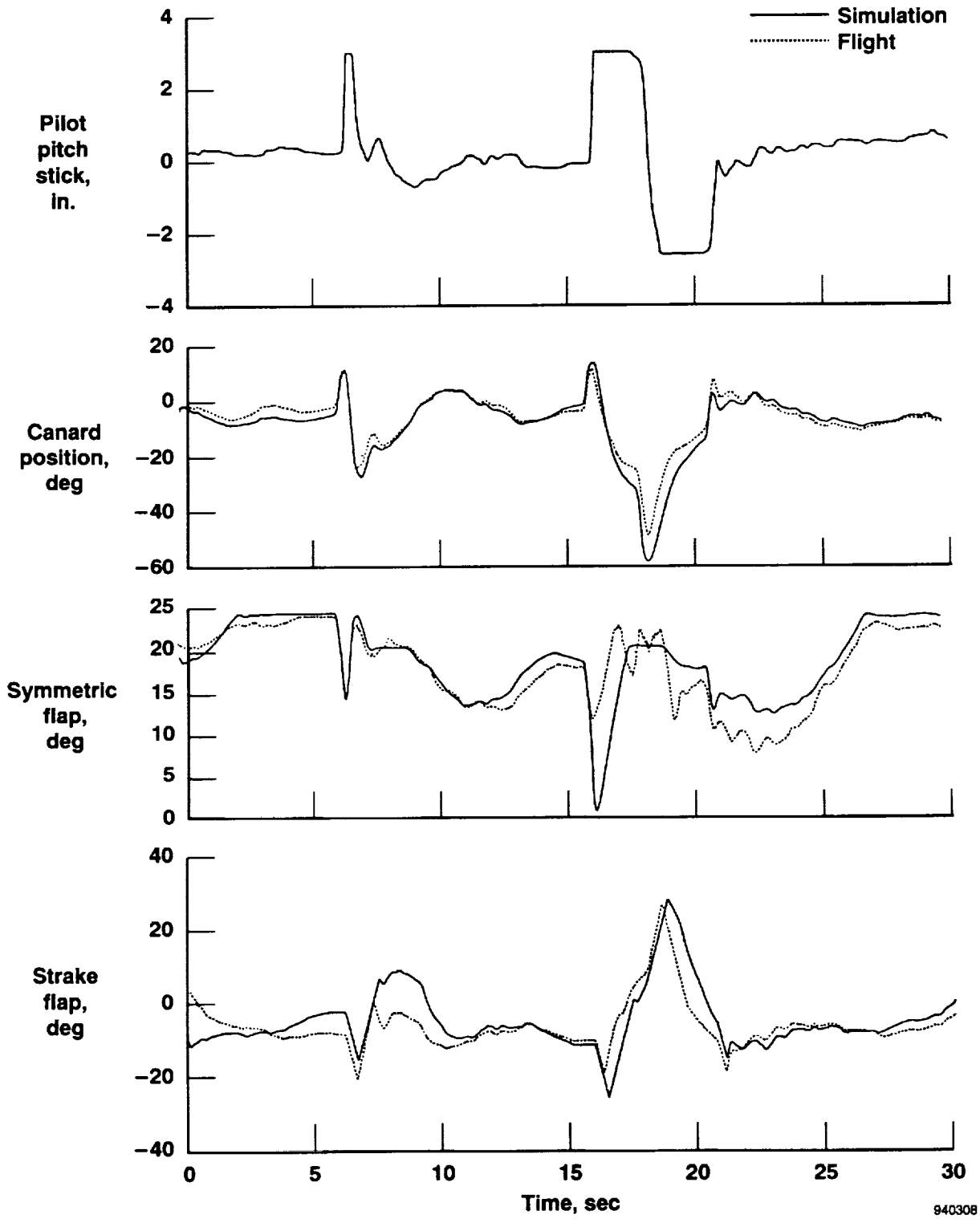

Figure 14. Concluded.

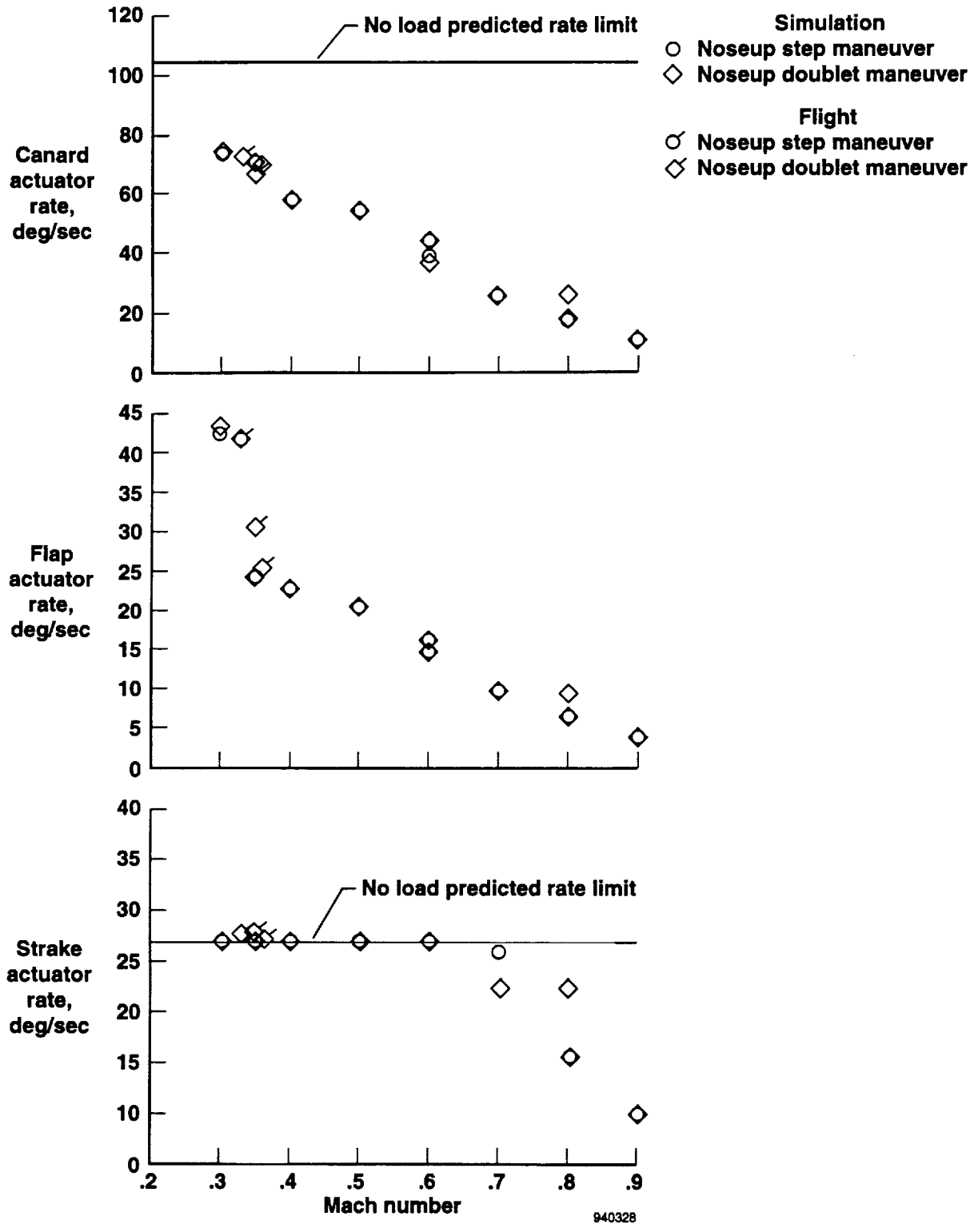

(a) Noseup maneuvers.

Figure 15. Surface rates during pitching steps.

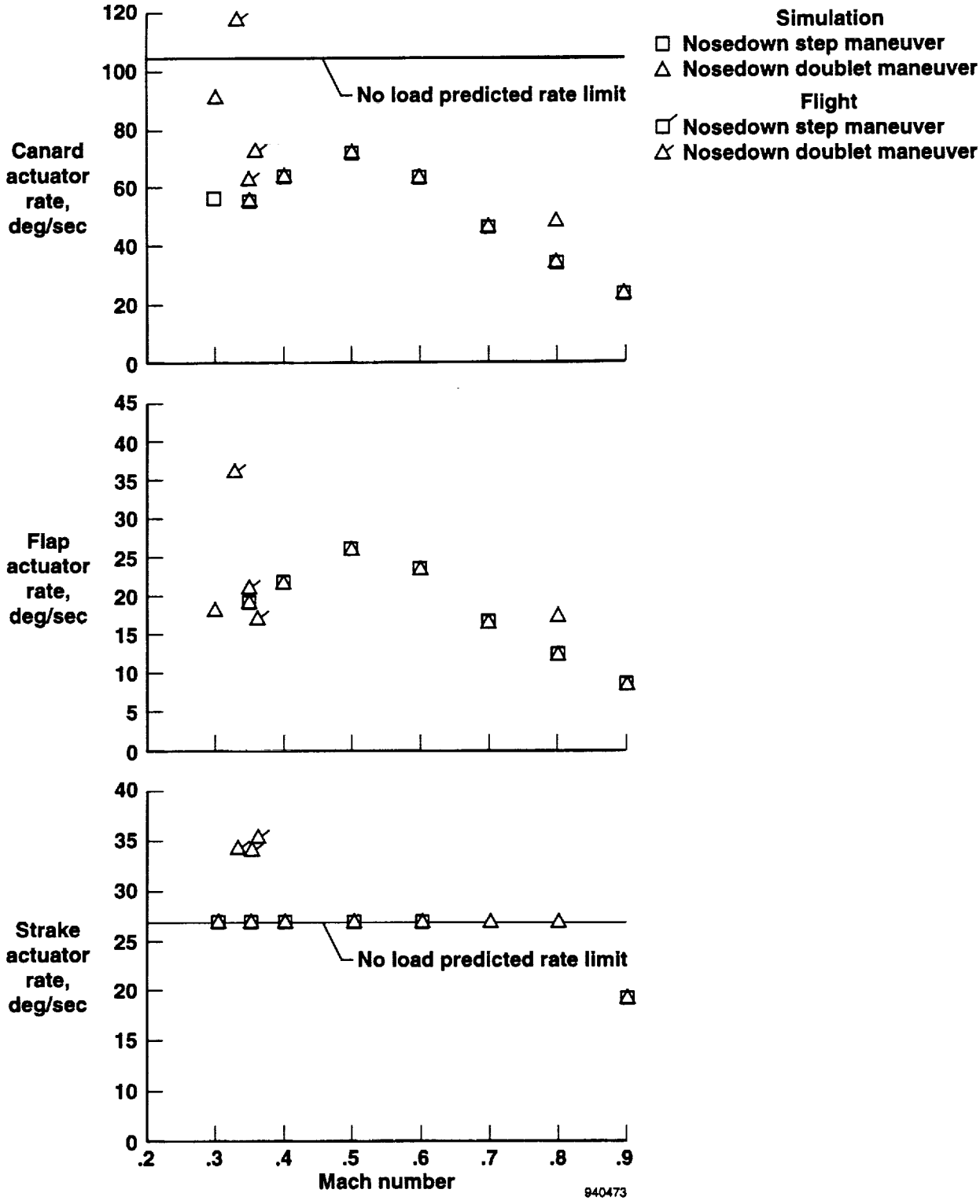

(b) Nosedown maneuvers.

Figure 15. Concluded.

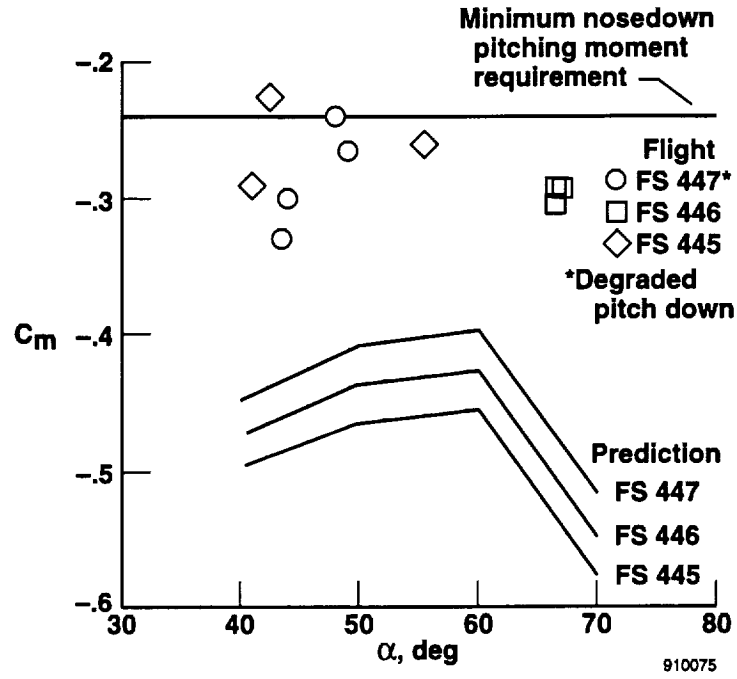

Figure 16. Minimum nosedown aerodynamic pitching moment.

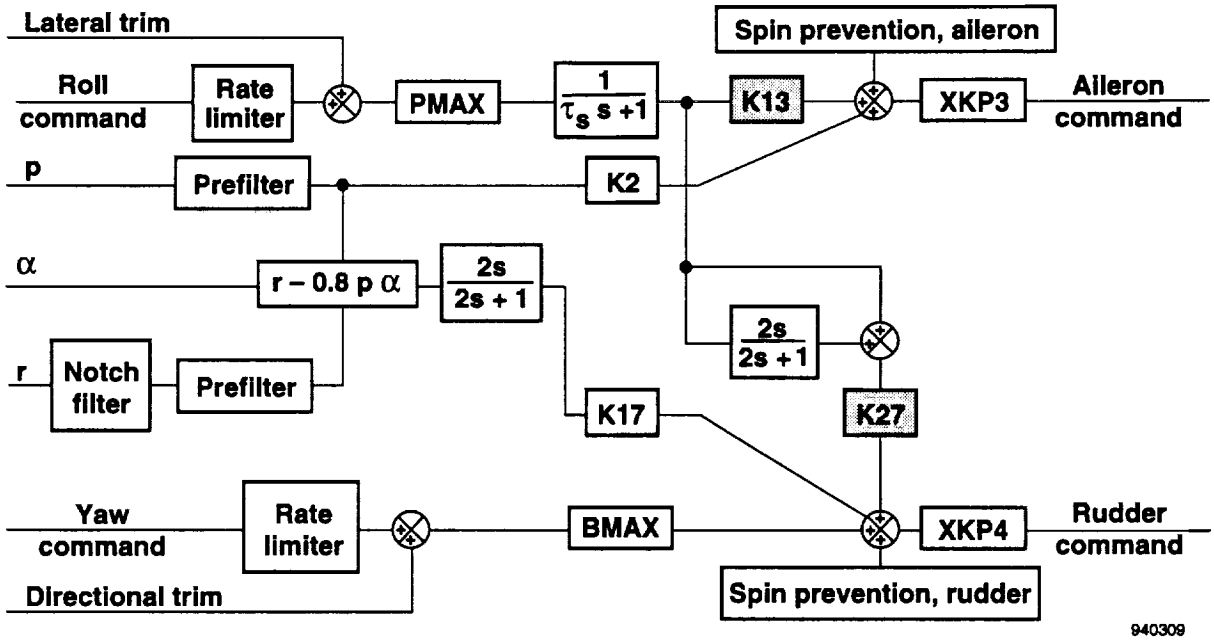

Figure 17. The X-29A high-angle-of-attack lateral–directional flight control system with variable gains highlighted.

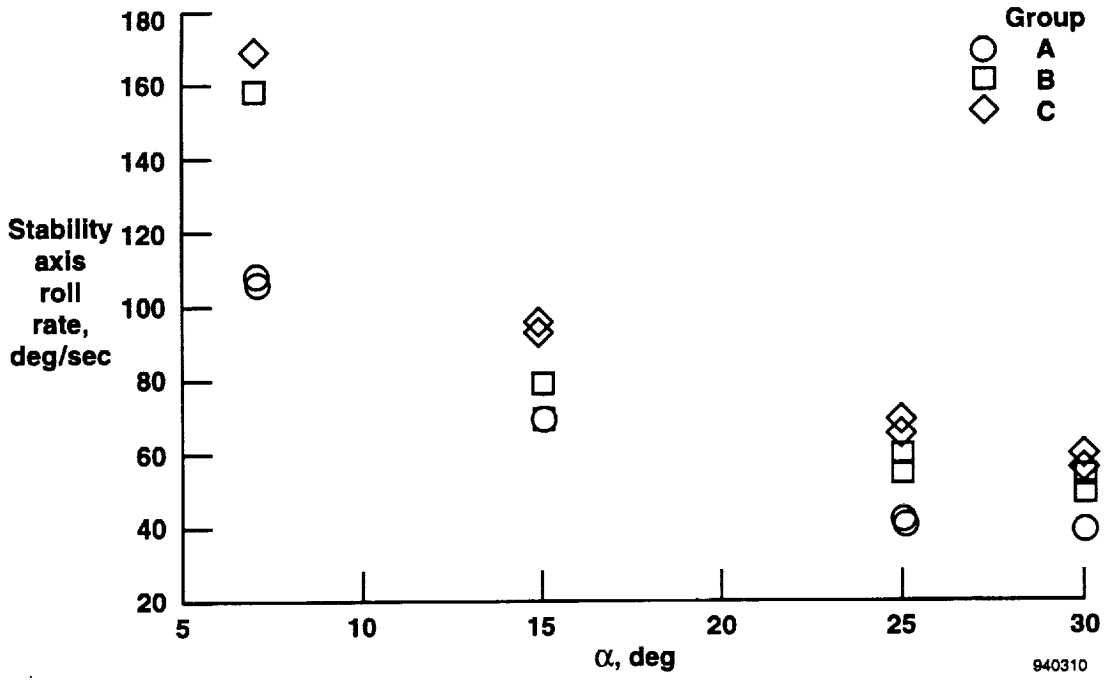

Figure 18. Stability axis roll rate (at 200 kn and an altitude of 20,000 ft) as a function of angle of attack.

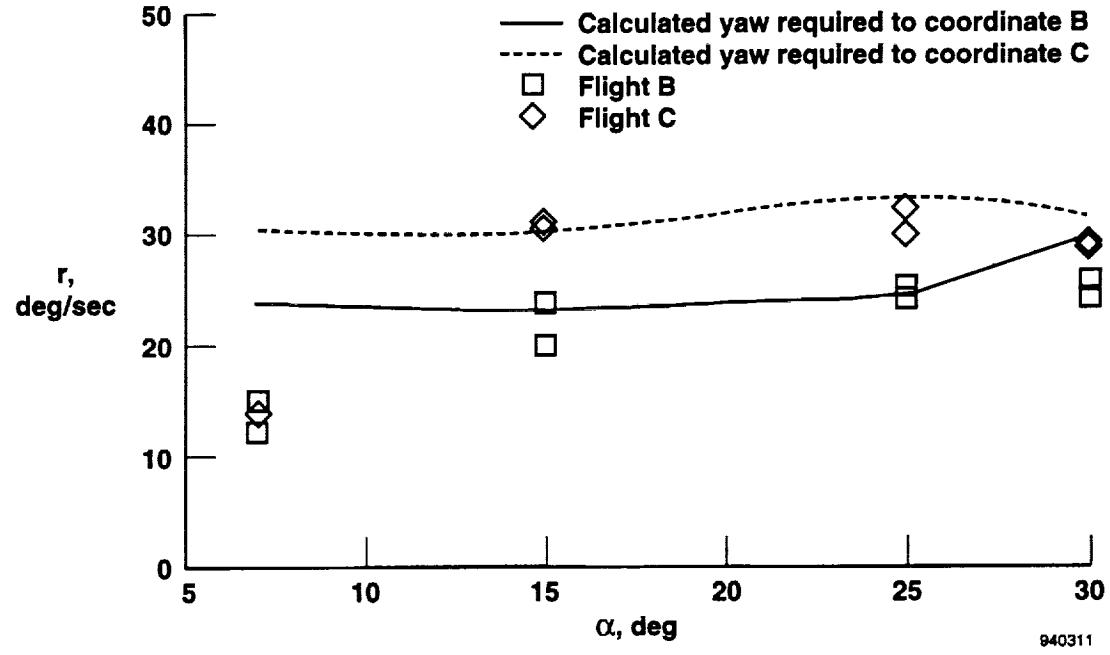

Figure 19. Body axis yaw rate required (at 200 kn and an altitude of 20,000 ft) for coordination of stability axis roll rate of figure 18.

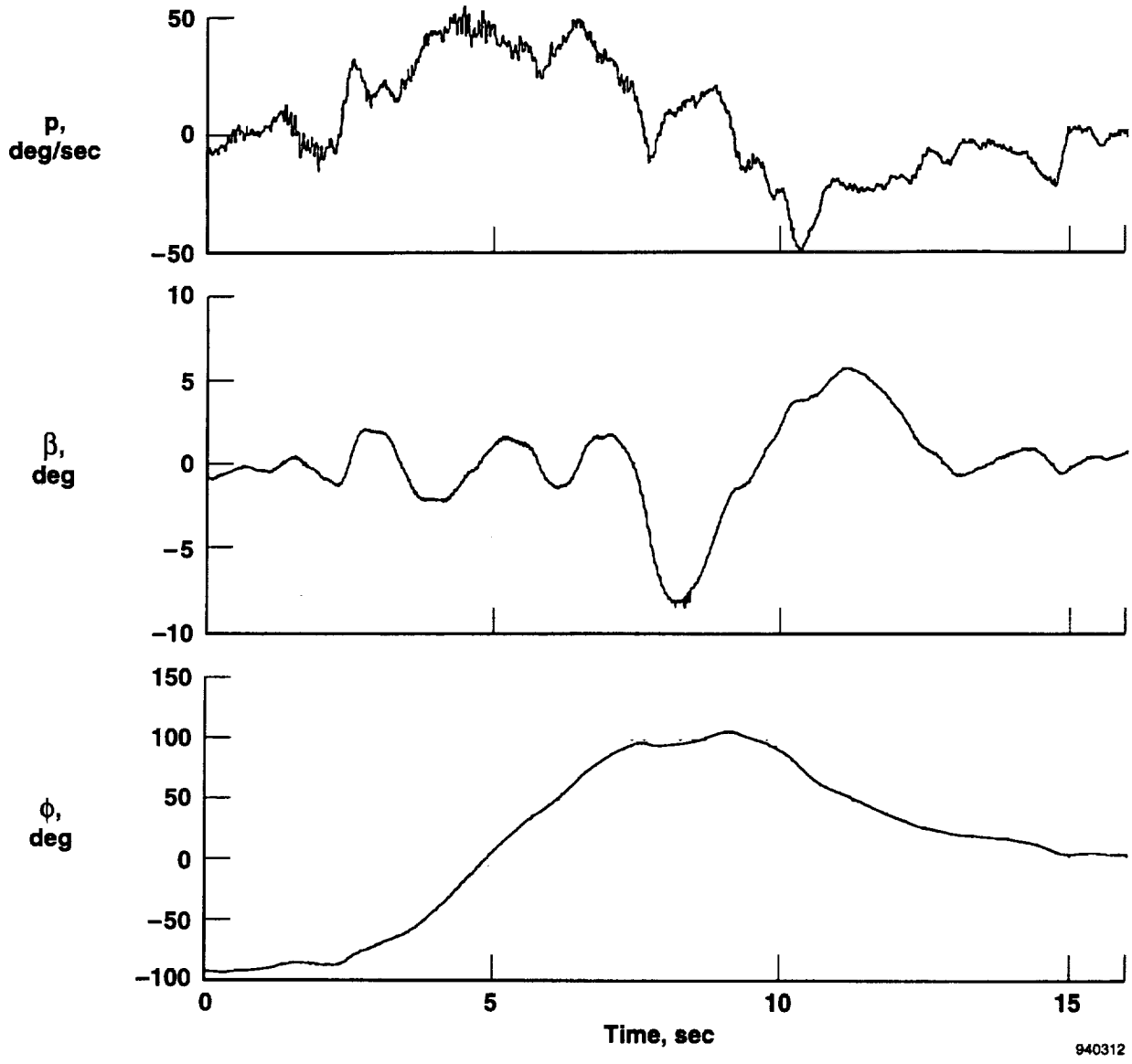

Figure 20. Effect of sideslip on roll coordination for a typical bank angle maneuver.

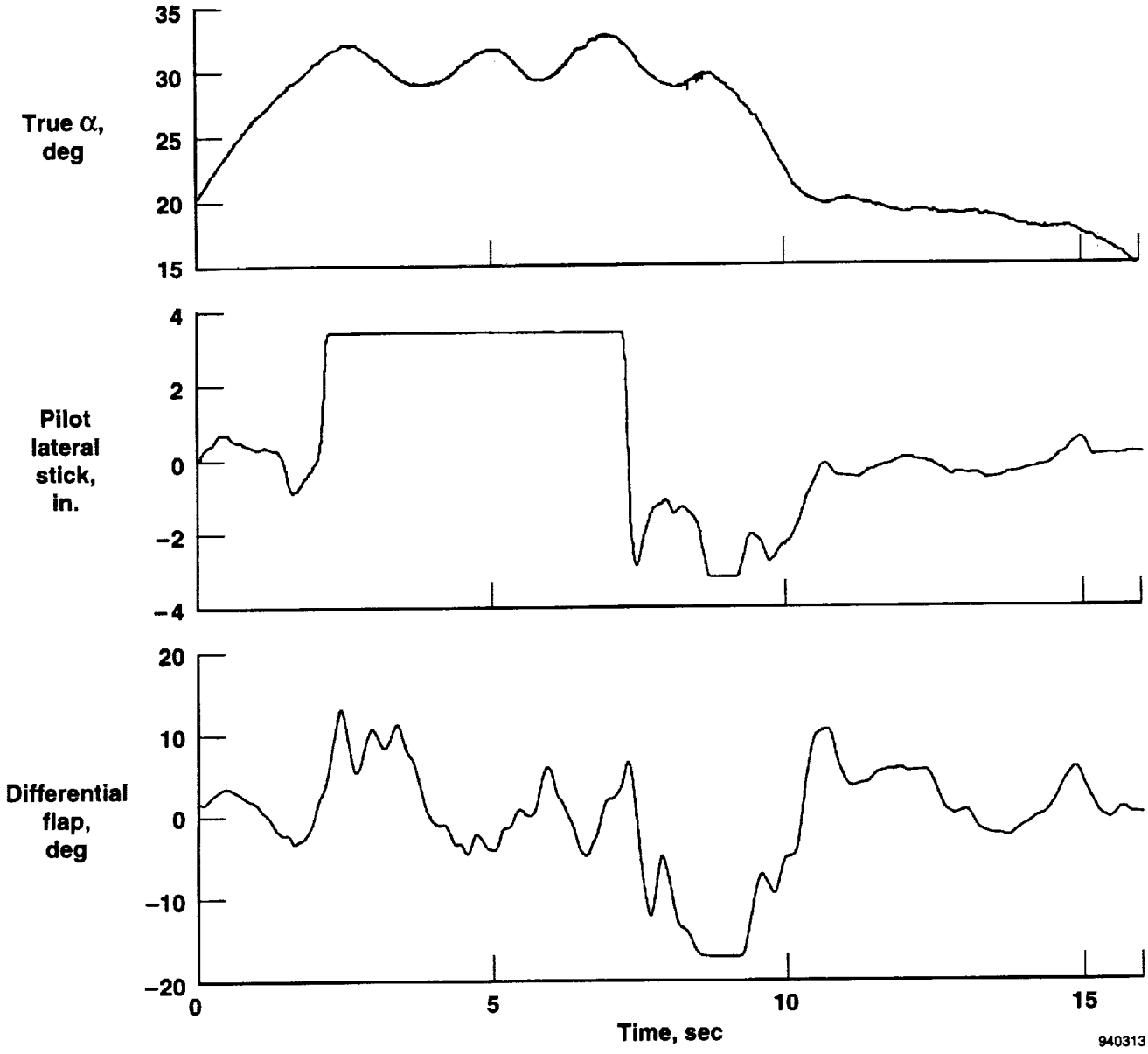

Figure 20. Concluded.

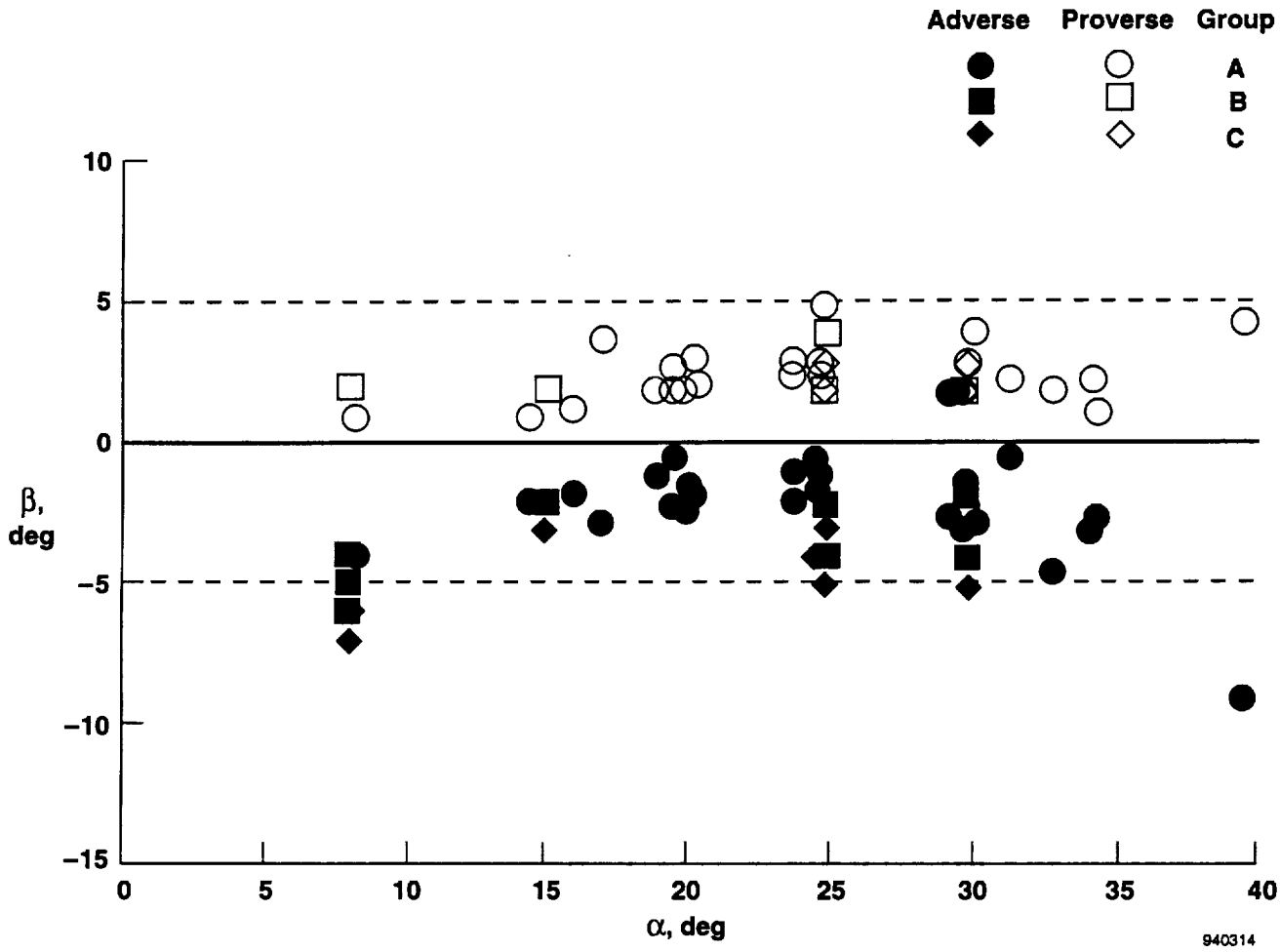

Figure 21. Roll coordination data (all data represented as if roll were negative (to the left)).

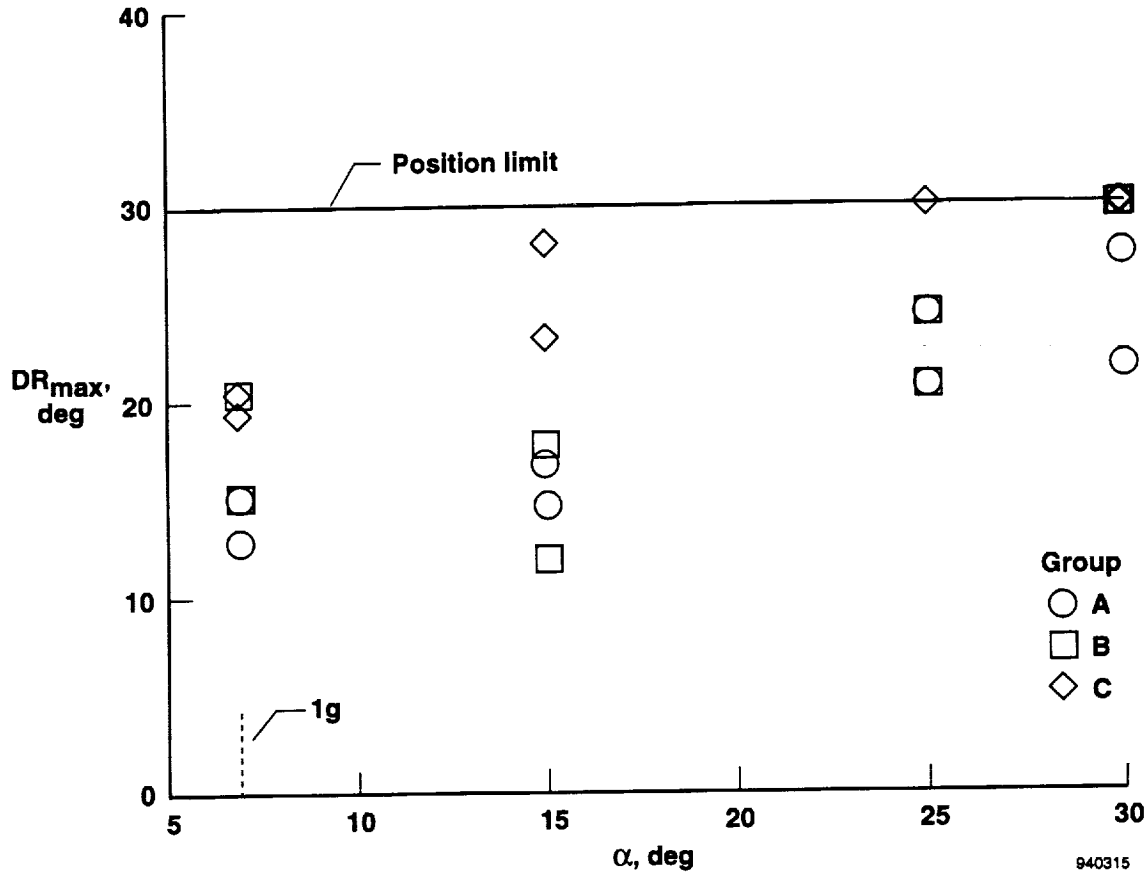

Figure 22. Maximum rudder deflection during 180° roll captures at 200 kn equivalent airspeed.

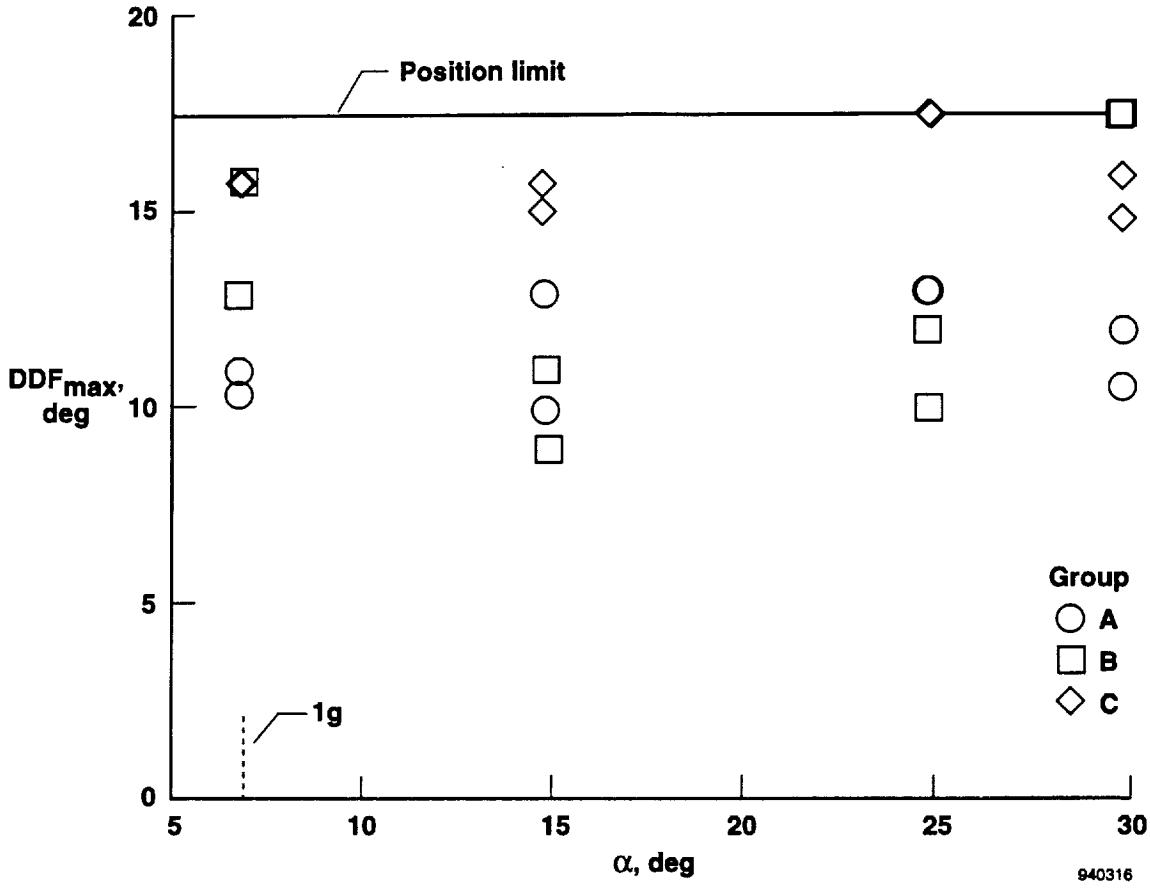

Figure 23. Maximum aileron deflection during 180° roll captures at 200 kn equivalent airspeed.

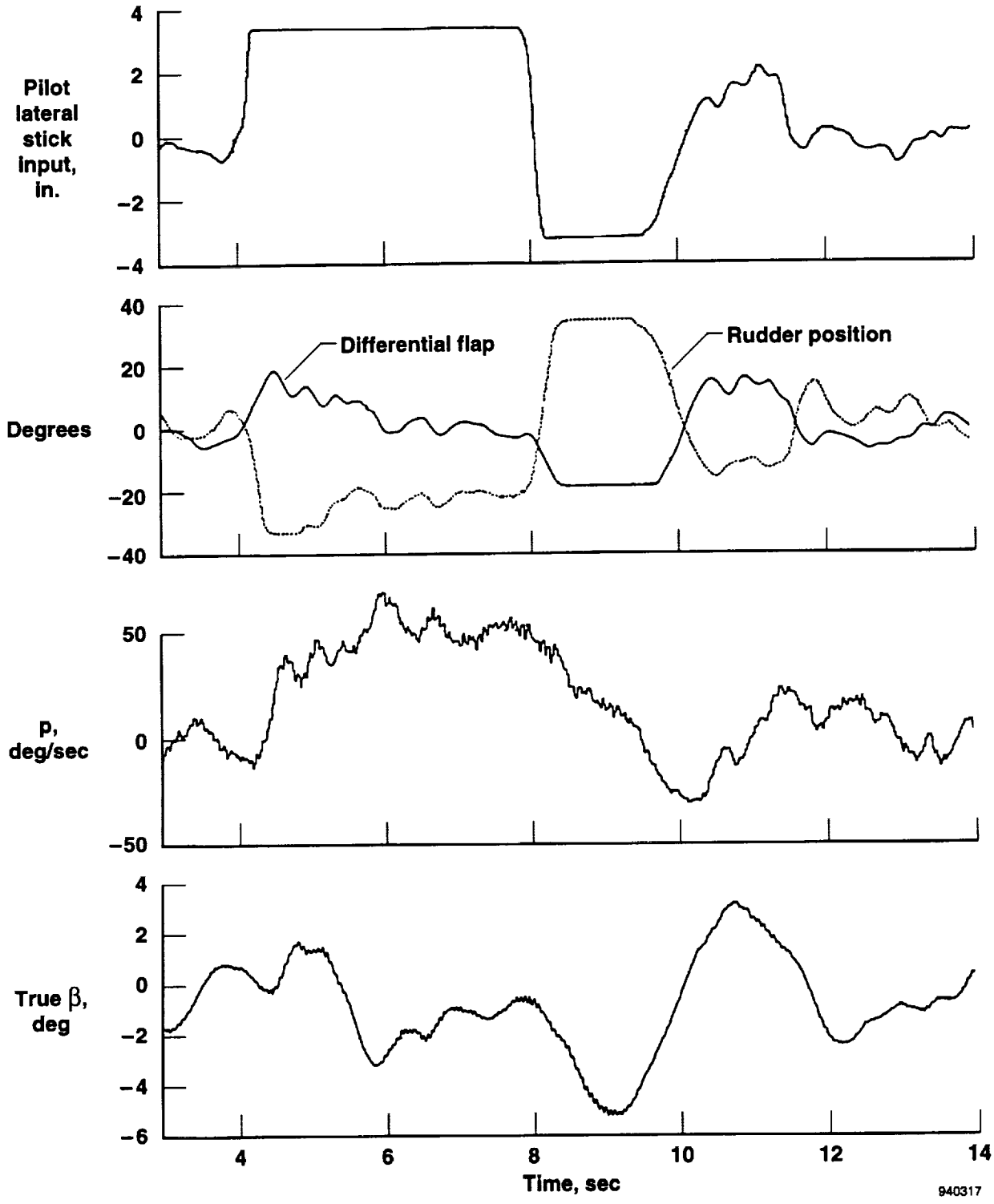

Figure 24. Angle of sideslip buildup during position limiting.

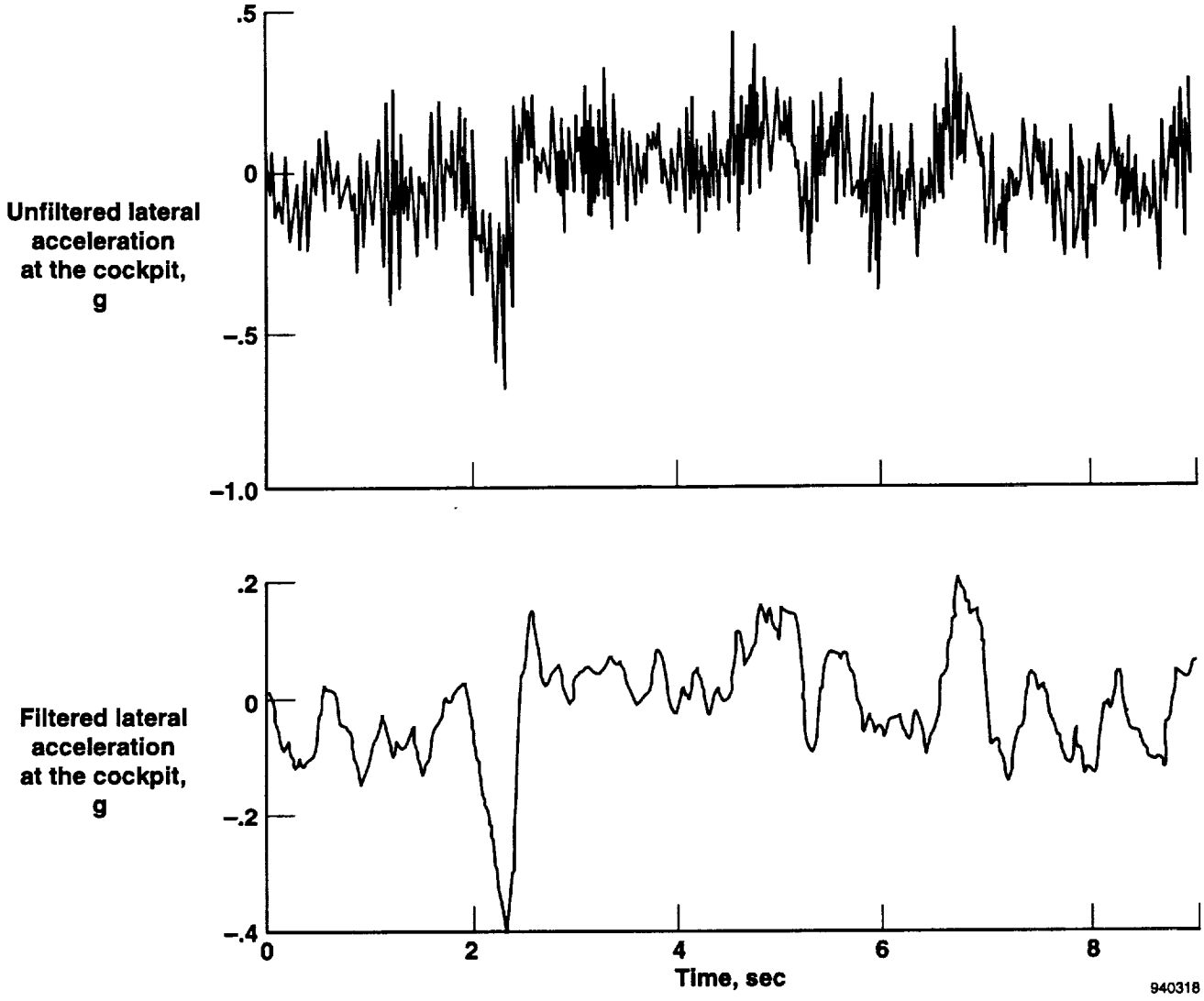

Figure 25. Effects of filtering on lateral acceleration components.

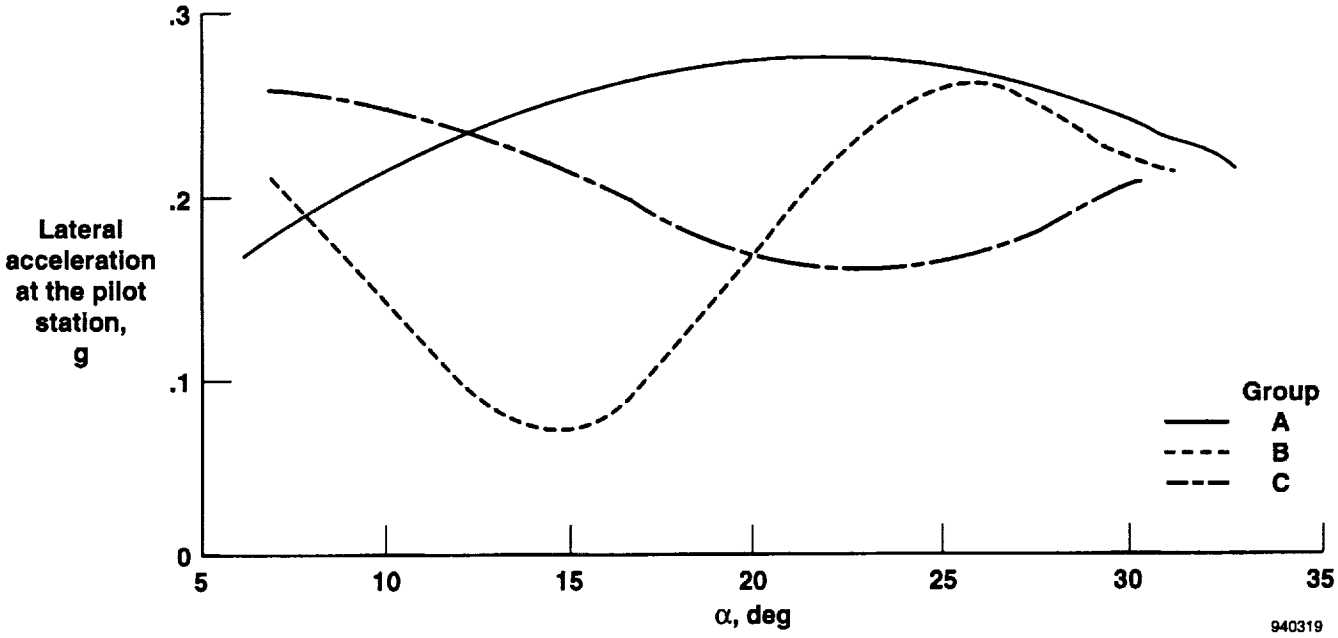

Figure 26. Cockpit lateral acceleration at roll initiation.

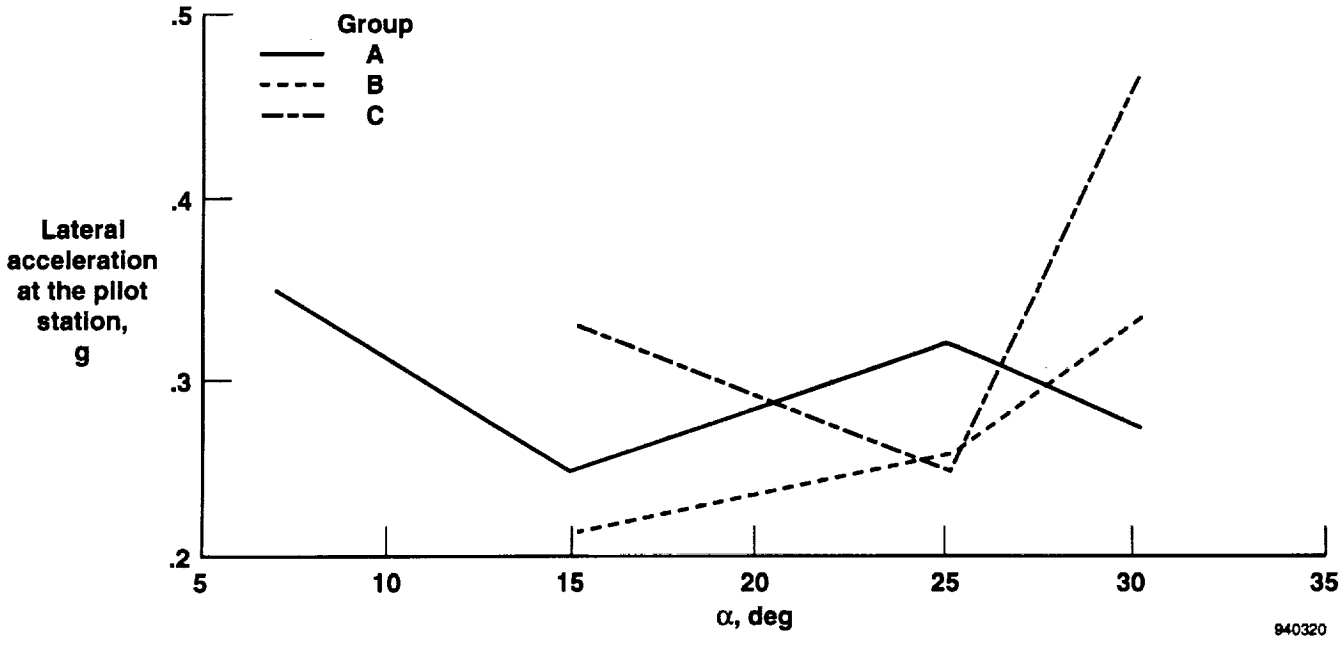

Figure 27. Largest cockpit lateral acceleration components during maneuver.

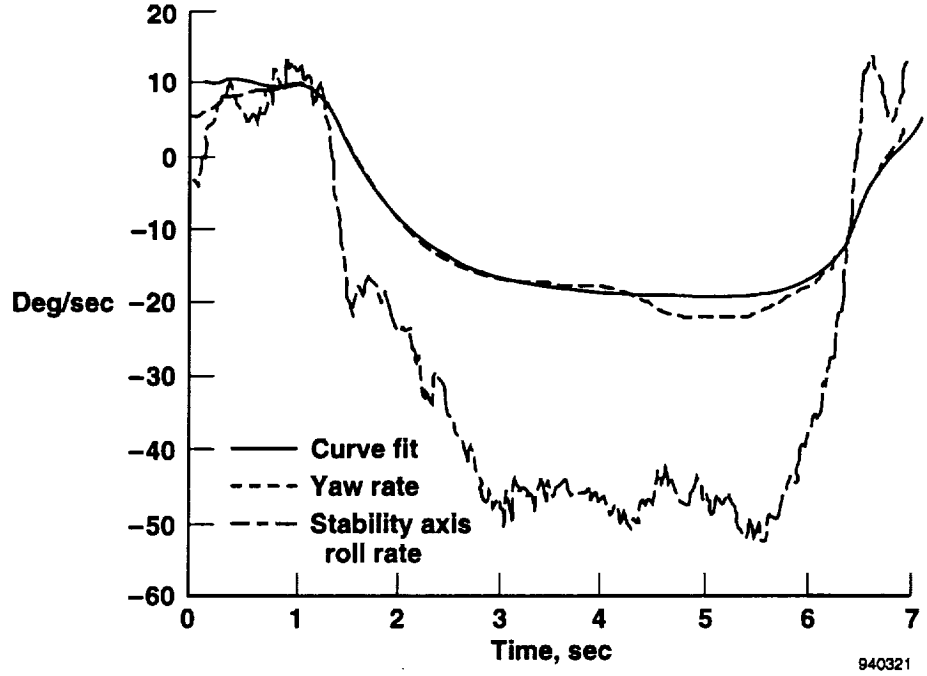

(a) Fit of body axis yaw rate.

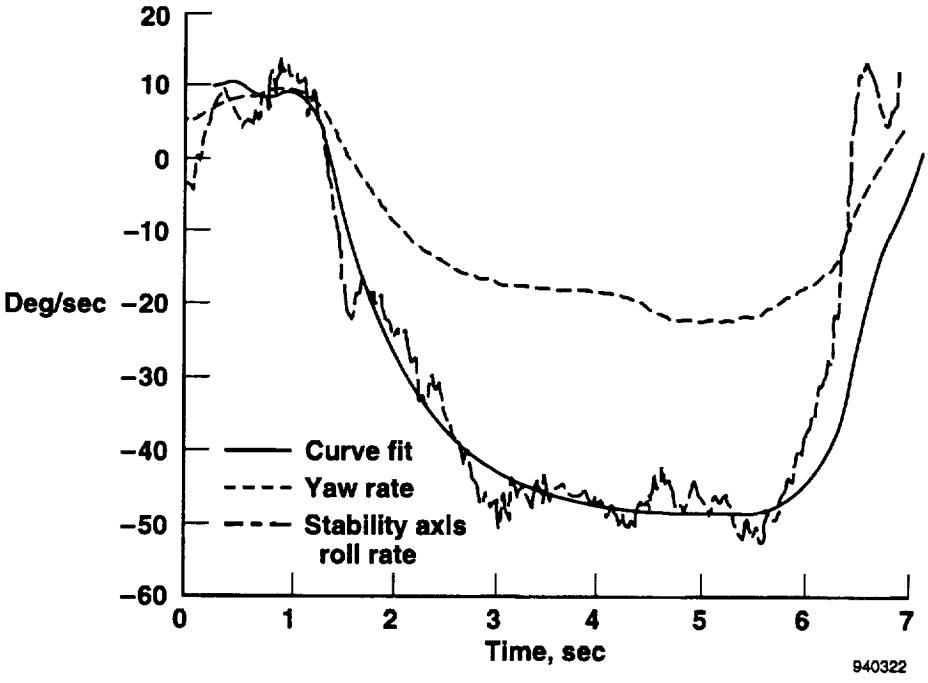

(b) Fit of stability axis roll rate.

Figure 28. Flight data fit to determine roll mode time constant.

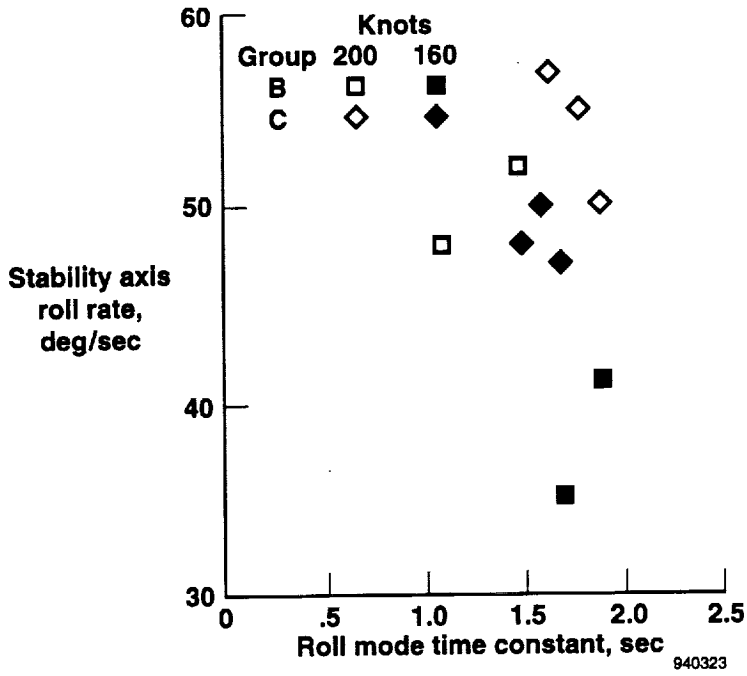

Figure 29. Roll mode time constant as a function of stability axis roll rate at a 30° angle of attack.

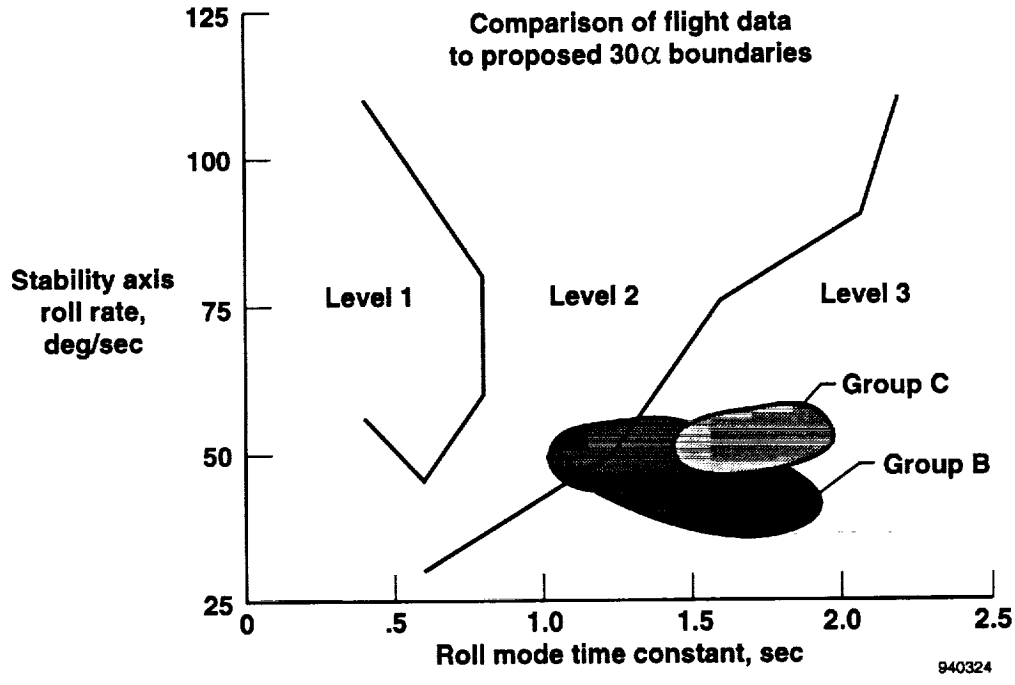

Figure 30. Proposed criteria for a 30° angle of attack.

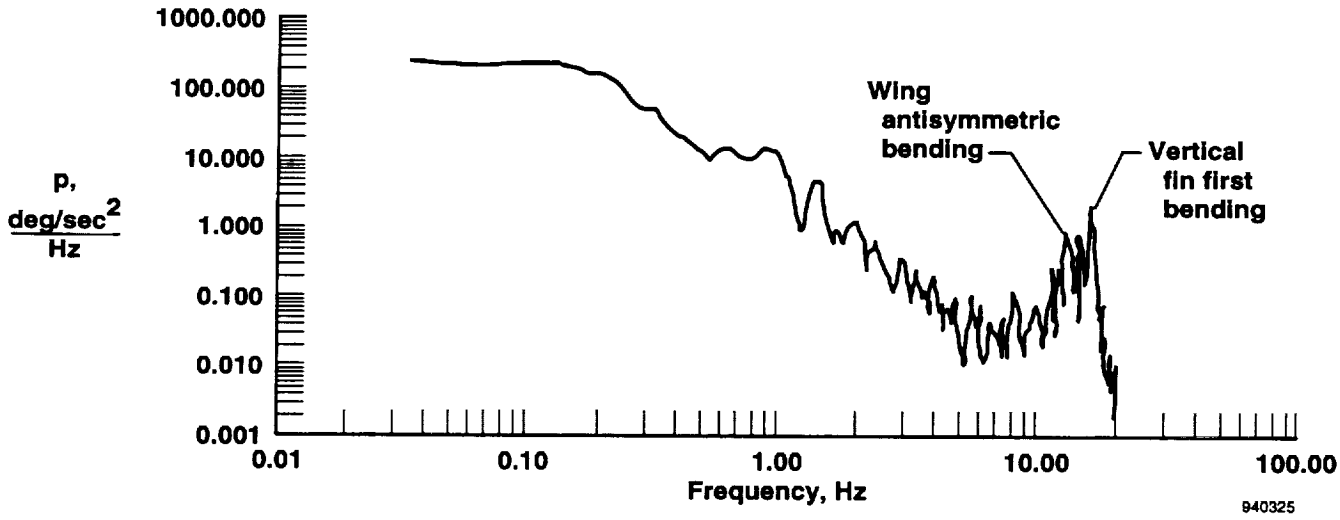

Figure 31. Roll rate gyroscope signal power spectral density.

SIMULATION DATA DISPLAY:

P	0.00	PDOT	0.00	AMCH	0.45				
Q	6.11	QDOT	0.00	QBAR	136.	NORMAL MODE			
R	0.00	RDOT	0.00	GMA	-5.00				
V	463.	VDOT	0.00	DEL	0.00				
ALP	15.00	ALPD	0.00	UB	447.				
BTA	0.00	BTAD	0.00	VB	0.				
THA	10.00	THAD	6.11	WB	120.				
PSI	0.00	PSID	0.00						
PHI	0.00	PHID	0.00	ANX	0.57				
H	20000.	HDOT	-40.	ANY	0.00				
X	0.00	XDOT	461.	ANZ	-2.46	VEAS	200.		
Y	0.00	YDOT	0.	AN	2.46	VCAS	203.	CL	0.00000
DAP	------	DEP	--------	DRP	------	DC	-4.41	CM	0.10208
DFL	20.74	DFR	20.74	DR	0.00	DST	8.79	CN	0.00000
ERP	1.000	AIX	4547.	AIY	51888.	AIZ	57063.	CD	0.36395
PLA	130.000	DELX	0.30	DELZ	0.12	AIXZ	2559.	CY	0.00000
THS	8051.	EWT	--------	FWT	------	TWT	------	CLFT	1.48527

FA

VTOT	ALPHA	Q	THETA	BETA	P	R	PHI
-0.7739E-01	-0.8229E+02	-0.7478E+00	-0.3199E+02	0.7000E-01	-0.9334E-08	0.0000E+00	0.5764E-08
-0.4778E-03	-0.2928E+00	0.9940E+00	0.6048E-02	0.3889E-07	-0.7531E-10	0.0000E+00	0.4651E-10
0.4048E-03	0.4035E+01	-0.2314E+00	-0.1655E-03	0.2026E-05	-0.5125E-08	0.0000E+00	0.3165E-08
0.0000E+00	0.0000E+00	0.1000E+01	0.0000E+00	0.0000E+00	0.0000E+00	0.0000E+00	0.0000E+00
A = 0.0000E+00	0.0000E+00	0.0000E+00	0.0000E+00	-0.1274E+00	0.2591E+00	-0.9625E+00	0.6837E-01
0.0000E+00	0.0000E+00	0.0000E+00	0.0000E+00	-0.2283E+02	-0.1091E+01	0.1151E+01	0.3177E-07
0.0000E+00	0.0000E+00	0.0000E+00	0.0000E+00	0.2359E+01	-0.1657E+00	-0.4863E-01	-0.1813E-07
0.0000E+00	0.0000E+00	0.0000E+00	0.0000E+00	0.0000E+00	0.1000E+01	0.1763E+00	0.1879E-01

FH

VTOT	ALPHA	Q	THETA	BETA	P	R	PHI
0.1046E-01	0.4187E+01	0.1039E+00	-0.2665E-03	-0.1478E+00	-0.7063E-02	0.8140E-02	-0.5875E-09
C = 0.1046E-01	0.4187E+01	0.1039E+00	-0.2665E-03	-0.1478E+00	-0.7063E-02	0.8140E-02	-0.5875E-09
0.0000E+00	0.0000E+00	0.0000E+00	0.0000E+00	-0.1140E+01	0.4177E-01	0.1713E-01	-0.1747E-02

FB

DC	DSF	DSTF	PLA	DDF	DR
-0.1753E+00	-0.2178E+00	-0.7165E-01	0.1282E+00	-0.1430E-11	0.4567E-09
-0.5187E-03	-0.1089E-02	-0.3993E-03	-0.7423E-04	-0.1154E-13	0.3685E-11
0.4279E-01	-0.1264E-01	-0.2349E-01	-0.1069E-02	-0.7853E-12	0.2508E-09
0.0000E+00	0.0000E+00	0.0000E+00	0.0000E+00	0.0000E+00	0.0000E+00
B = -0.1046E-10	-0.1369E-11	-0.6718E-12	0.7865E-13	-0.5023E-03	0.4928E-03
0.6306E-08	0.1859E-09	0.9124E-10	-0.1068E-10	0.4195E+00	0.1057E+00
0.3045E-09	-0.1061E-09	-0.5206E-10	0.6095E-11	0.1706E-01	-0.2841E-01
0.0000E+00	0.0000E+00	0.0000E+00	0.0000E+00	0.0000E+00	0.0000E+00

FF

DC	DSF	DSTF	PLA	DDF	DR
0.7251E-02	0.1728E-01	0.6871E-02	0.3363E-04	0.2716E-02	0.6845E-03
D = 0.7251E-02	0.1728E-01	0.6871E-02	0.3363E-04	0.2716E-02	0.6845E-03
-0.3660E-09	-0.2244E-10	-0.1102E-10	0.1290E-11	-0.2147E-01	0.4517E-02

Figure A-1. Linear matrices.

SIMULATION DATA DISPLAY:

P	0.00	PDOT	0.00	AMCH	0.45				
Q	9.86	QDOT	0.00	QBAR	136.	NORMAL MODE			
R	0.00	RDOT	0.00	GMA	-50.00				
V	463.	VDOT	0.00	DEL	0.00				
ALP	25.00	ALPD	0.00	UB	419.				
BTA	0.00	BTAD	0.00	VB	0.				
THA	-25.00	THAD	9.86	WB	195.				
PSI	0.00	PSID	0.00						
PHI	0.00	PHID	0.00	ANX	0.62				
H	20000.	HDOT	-354.	ANY	0.00				
X	0.00	XDOT	297.	ANZ	-3.15	VEAS	200.		
Y	0.00	YDOT	0.	AN	3.15	VCAS	203.	CL	0.00000
DAP	------	DEP	--------	DRP	------	DC	-11.40	CM	0.11905
DFL	20.74	DFR	20.74	DR	0.00	DST	19.53	CN	0.00000
ERP	1.000	AIX	4547.	AIY	51888.	AIZ	57063.	CD	0.75610
PLA	130.000	DELX	0.30	DELZ	0.12	AIXZ	2559.	CY	0.00000
THS	7791.	EWT	--------	FWT	------	TWT	------	CLFT	1.80273

A = FA

VTOT	ALPHA	Q	THETA	BETA	P	R	PHI
-0.1673E+00	-0.1368E+03	-0.1221E+01	-0.2065E+02	0.1442E+00	0.2825E-03	0.1319E-03	0.4294E-06
-0.4936E-03	-0.3261E+00	0.9943E+00	0.5316E-01	0.1176E-06	-0.2850E-06	-0.1331E-06	-0.3897E-09
0.2451E-03	0.2197E+01	-0.1998E+00	-0.1454E-02	0.2567E-04	0.8359E-04	0.3905E-04	0.1274E-06
0.0000E+00	0.0000E+00	0.1000E+01	0.0000E+00	0.0000E+00	0.0000E+00	0.0000E+00	0.0000E+00
-0.9687E-12	0.2672E-08	-0.5384E-09	-0.5207E-09	-0.8656E-01	0.4188E+00	-0.9024E+00	0.6292E-01
-0.4119E-10	-0.3355E-05	-0.6204E-08	-0.6001E-08	-0.3560E+02	0.1325E+01	-0.1078E+01	0.1388E-06
0.5082E-10	-0.1325E-06	0.7654E-08	0.7403E-08	0.7420E+00	-0.1317E+00	0.2307E-01	-0.2581E-06
0.0000E+00	0.0000E+00	0.0000E+00	0.0000E+00	0.0000E+00	0.1000E+01	-0.4663E+00	-0.2023E-01

C = FH

VTOT	ALPHA	Q	THETA	BETA	P	R	PHI
0.1350E-01	0.4901E+01	0.1070E+00	0.1114E-02	-0.2305E+00	0.8576E-02	-0.5867E-02	-0.3724E-08
0.1350E-01	0.4901E+01	0.1070E+00	0.1114E-02	-0.2305E+00	0.8576E-02	-0.5867E-02	-0.3724E-08
-0.5164E-10	0.1522E-06	-0.7777E-08	-0.7522E-08	-0.7072E-01	-0.9984E-01	0.9662E-01	-0.1607E-02

B = FB

DC	DSF	DSTF	PLA	DDF	DR
-0.3152E+00	-0.1109E+00	-0.1223E+00	0.1203E+00	0.7325E-09	0.7040E-09
-0.6335E-03	0.3419E-04	-0.4144E-03	-0.1212E-03	-0.7622E-12	-0.7138E-12
0.3929E-01	-0.3961E-02	-0.1891E-01	-0.1068E-02	0.2166E-09	0.2083E-09
0.0000E+00	0.0000E+00	0.0000E+00	0.0000E+00	0.0000E+00	0.0000E+00
0.1137E-08	0.5691E-10	0.4202E-10	-0.4919E-11	-0.5015E-03	0.3623E-03
0.7641E-07	0.5431E-09	0.4010E-09	-0.4694E-10	0.2268E+00	0.6077E-01
-0.7185E-07	-0.1009E-08	-0.7453E-09	0.8726E-10	0.1949E-01	-0.2421E-01
0.0000E+00	0.0000E+00	0.0000E+00	0.0000E+00	0.0000E+00	0.0000E+00

D = FF

DC	DSF	DSTF	PLA	DDF	DR
0.1114E-01	0.1137E-02	0.7609E-02	0.3331E-04	0.1469E-02	0.3935E-03
0.1114E-01	0.1137E-02	0.7609E-02	0.3331E-04	0.1469E-02	0.3935E-03
0.1609E-07	0.8321E-09	0.6143E-09	-0.7192E-10	-0.1523E-01	0.3979E-02

Figure A-1. Continued.

SIMULATION DATA DISPLAY:

P	0.00	PDOT	0.00	AMCH	0.45			
Q	9.21	QDOT	0.00	QBAR	136.	NORMAL MODE		
R	0.00	RDOT	0.00	GMA	0.00			
V	463.	VDOT	-41.21	DEL	0.00			
ALP	30.00	ALPD	0.00	UB	401.			
BTA	0.00	BTAD	0.00	VB	0.			
THA	30.00	THAD	9.21	WB	231.			
PSI	0.00	PSID	0.00					
PHI	0.00	PHID	0.00	ANX	0.55			
H	20000.	HDOT	0.	ANY	0.00			
X	0.00	XDOT	463.	ANZ	-3.51	VEAS 200.		
Y	0.00	YDOT	0.	AN	3.51	VCAS 203.	CL	0.00000
DAP	------	DEP	--------	DRP	------	DC -15.34	CM	0.12021
DFL	20.74	DFR	20.74	DR	0.00	DST 19.95	CN	0.00000
ERP	1.000	AIX	4547.	AIY	51888.	AIZ 57063.	CD	1.00322
PLA	130.000	DELX	0.30	DELZ	0.12	AIXZ 2559.	CY	0.00000
THS	6028.	EWT	--------	FWT	------	TWT ------	CLFT	1.93459

A =

VTOT	ALPHA	Q	THETA	BETA	P	R	PHI
-0.2321E+00	-0.1477E+03	-0.1445E+01	-0.3211E+02	0.5089E-01	-0.1245E-01	-0.4077E-02	-0.2787E-04
-0.6005E-03	-0.2519E+00	0.9946E+00	-0.1822E-08	-0.8538E-06	-0.1000E-03	-0.3275E-04	-0.2039E-06
0.1709E-03	0.2352E+01	-0.3633E+00	0.4329E-07	0.3748E-04	0.2252E-02	0.7372E-03	0.5043E-05
0.0000E+00	0.0000E+00	0.1000E+01	0.0000E+00	0.0000E+00	0.0000E+00	0.0000E+00	0.0000E-00
0.2597E-11	-0.8516E-07	0.1443E-08	0.9334E-09	0.7681E-01	0.4956E+00	-0.8576E+00	0.6[illegible]E-01
0.1137E-07	0.2866E-04	0.1712E-05	0.1107E-05	-0.3490E+02	0.1765E+01	-0.3448E+01	-0.[illegible]49E-03
0.5337E-09	0.4847E-05	0.8038E-07	0.5197E-07	0.1223E+01	-0.9104E-01	-0.2021E+00	-0.[illegible]63E-05
0.0000E+00	0.0000E+00	0.0000E+00	0.0000E+00	0.0000E+00	0.1000E+01	0.5774E+00	0.9[illegible]3E-01

C =

VTOT	ALPHA	Q	THETA	BETA	P	R	PHI
0.1555E-01	0.5155E+01	0.1115E+00	-0.8867E-03	-0.2260E+00	0.1279E-01	-0.2084E-01	0.2[illegible]87E-05
0.1555E-01	0.5155E+01	0.1115E+00	-0.8867E-03	-0.2260E+00	0.1279E-01	-0.2084E-01	0.2[illegible]87E-05
-0.2503E-09	-0.2313E-05	-0.3770E-07	-0.2438E-07	0.1056E+01	-0.1229E+00	0.2447E+00	-0.[illegible]33E-02

B =

DC	DSF	DSTF	PLA	DDF	DR
-0.3558E+00	-0.1014E+00	-0.1435E+00	0.1149E+00	-0.4871E-07	-0.4659E-07
-0.9386E-03	0.7000E-05	-0.3907E-03	-0.1434E-03	-0.3912E-09	-0.3742E-09
0.5196E-01	-0.8818E-02	-0.2016E-01	-0.1067E-02	0.8803E-08	0.8421E-08
0.0000E+00	0.0000E+00	0.0000E+00	0.0000E+00	0.0000E+00	0.0000E+00
-0.7623E-08	-0.4431E-09	-0.3272E-09	0.3830E-10	-0.4645E-03	0.2504E-03
-0.2318E-04	-0.5278E-06	-0.3897E-06	0.4563E-07	0.1392E+00	0.5544E-02
0.9551E-06	-0.2880E-07	-0.2126E-07	0.2489E-08	0.1372E-01	-0.2079E-01
0.0000E+00	0.0000E+00	0.0000E+00	0.0000E+00	0.0000E+00	0.0000E+00

D =

DC	DSF	DSTF	PLA	DDF	DR
0.1556E-01	0.1770E-02	0.7739E-02	0.3315E-04	0.9014E-03	0.3591E-04
0.1556E-01	0.1770E-02	0.7739E-02	0.3315E-04	0.9014E-03	0.3591E-04
0.6183E-06	0.1178E-07	0.8697E-08	-0.1018E-08	-0.1166E-01	0.4068E-02

Figure A-1. Concluded.

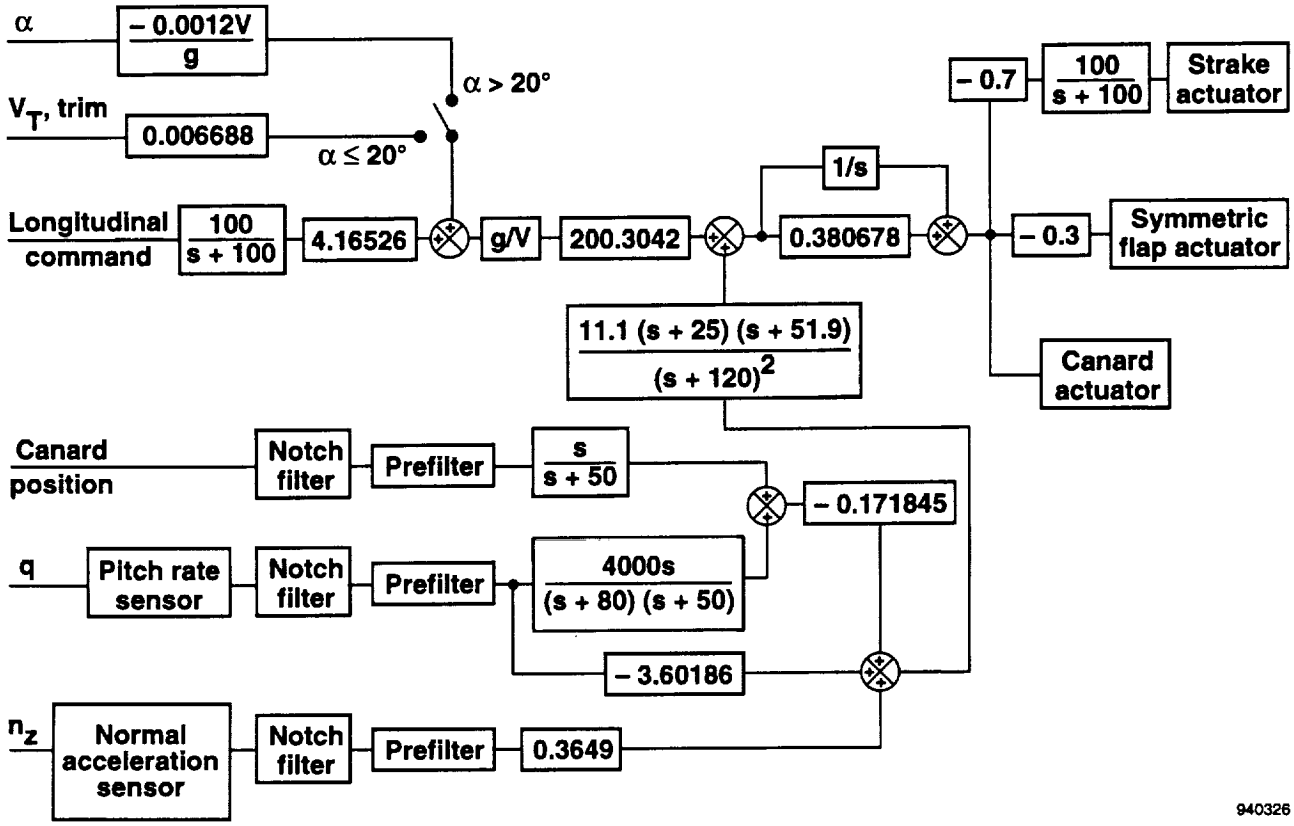

Figure A-2. Longitudinal control system.

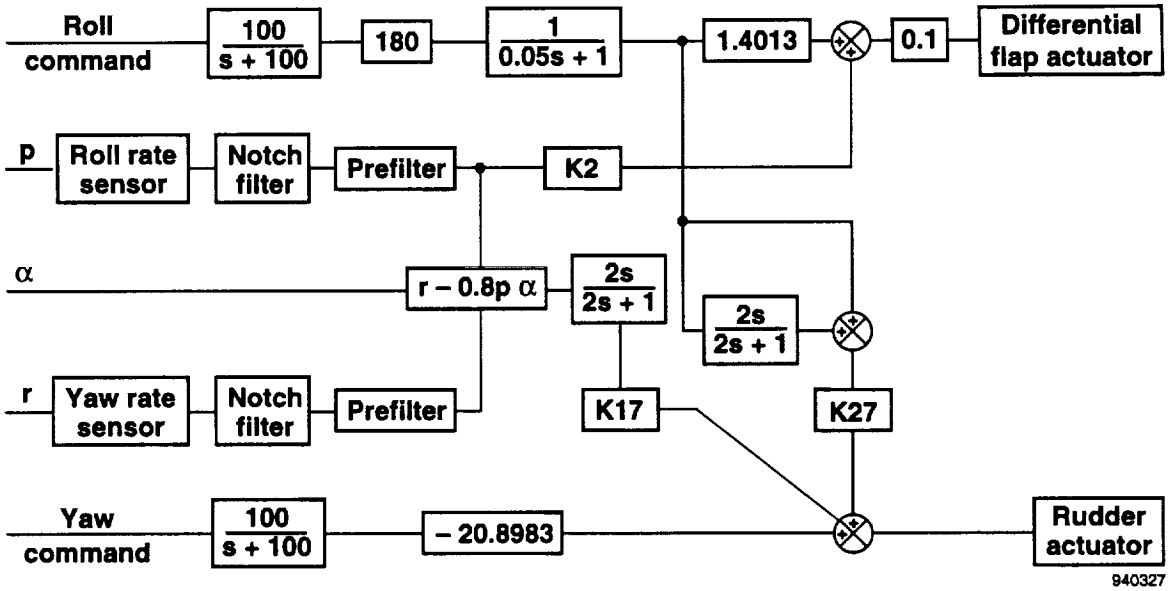

Figure A-3. Lateral–directional control system.

REPORT DOCUMENTATION PAGE

Form Approved
OMB No. 0704-0188

1. AGENCY USE ONLY (Leave blank)	2. REPORT DATE	3. REPORT TYPE AND DATES COVERED
	February 1995	Technical Paper

4. TITLE AND SUBTITLE

Flight Test of the X-29A at High Angle of Attack: Flight Dynamics and Controls

5. FUNDING NUMBERS

WU 505-64-30

6. AUTHOR(S)

Jeffrey E. Bauer, Robert Clarke, and John J. Burken

7. PERFORMING ORGANIZATION NAME(S) AND ADDRESS(ES)

NASA Dryden Flight Research Center
P.O. Box 273
Edwards, California 93523-0273

8. PERFORMING ORGANIZATION REPORT NUMBER

H-1984

9. SPONSORING/MONOTORING AGENCY NAME(S) AND ADDRESS(ES)

National Aeronautics and Space Administration
Washington, DC 20546-0001

10. SPONSORING/MONITORING AGENCY REPORT NUMBER

NASA TP-3537

11. SUPPLEMENTARY NOTES

12a. DISTRIBUTION/AVAILABILITY STATEMENT

Unclassified—Unlimited
Subject Category 05

12b. DISTRIBUTION CODE

13. ABSTRACT (Maximum 200 words)

The NASA Dryden Flight Research Center has flight tested two X-29A aircraft at low and high angles of attack. The high-angle-of-attack tests evaluate the feasibility of integrated X-29A technologies. More specific objectives focus on evaluating the high-angle-of-attack flying qualities, defining multiaxis controllability limits, and determining the maximum pitch-pointing capability. A pilot-selectable gain system allows examination of tradeoffs in airplane stability and maneuverability. Basic fighter maneuvers provide qualitative evaluation. Bank angle captures permit qualitative data analysis.

This paper discusses the design goals and approach for high-angle-of-attack control laws and provides results from the envelope expansion and handling qualities testing at intermediate angles of attack. Comparisons of the flight test results to the predictions are made where appropriate. The pitch rate command structure of the longitudinal control system is shown to be a valid design for high-angle-of-attack control laws. Flight test results show that wing rock amplitude was overpredicted and aileron and rudder effectiveness were underpredicted. Flight tests show the X-29A airplane to be a good aircraft up to 40° angle of attack.

14. SUBJECT TERMS

Digital flight controls; Flight test; Flying qualities; Forward-swept wing; High alpha; Unstable

15. NUMBER OF PAGES

70

16. PRICE CODE

AO4

17. SECURITY CLASSIFICATION OF REPORT	18. SECURITY CLASSIFICATION OF THIS PAGE	19. SECURITY CLASSIFICATION OF ABSTRACT	20. LIMITATION OF ABSTRACT
Unclassified	Unclassified	Unclassified	Unlimited

National Aeronautics and
Space Administration
Code JTT
Washington, D.C.
20546-0001

Official Business
Penalty for Private Use, $300

SPECIAL FOURTH-CLASS RATE
POSTAGE AND FEES PAID
NASA
PERMIT No. G27

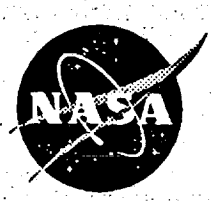

POSTMASTER: If Undeliverable (Section 158
Postal Manual) Do Not Return